HERSCHEL / PLANCK

Radio Frequency Development Model (RFDM) modeling and analysis

H-P-3-ASPI-AN-0324

Product Code : 220000

Rédigé par/*Written by*	**Responsabilité-Service-Société** ***Responsibility-Office -Company***	**Date**	**Signature**
D. Dubruel	Planck RF analysis.	19-06-2002	
M. Nadarassin	Planck RF analysis.	19-06-2002	
Vérifié par/*Verified by*			
G. Forma	Planck RFDM mock up and test manager	30/06/02	
JB. Riti	Planck engineering manager	30/06/02	
T. Banos	Planck PLM manager	30/06/02	
Approbation/*Approved*			
V. Grossetete	Product Assurance Manager	30/06/02	
J-J. JUILLET	Project Manager	30/06/02	

Data management : G. SERRA

Entité Emettrice : Alcatel Space - Cannes
(détentrice de l'original) :

SPIRE-ALC-DOC-002363

HERSCHEL / PLANCK

Radio Frequency Development Model (RFDM) modeling and analysis

H-P-3-ASPI-AN-0324

Product Code : 220000

Rédigé par/ *Written by*	**Responsabilité-Service-Société** ***Responsibility-Office -Company***	**Date**	**Signature**
D. Dubruel	Planck RF analysis.	19-06-2002	
M. Nadarassin	Planck RF analysis.	19-06-2002	
Vérifié par/ *Verified by*			
G. Forma	Planck RFDM mock up and test manager		
JB. Riti	Planck engineering manager		
T. Banos	Planck PLM manager		
Approbation/ *Approved*			
V. Grossetete	Product Assurance Manager		
J-J. JUILLET	Project Manager		

Data management : G. SERRA

Entité Emettrice : Alcatel Space - Cannes
(détentrice de l'original) :

HERSCHEL/PLANCK	DISTRIBUTION RECORD

DOCUMENT NUMBER : H-P-3-ASPI-AN-0323

Issue 1/ Rev. : 0
Date: 19-06-2002

EXTERNAL DISTRIBUTION		INTERNAL DISTRIBUTION	
ESA	X	HP team	X
ASTRIUM			
ALENIA			
CONTRAVES			
TICRA			
TECNOLOGICA			
		Clt Documentation	Orig.

ENREGISTREMENT DES EVOLUTIONS / *CHANGE RECORDS*

ISSUE	DATE	§ : DESCRIPTION DES EVOLUTIONS *§ : CHANGE RECORD*	REDACTEUR *AUTHOR*
1	19-06-2002	Initial release	D. Dubruel

TABLE OF CONTENTS

LIST OF FIGURES

LIST OF TABLES

1. INTRODUCTION

1.1 Purpose of this note

This note introduces the analyses performed on the radio frequency development model. The RFDM has been modeled and tested in Cannes. The test facility is a Compact Antenna Test Range.

The report is complementary in term of analysis to the RFDM CATR test reporrt (see below RD4).

1.2 Reference documents

1.2.1 Reference documents

[RD1] Planck RFDM RF Test Requirement Doc. n° : H-P-3-ASPI-SP-0221 issue 1 rev 0
[RD2] Technical note defining the 3D reflector measurement list of points Doc. n° : H-P-3-ASPI-TN-0222 issue 1 rev 0
[RD3] Planck RFDM RF Test Procedure Doc. n° : H-P-3-ASPI-TP-0223 issue 1 rev 0
[RD4] PLANCK RFDM RF TEST REPORT Doc. n° : H-P-3-ASPI-TR-0240 issue 1 rev 0
[RD5] H-P-3-ASPI-DD-0345 RFDM mathematical model issue 1 rev 0

2. RFDM DESCRIPTION

The Planck RFDM is an off-axis Gregorian telescope composed of a parabolic primary, an elliptical secondary and a corrugated horn. The reflectors were part of the Archeops balloon borne payload and were designed by the University of Minnesota to have an entrance aperture of 1500 mm providing a diffraction limited beam with 8 arcminute full width at half maximum at 143 GHz. The circular entrance aperture of 1500 mm gives an elliptical primary with dimensions of ~1800 mm X 1500 mm and a circular secondary with diameter of ~800 mm. Remmelle Engineering of New Brighton, Minnesota manufactured the primary and secondary reflectors by milling slabs of Al-6061 and thermally treating them to T6. The overall figure accuracy is better than 60 micron RMS and the local surface quality is better than 2 micron roughness average.

The 100 GHz horn (circular aperture $\varnothing \cong 15$ mm, corrugation width $\cong 0.3$ mm) has been manufactured using electroforming process by SAP (Société Audoise de Précision, France). The horn and the sub-reflector assembly are mounted on high precision hexapods allowing accurate positioning with respect to the main reflector. The feed geometry at 100 GHz is a scaled version of the 30 GHz horn. The geometry has been provided by the LFI team, it corresponds to one version of the potential candidates for the Planck focal plane flight model. This horn is providing a representative illumination of the secondary relfector.

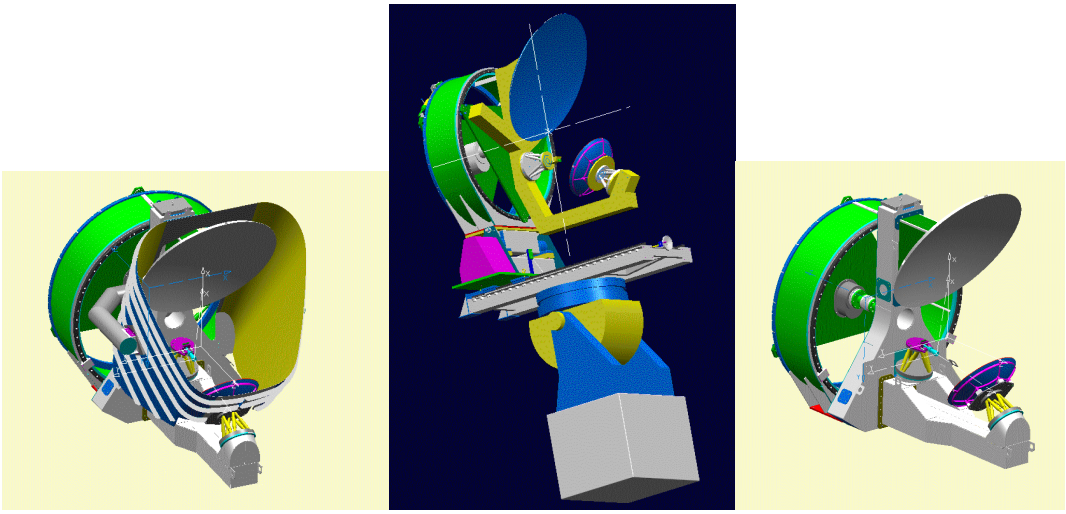

Figure 2-1: RFDM in test configuration.

Figure 2-2 : RFDM under test configuration in CATR.

3. REFLECTORS SURFACE MEASUREMENTS AND ANALYSES.

3.1 Initial 3D measurement (after reflectors manufacturing).

The RFDM reflectors have been mechanically measured after the manufacturing using a laser tracker method : an optical target is rolled over the reflector surface and tracked by a laser to obtain its spatial location. Around 19000 points have been obtained. The figure 3-1 displays the track of points.

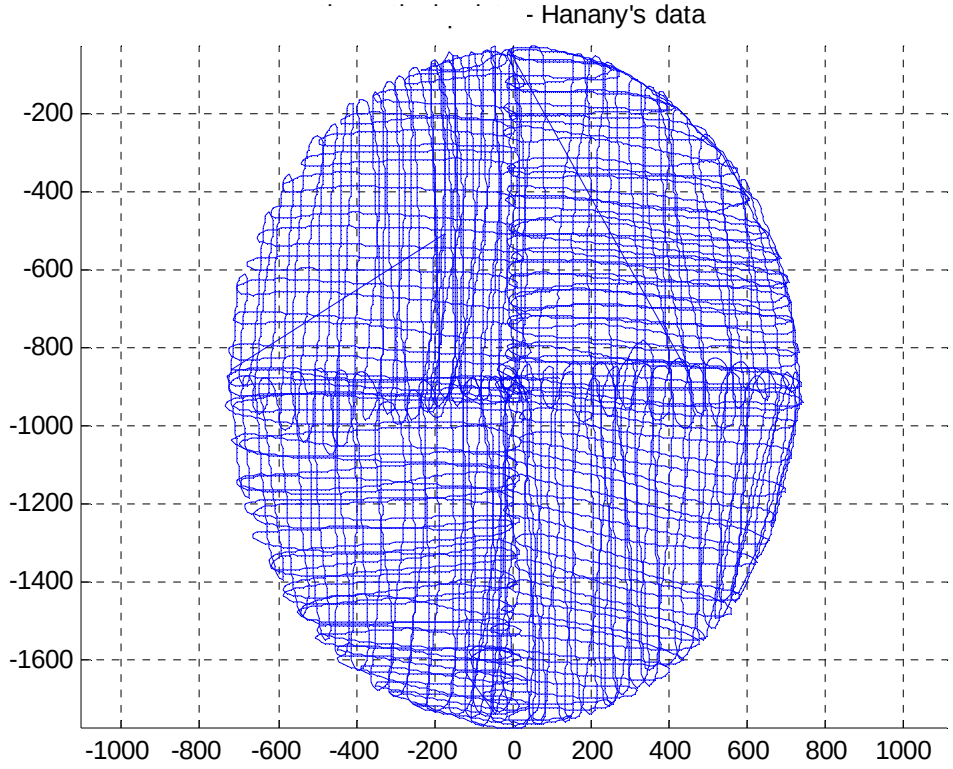

Figure 3-1 : track of measured points on the primary reflector.

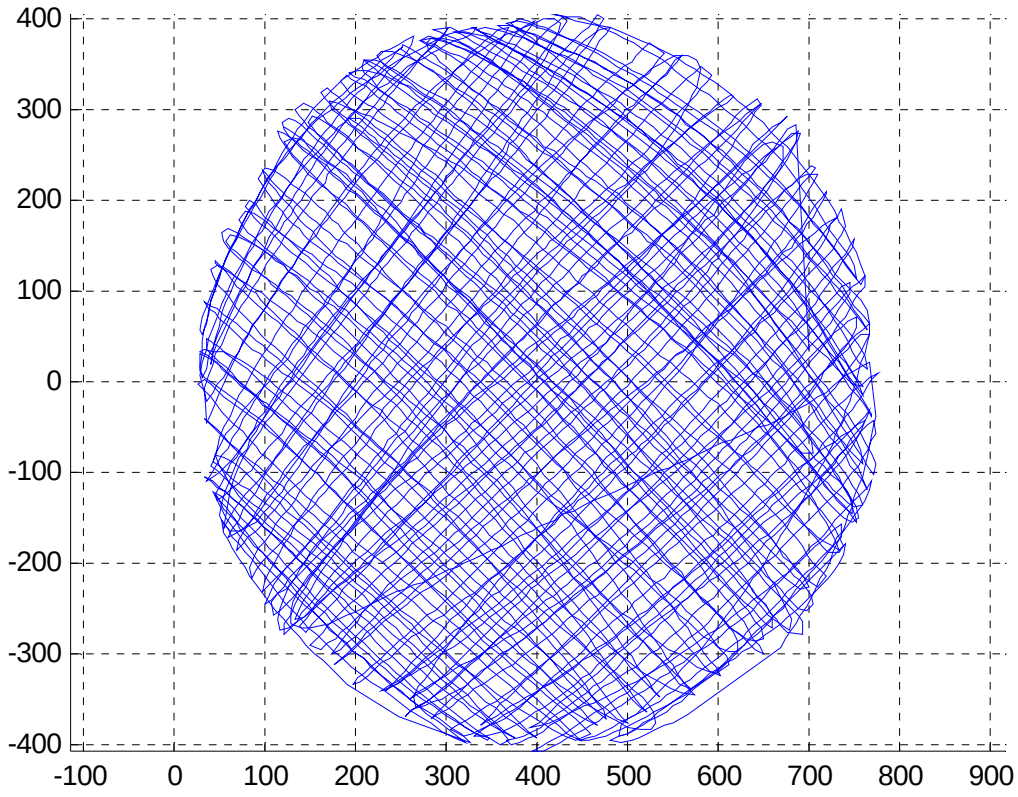

Figure 3-2 : track of measured points on the secondary reflector.

The measured points are displayed as deviation (actual theoretical surface – measured one) in the figure 3-3 for the primary reflector and figure 3-4 for the secondary reflector. For the primary (respectively secondary) reflector the surface error root mean square is of the order of 58 µm (respectively 62µm) . This was the surface deviation state prior to any balloon flight.

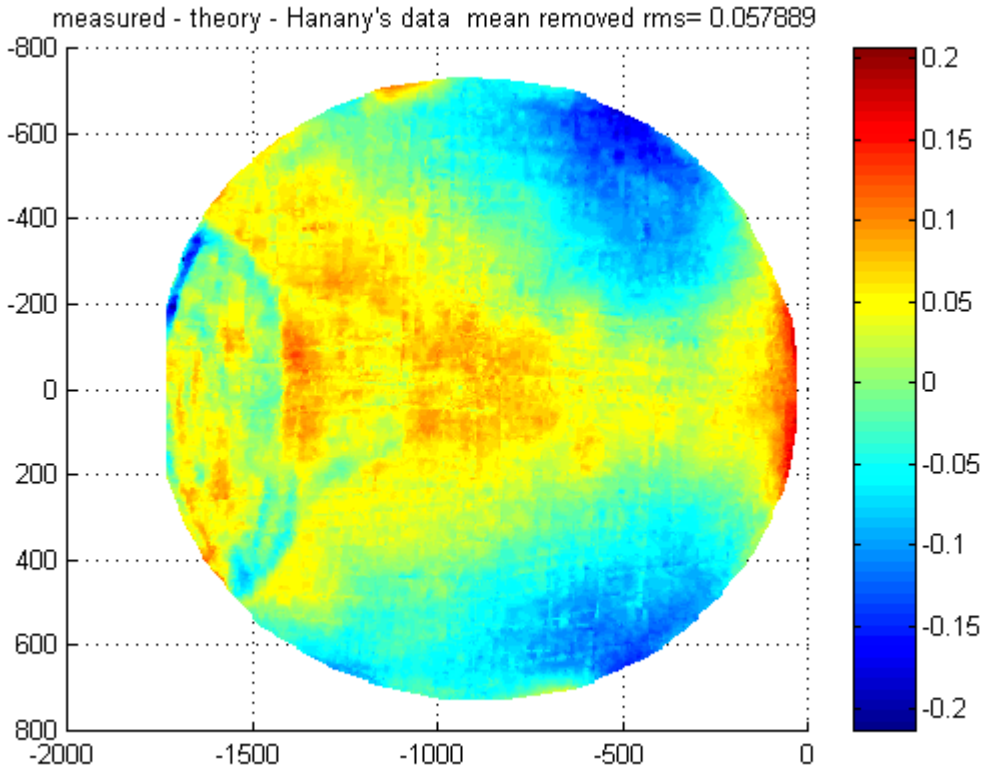

Figure 3-3 : deviation of the manufactured primary reflector.

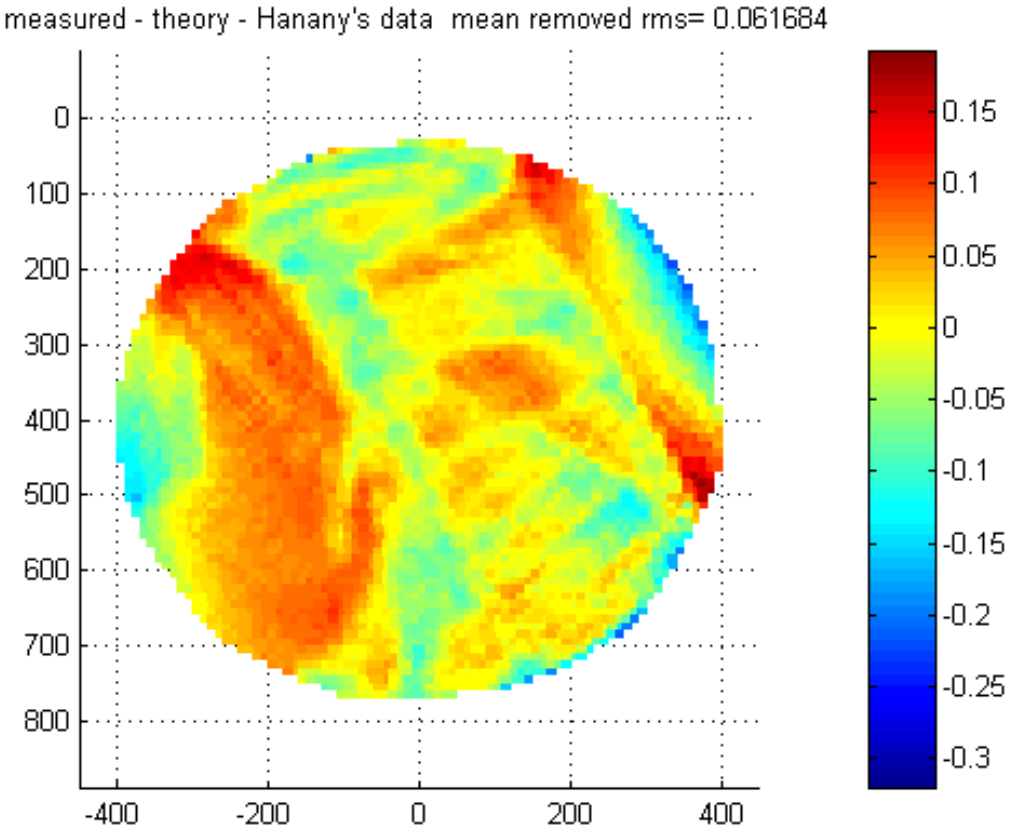

Figure 3-4 : deviation of the manufactured secondary reflector.

3.2 3D mechanical measurements after balloon flights and comparison with initial measurements.

The Archeops telescope, called RFDM in the Planck program has been equiped with tooling balls on both reflectors and reference optical cubes. The two reflectors have been delivered without any optical reference.
The following process has then been performed :

-assesment of a mechanical coordinate system thanks to the available interface holes (CAD work).
-optical reference set up (1 cube + ball and 3 single optical balls for each reflector).
-mechanical probing of the reflector surface.
-numerical processing of the surface.
-numerical processing of the pointing data.

The reference document [RD2] details the list of measurement point. 5265 points have been defined for the primary reflector and 5995 for the secondary. 340 fake points have been removed from the measured data of the secondary. These points are located at the edge of the reflector where the probing tool composed of a sphere is touching the edge of the surface leading to an error going up to the radius of the sphere. In fact the probe is descending too low wrt to the surface. The secondary reflector was measured through paralell lines, the first and last points of the170 final lines have been removed.

The numerical processing of the surface consists in loading the 3D data as an irregular grid. Then this irregular grid is converted into a regular grid thanks to a matlab procedure. A translation along x,y,z is applied followed by a rotation around X,Y, axis followed by a translation along z prior to the computation of the root mean square deviation. The following transformations have been applied :

- translation along X of 0 mm
- translation along Y of 0.05 mm
- translation along Z of 0.2399 mm
- rotation around X_axis of 0.015°
- rotation around Y axis of 0.008°.
- translation along Z axis of 0.1763 mm

The primary reflector deviation is displayed in figure 3-5.
The obtained rms is 61.5 microns.

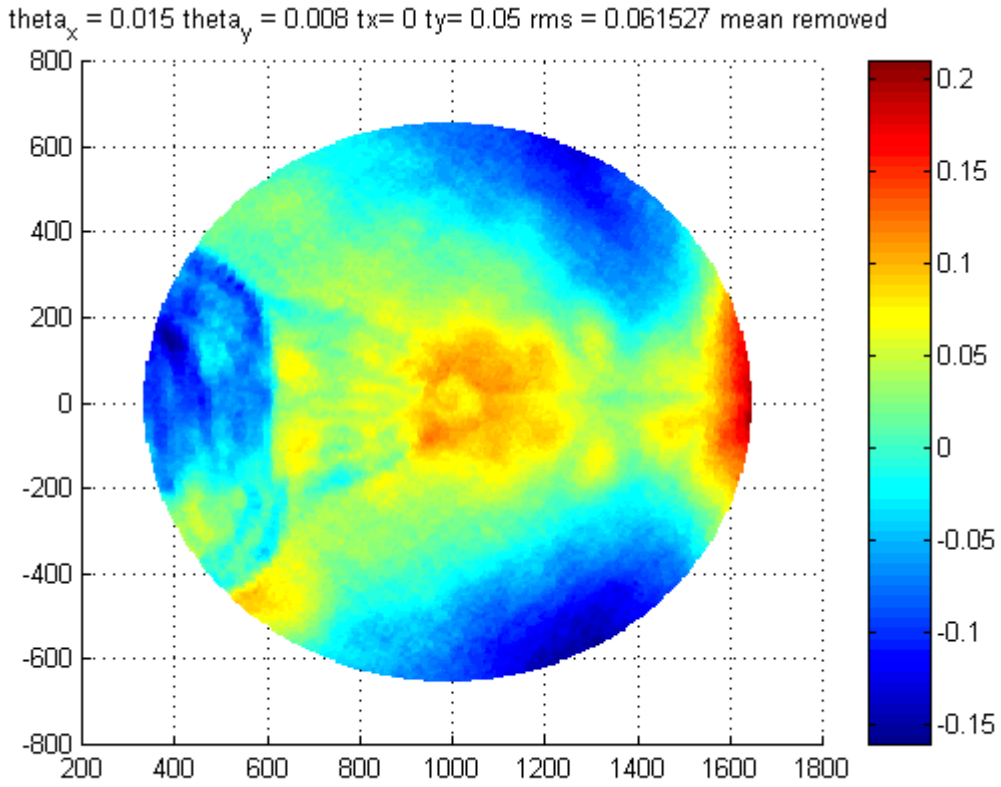

Figure 3-5 : Display of the difference between the 3D primary reflector measured surface and the theoretical paraboloid

Conclusion for the Primary reflector: the figure 3-5 has to be compared to the figure 3-3. A nice correlation of the surface deviation is visible. The primary reflector surface has not changed since the manufacturing. The rms difference of 3.5 microns could certainly be reduced by further optimisation of the surface shift.

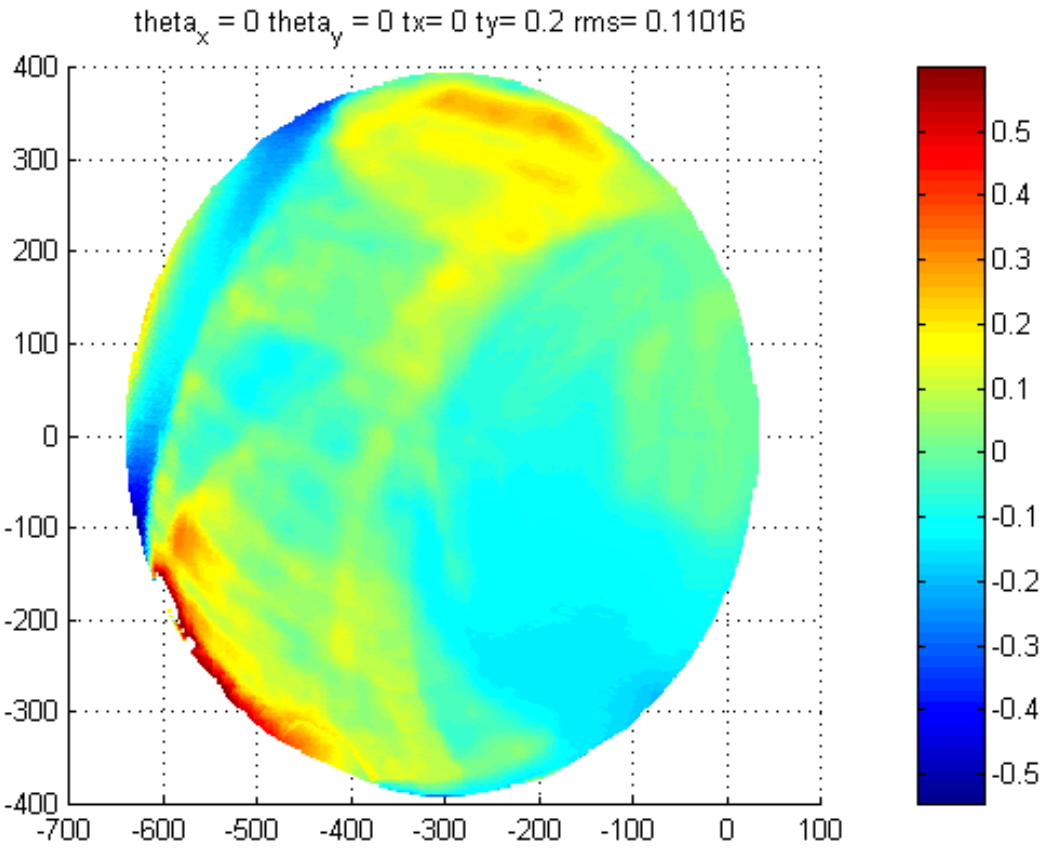

Figure 3-6 : Display of the difference between the 3D secondary reflector measured surface and the initial ellipsoid.

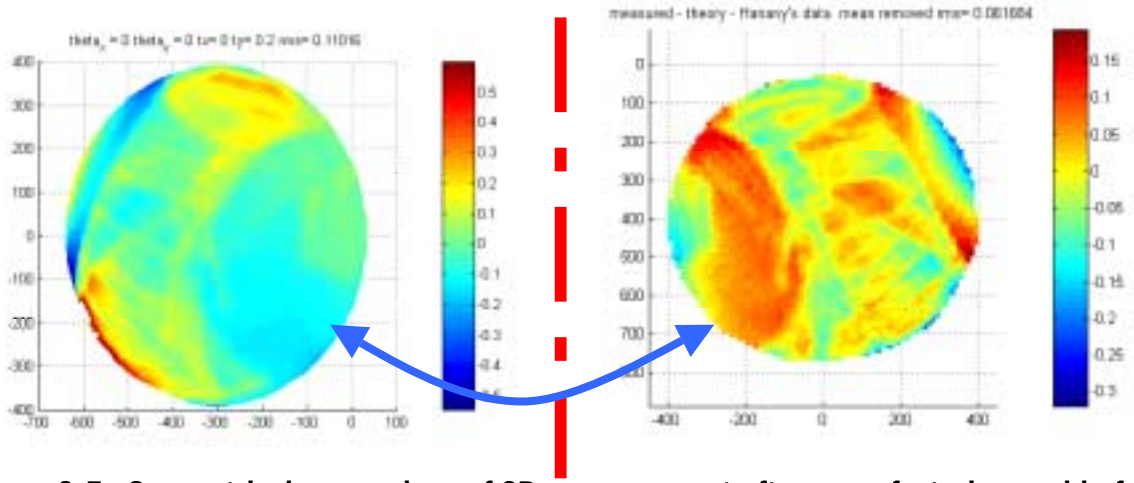

Figure 3-7 : Symmetrical comparison of 3D measurement after manufacturing and before RF tests.

Conclusion for the secondary reflector : the figure 3-7 displays the mirroring comparison of the theoretical surface and the surface measured in Cannes. The rms deviation is of order of 61 µm for the surface after manufacturing and 110 µm for the surface after balloon flights. This deviation cannot be explained by a non optimum set of rotations and translations of the measured cloud of points. In fact by looking carefully at the shape, a surface change is visible at one edge of the secondary reflector. This could correspond to a event in hte Archeops experiment (balloon hard landing ????).
This surface modification has no significant RF impact thanks to the very low level of illumination in this area. The RFDM test is producing the RF performance of the distorted surface not the performance of the manufactured telescope. This is sufficient to reach one of the RFDM test goals : the validation of the numerical model.

As a conclusion, the surface shape of both reflectors is known with a difference to theory of 60µm for the primary and 110µm rms for the secondary.

3.3 Videogrammetry of the reflector

A videogrammetry measurement of the primary reflector has been performed using a target projector (see fig 3-9). 4000 optical targets have been projected on the front face of the primary reflector. The cloud of points has been obtained together with the optical balls at the periphery of the primary reflector (see fig 3-8). This test has also provided the relative distance of the optical balls of the primary reflector with regards to the balls of the secondary reflector. As a summary the following set of data is available form the videogrammetry :

-cloud of points of the reflector surface AND the optical peripheral balls.
-relative distance between primary and secondary reflectors.

In other words, this test has provided the shape of the primary reflector as well as the alignement of the telescope under test configuration.

The displayed deviations have to be compared with the former results (fig 3-3 and 3-5). A nice correlation is obtained for the shape. The rms is slightly worse in the vidoegrammetry results, but the cloud of points is known in the optical balls coordinate system (telescope alignement known).

The secondary reflector has not yet (at release date of this document) been measured. The target projector could not illuminate completely the secondary reflector in the integrated configuration. The secondary reflector is planned to be measured using videogrammetry in a dismounted configuration on a table in July 2002.

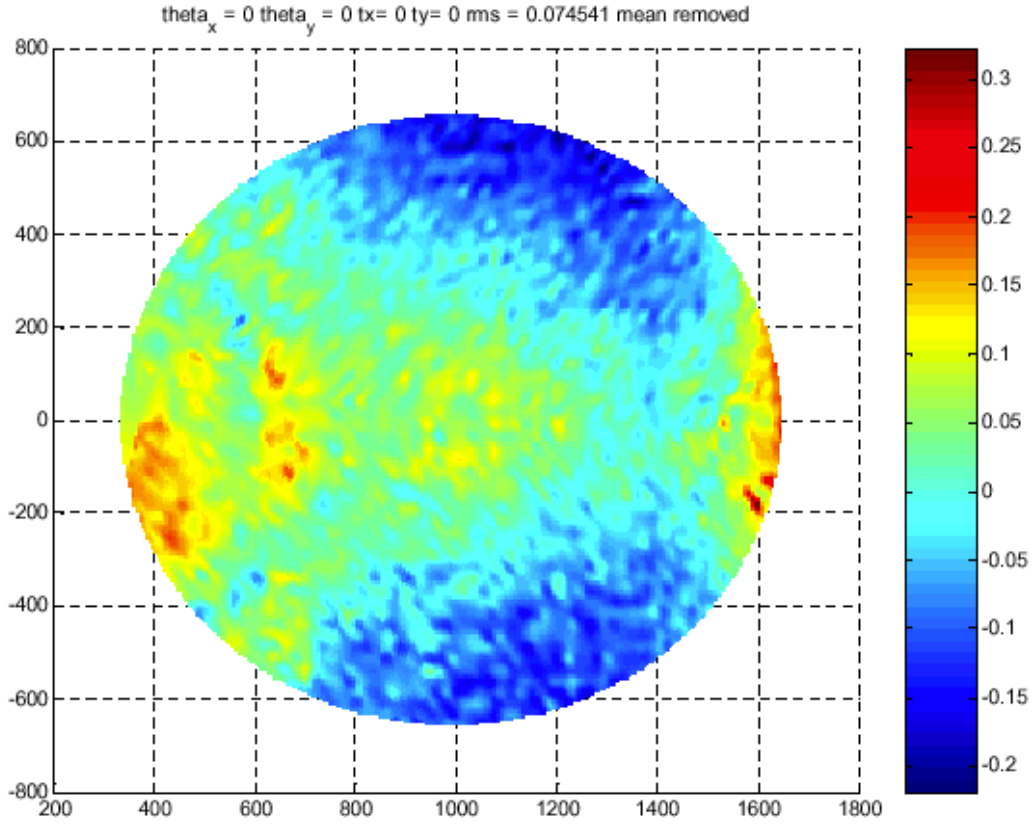

Figure 3-8 : primary reflector deviation measured by videogrammetry.

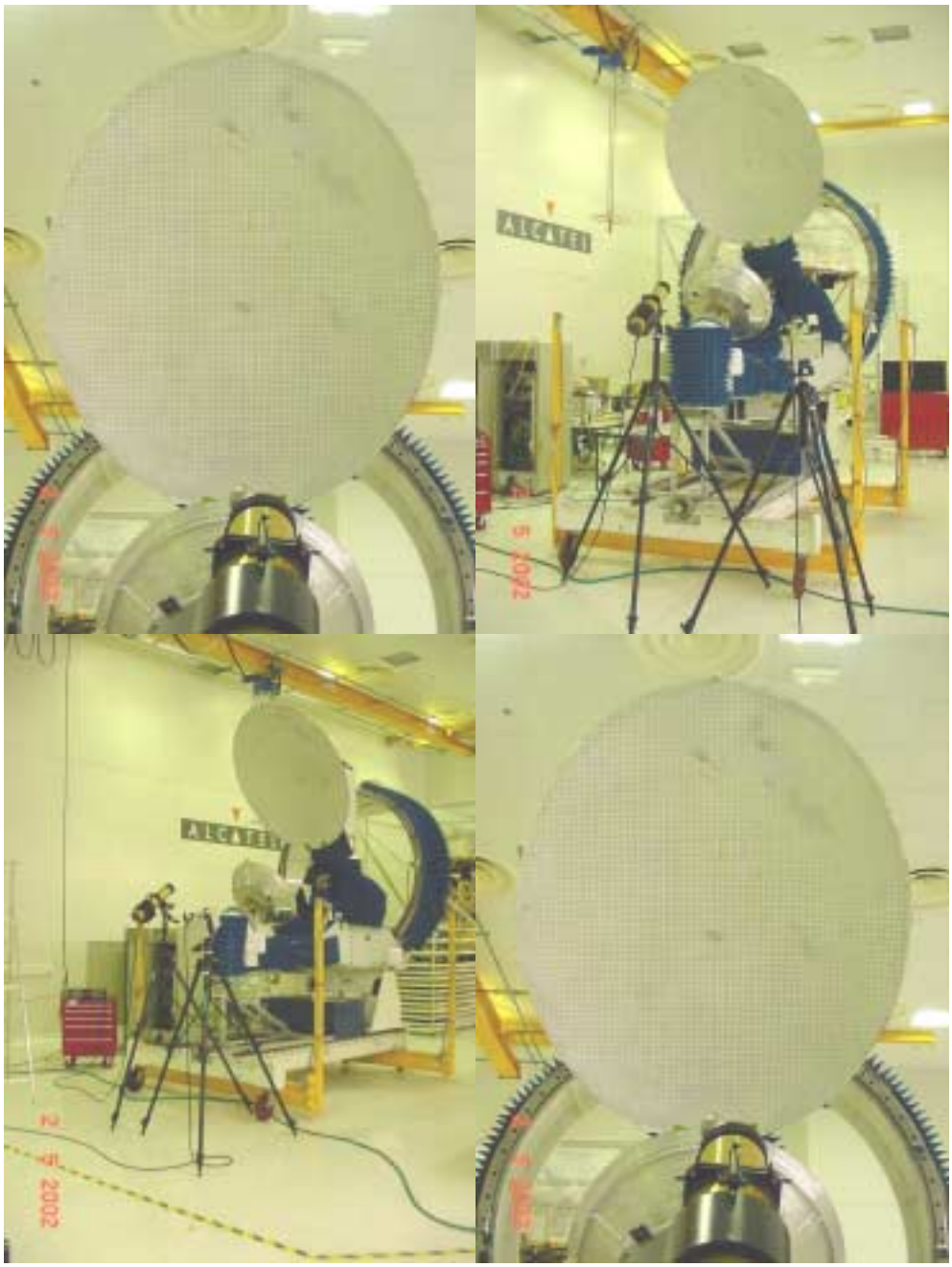

Figure 3-9 : primary reflector videogrametry test.

4. PRIMARY FEED PREDICTION AND MEASUREMENT.

The feed geoemetry has been provided by the LFI team, it corresponds to one version of the potential candidates for the Planck focal plane flight model. Its main characteristic is a very low taper at the edge of the secondary reflector. Its geometry is described in the mathematical model [RD6].

The primary feed radiation pattern has been computed and matched in terms of frequency using the SRSR software written by France Telecom (see fig 4-2). This software is a finite element software solving the Maxwell equations. The geometry of the corrugated horn is of revolution and fed by the TE11 mode. The geometry is given by a set of (X,Z) points, Z being the coordinate along the RF axis and X, the local radius. The third component is deduced by revolution.

Two predictions have been performed : the prediction of the initial geometry and the prediction of the manufactured geometry. The manufacturing tolerance is so small compared to the meshing of the corrugation that no impact is visible on the diagram.

The manufactured geometry is obtained by the mechanical measurement of the mandrin used in the electroerosion manufacturing process.

Figure 4-1 : photo of the 30 GHz primary feed.

The 100 GHz horn is a scaled version of the 30 GHz one. The scale factor is 30/100. From an electromagnetic point of view, the radiation patterns of the two corrugated horns are the same. In both cases the non-sized ratio (distance/wavelength) is constant. The predictions of the 30 GHz horn and 100 GHz are then identical. In order to cope with the actual internal transition diameter, the matching of the resulting horn has been matched thanks to the SRSR software. This optimisation loop has been performed because the scaling of the 30 GHz horn has led to a non conventional transition diameter. A local geometrical change on the first corrugation has been performed in order to obtain a horn input diameter compatible and matched with the existing 100 GHz transition. This local geometrical modification does not impact the far field radiation pattern of the primary feed.

The 30 GHz horn radiation pattern has been measured in France Telecom R&D La Turbie facility. The measurement results are presented in fig 4-3.

The measurements show a very good agreement with the predictions for the Co-polarisation in the planes $\varphi=0°$, $\varphi=45°$, $\varphi=90°$, $\varphi=135°$. Nevertheless a significant difference is visible on the cross-polarization. The cross-polarization appears roughly as the attenuated image of the co-polarization shape. The

attenuation is of order of 30 dB. This difference will have an impact on the cross polarization of the overall telescope radiation pattern (see section 9-2).

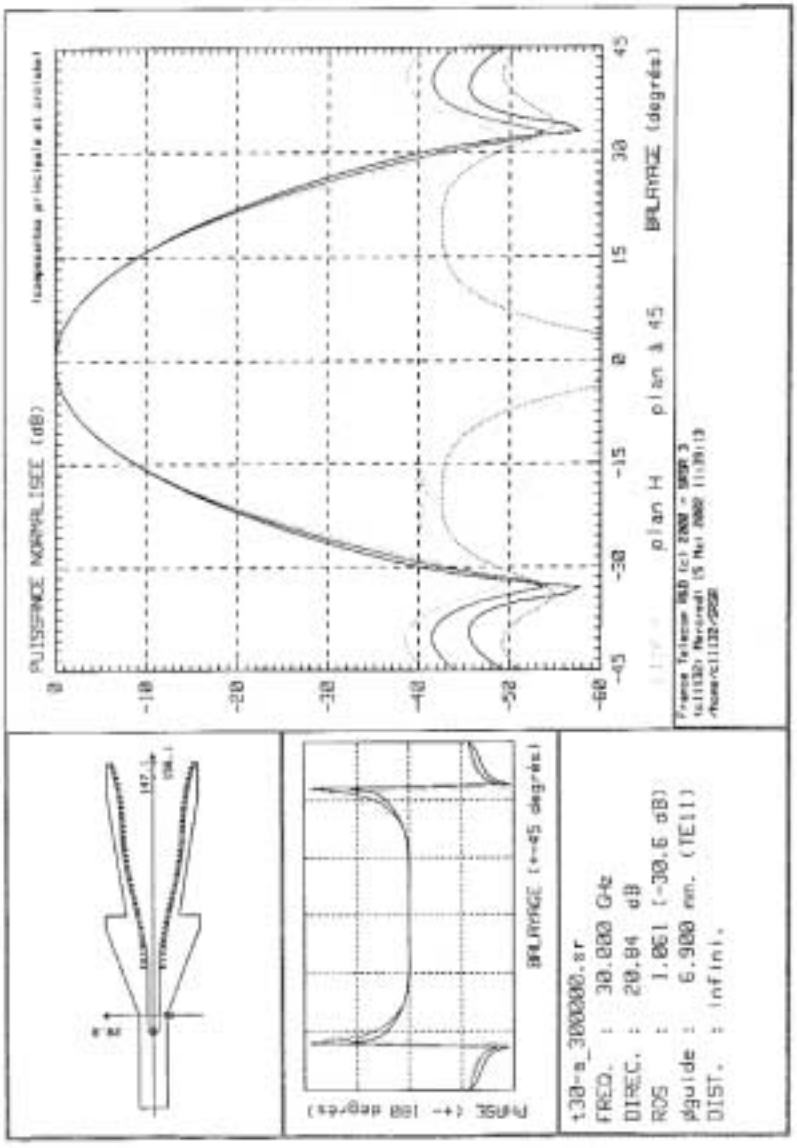

Figure 4-2 : Predicted radiation pattern of the 30 GHz and 100 GHz feed.

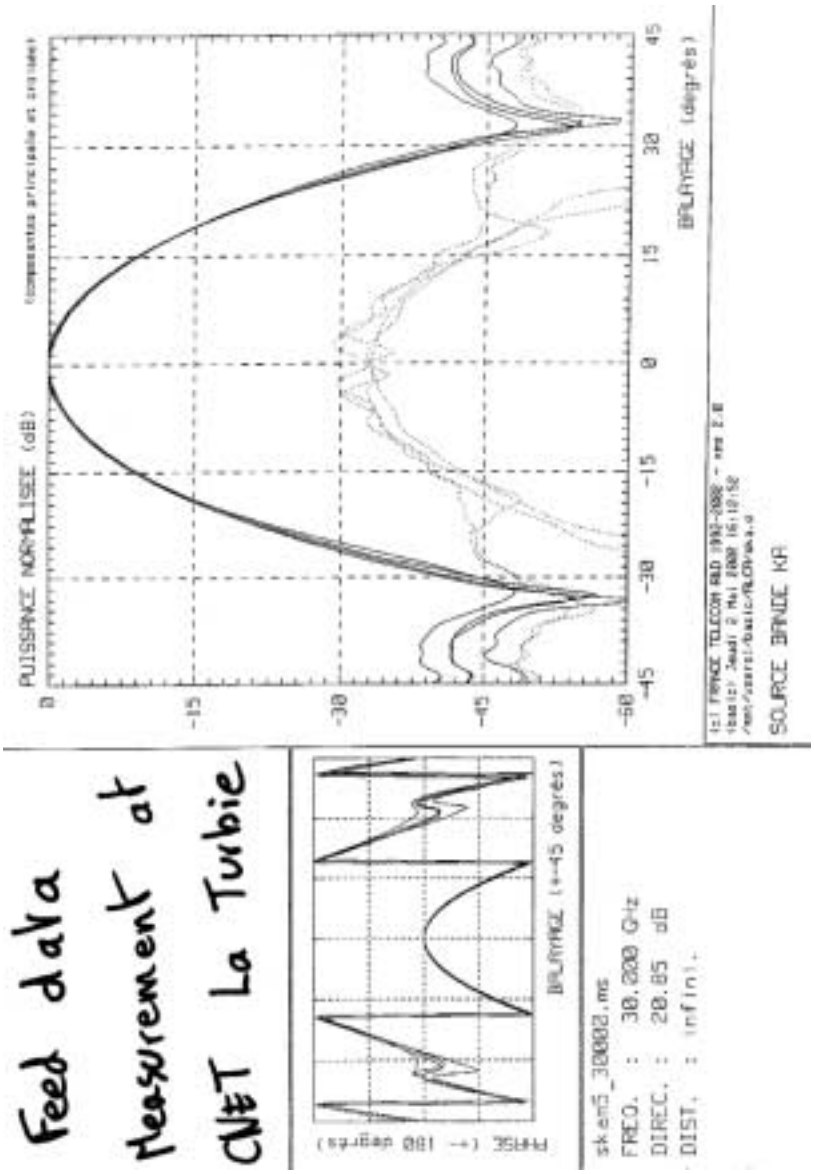

Figure 4-3 : 30 GHz measurement at France Telecom R&D la Turbie.

5. TELESCOPE FAR FIELD RADIATION PATTERN PREDICTION AT 30 GHZ

This section presents the prediction. Detailed analyses (correlation with measurement) are provided in the next section.

The main lobe is computed using the grasp8 software and the telescope mathematical model [RD 6]. This model corresponds to the nominal geometry realigned with the distance data provided by the videogrammetry. The primary reflector surface is composed of the cloud of points measured with the videogrammetry, the secondary surface is composed of the set of points measured with the 3D mechanical machine. A cross check will nevertheless be performed with the surface data provided by the vidogrammetry measurement of the secondary. At the moment the correlation is excellent at 30GHz. This means that the uncertainty remaining on the 3D mechanical data is small at 30GHz.

5.1 Angle convention

The angle convention corresponds to the TICRA definition of angles (θ,φ). A direction defined by (θ,φ) is found using the following procedure in a regular coordinate system.

1) a plane perpendicular to the X,Y plane is rotated by an angle φ around the Z_axis.

2) In the former plane θ is defined as the angle between the pointed direction and the Z_axis.

Example $\varphi=0$,corresponds to the plane of symmetry of the telescope (Plane X,Z).
$\varphi=90$, corresponds to the plane (X,Y)

$\varphi=$anyvalue, $\theta=0$ corresponds to the telescope boresight.

$\varphi=180°$, $\theta=2.65°$ corresponds to the direction of the maximum of the beam for the selected feed location.

RF acquisitions have been performed for constant φ and with the θ angle varying.

The set of measured cuts is fully described in the CATR test report (see RD 4). In this present document a special attention has been paid to two cuts : the cuts in the telescope plane of symmetry, and the cut contained in the plane perpendicular to the plane of symmetry. This corresponds to cuts for $\varphi=0°$ and $\varphi=+/-90°$.

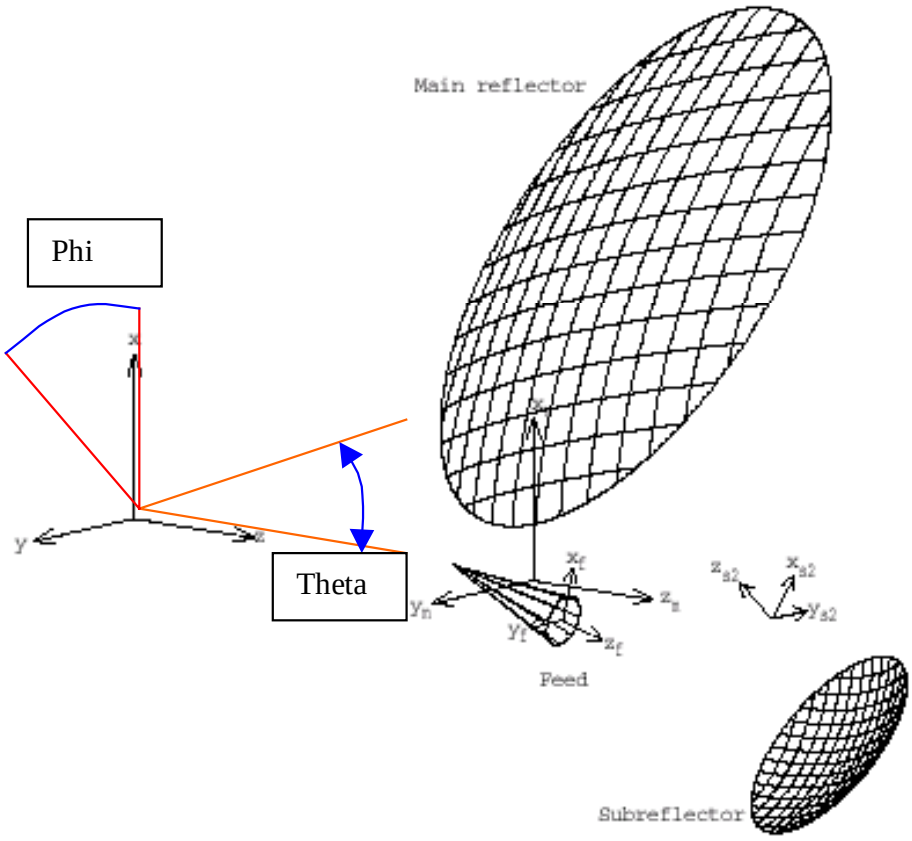

Figure 5-1 : axis convention

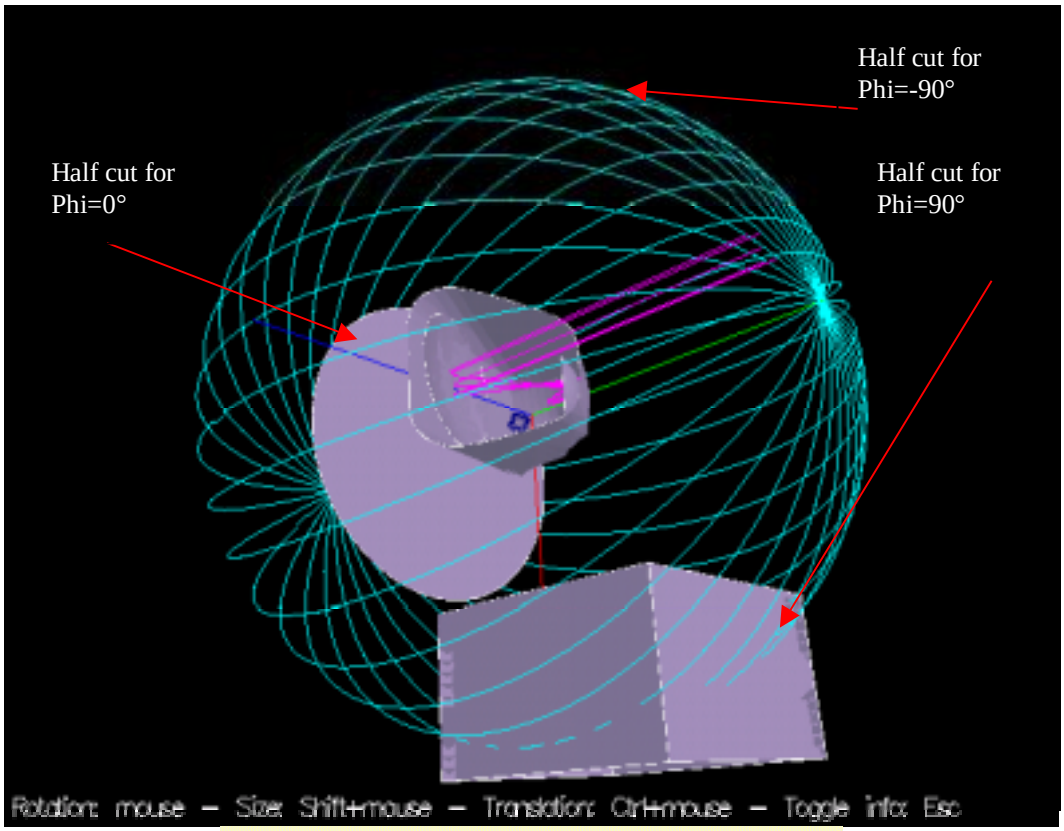

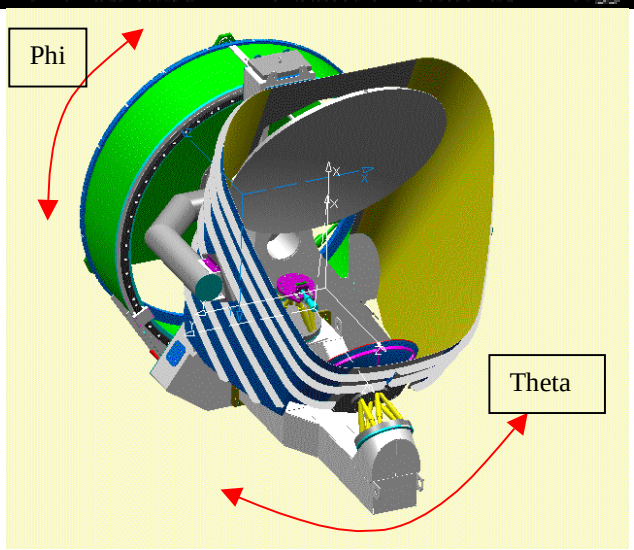

Figure 5-2 : example of cuts.

5.2 Main lobe prediction.

The computed on axis directivity is 52.1 dBi in co polarisation and the maximum cross-polarization level is 23.4 dBi. The maximum difference is 52.1 - 23.4 = 28.7 dB. The configuration is composed of the two reflectors alone. Predictions have been perfomed using PO on the secondary and PO on the primary reflector.

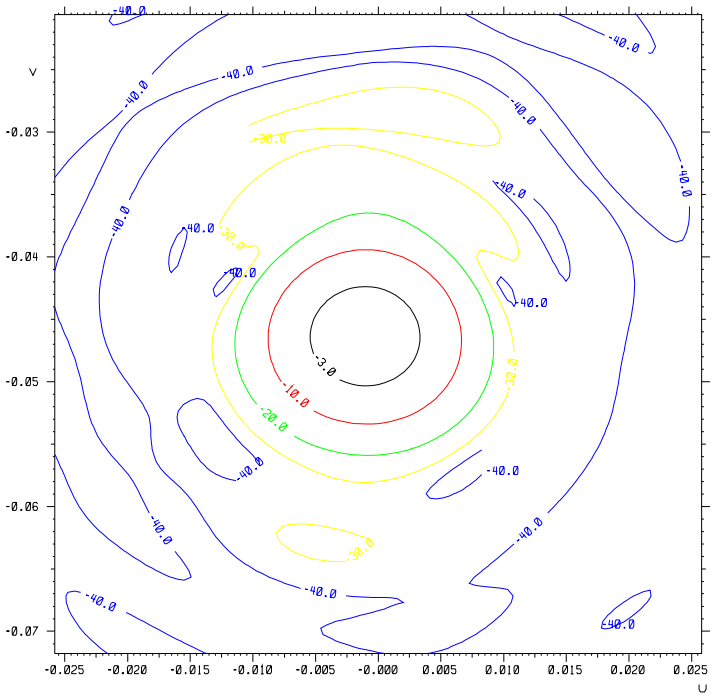

Figure 5-3 : Main lobe co-polarisation prediction relatively to the co-pol maximum.

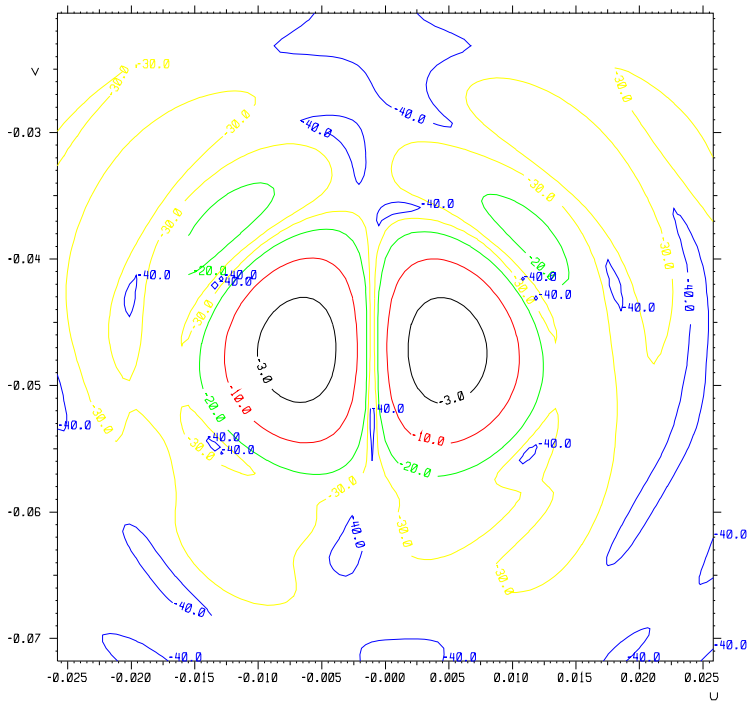

Figure 5-4 : Main lobe predicted cross polarisation relatively to the cross-pol maximum .

5.3 Far out side lobe prediction

The far out side lobes are computed using the grasp8 software and the telescope mathematical model [RD 6]. The diagram is computed in two cuts : the telescope plane of symmetry and the plane perpendicular to the plane of symmetry ($\varphi=0$ and $\varphi=90°$ in M1 coordinate system. The figure 5-5 displays the prediction in the plane $\varphi=0°$. This cut is passing through the main lobe (pointing in $\theta=-2.65°$, $\varphi=0°$). The spill over lobe past the primary reflector is clearly visible around $\theta=75°$ and $\theta=170°$. A numerical caustic is visible around $\theta=120°$ (in co and cross polarisation), this corresponds to the backward direction of the primary reflector.
The figure 5-6 displays the cut for $\varphi=+/-90°$ (this cut is a full circle composed of two half cuts of 180° angular length). This cut should be symmetrical in the nomical case, the non symmetry is induced by the surface shape errror and the reflector relative misalignement. Rem : the predictions are performed using the alignement data measured on the actual RFDM prior to the RF test.

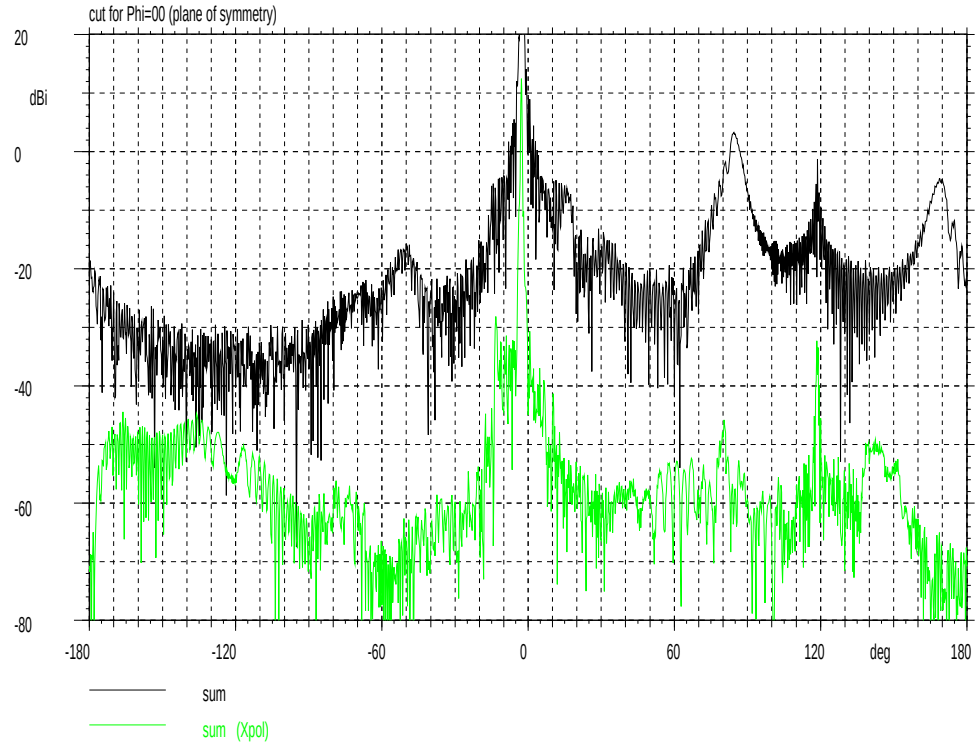

Figure 5-5 : far out side lobe prediction in the telescope plane of symmetry ($\varphi=0°$, $\varphi=180°$)

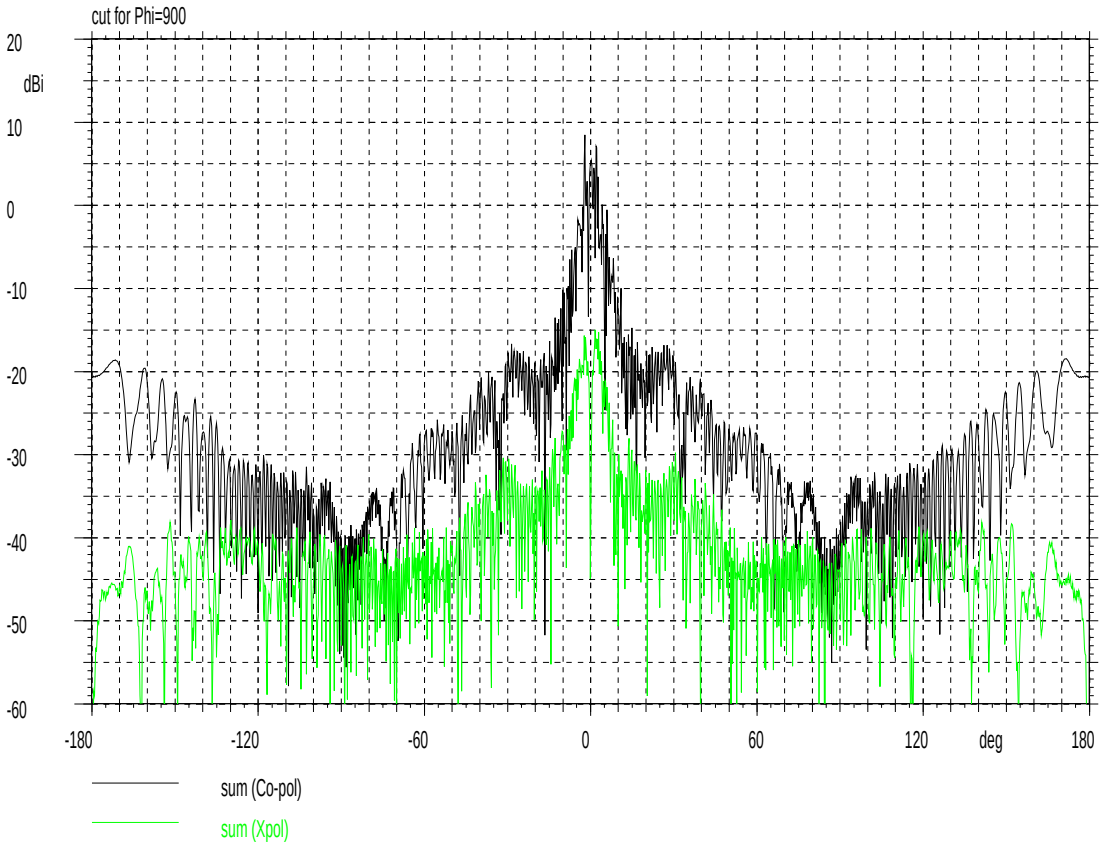

Figure 5-6 : far out side lobe prediction in the plane perpendicular to the plane of symmetry (φ=+/-90°)

6. 30 GHZ RFDM MEASUREMENT

This section introduces some measurements performed at 30 GHz. These measurements will be compared in future section (section 9) with predictions. All measurements plots are available in the reference document [RD 4].

6.1 Main lobe measurement

6.1.1 Main lobe measured with the MI Technology set up (vectorial network analyser) (telescope without baffle)

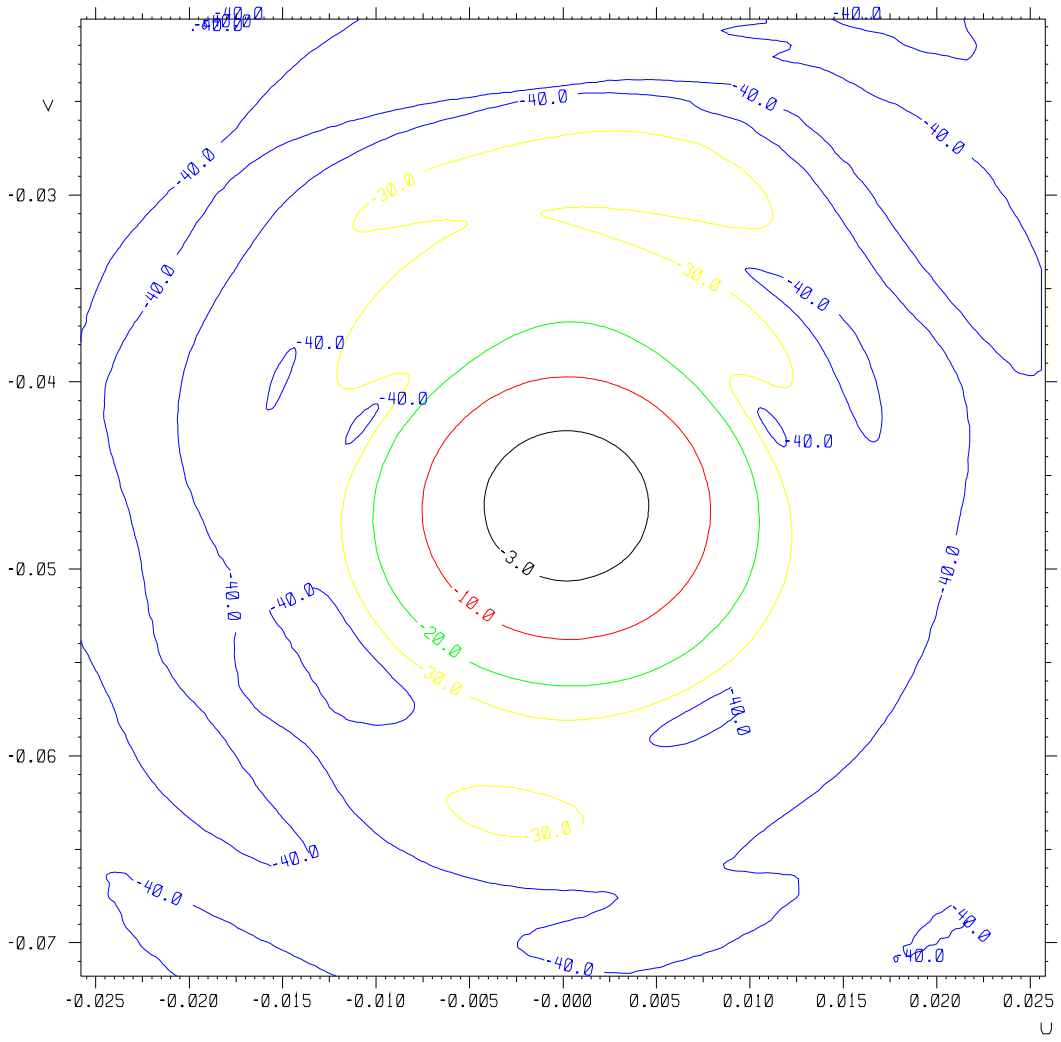

Figure 6-1 : Co pol MI Technology set up (vectorial network analyser), without baffle (-3 / -10 /-20 / –30 /-40 dB/max)

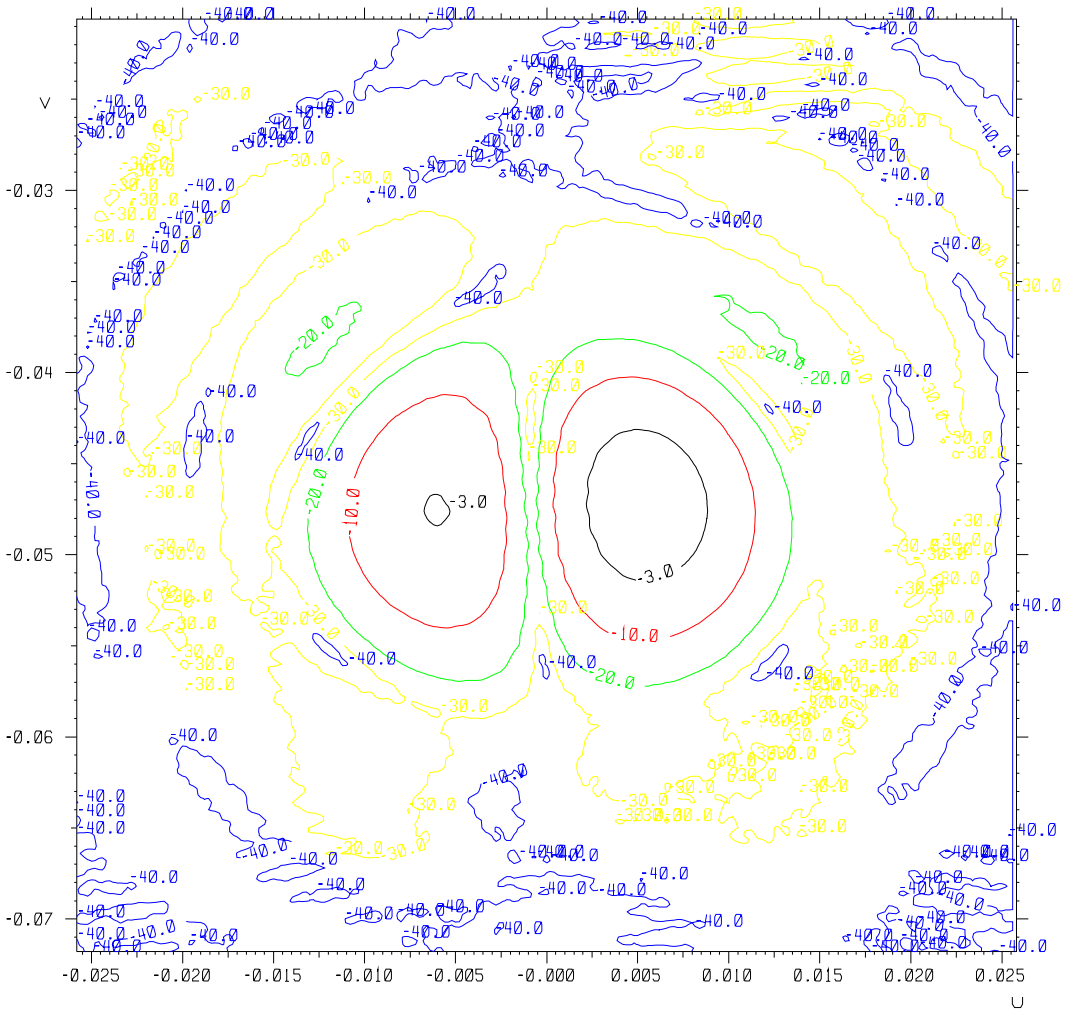

Figure 6-2 : X pol MI Technology set up (vectorial network analyser), without baffle (-3 / -10 /-20 / –30 /-40 dB/max)

6.1.2 Main lobe measured with spectrum analyser set up (telescope without baffle)

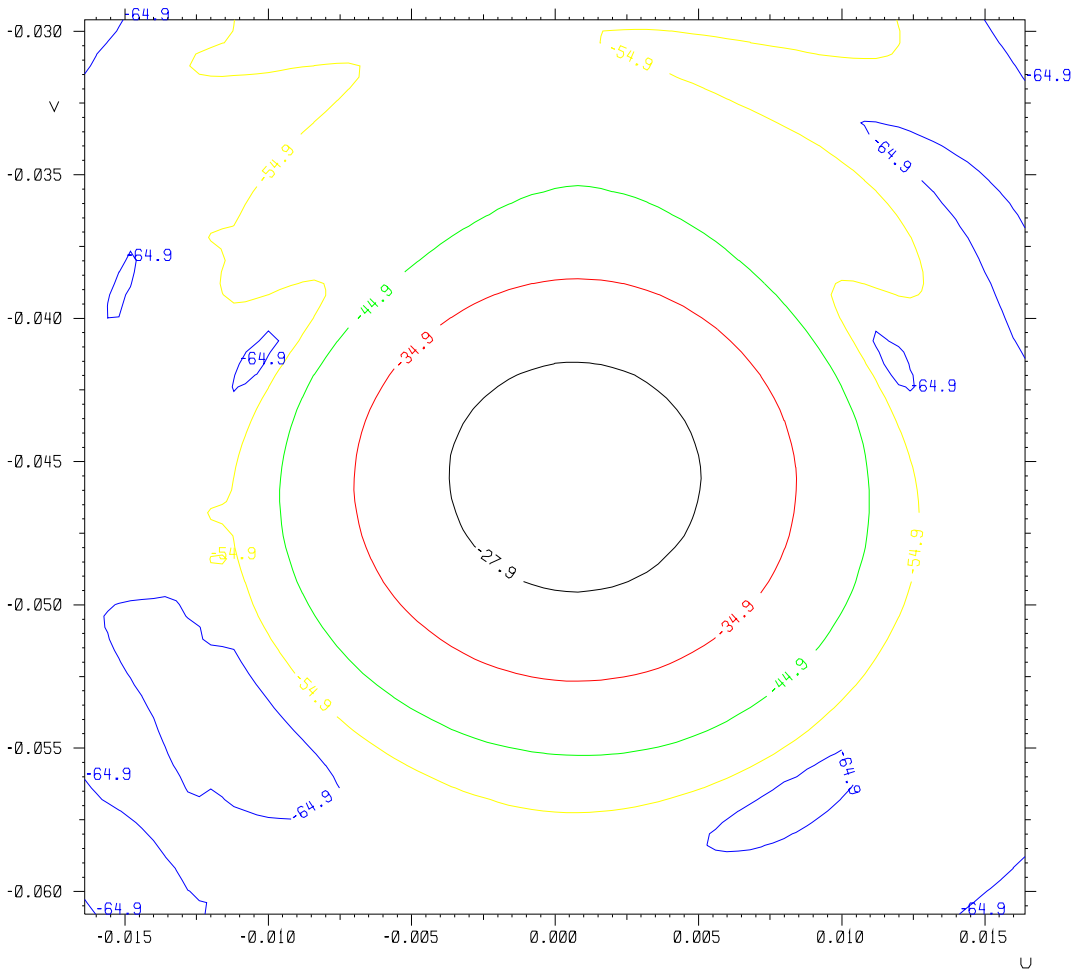

Figure 6-3 : Co pol measured with the Spectrum analyser set up , without baffle (-3 / -10 /-20 / –30 /-40 dB/max)

Plots displayed in absolute level –27.9 dB correspond to –3 dB/max etc…

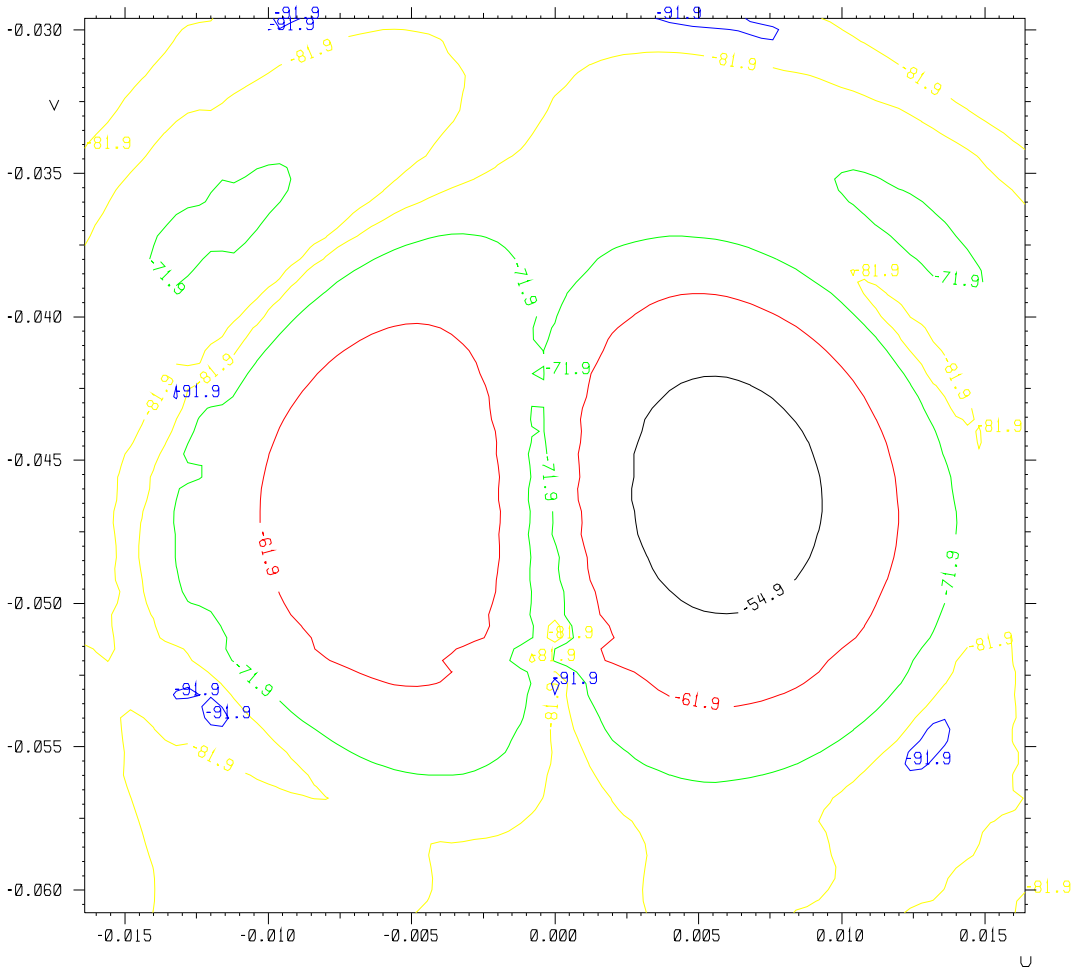

Figure 6-4 : X pol measured with the Spectrum analyser set up , without baffle (-3 / -10 /-20 / –30 /-40 dB/max)

6.1.3 Main lobe measured with the MI Technology set up (vectorial network analyser) (telescope with baffle)

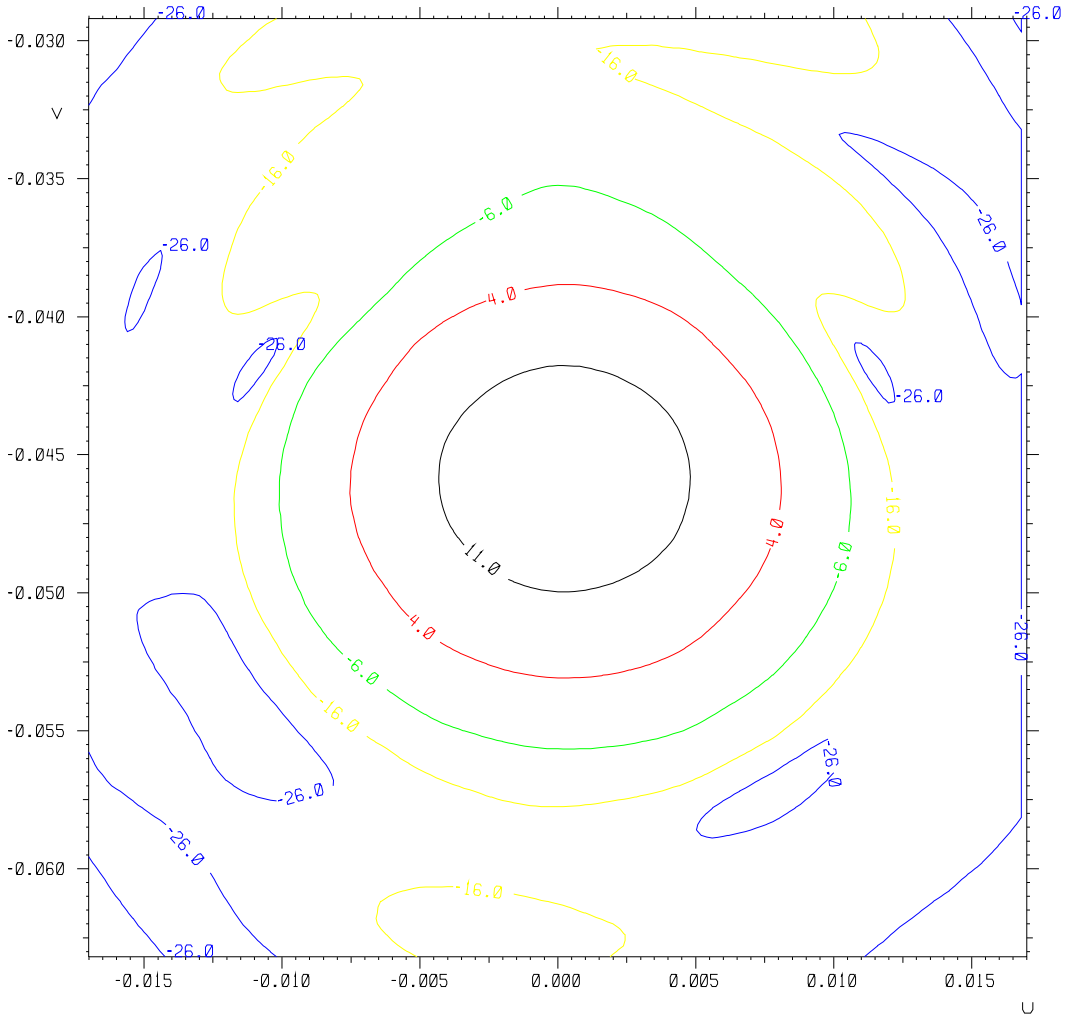

Figure 6-5 : Co pol MI Technology set up (vectorial network analyser), with baffle (-3 / -10 /-20 / –30 /-40 dB/max)

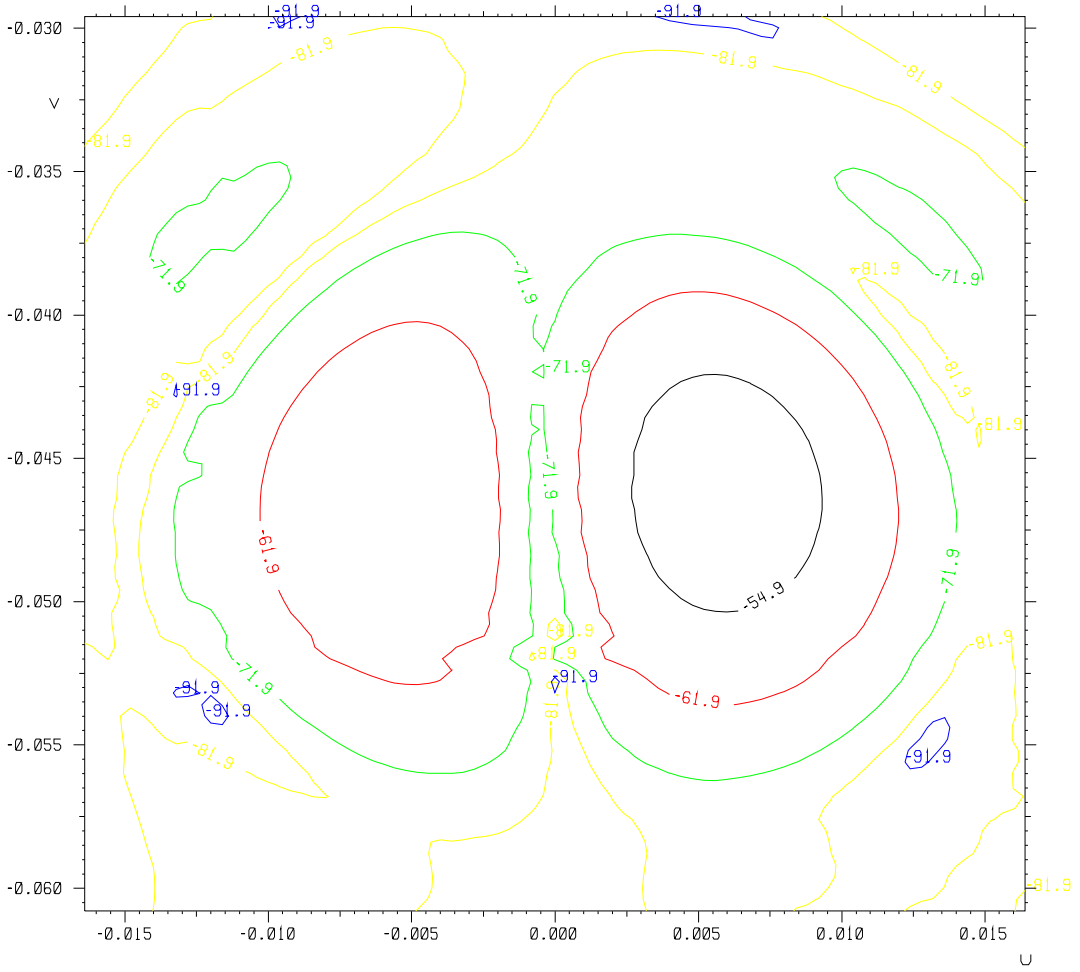

Figure 6-6 : X pol MI Technology set up (vectorial network analyser), with baffle (-3 / -10 /-20 / –30 /-40 dB/max)

6.2 Far out side lobe measurement

6.2.1 Far out side lobe measured with the MI Technology set up (vectorial network analyser) (telescope without baffle) cut for φ=0°.

The figure 6-7 displays the measured cut fot φ=0° using the MI Technology set up (vectorial network analyser). All other plots are displayed in the reference document [RD 4].

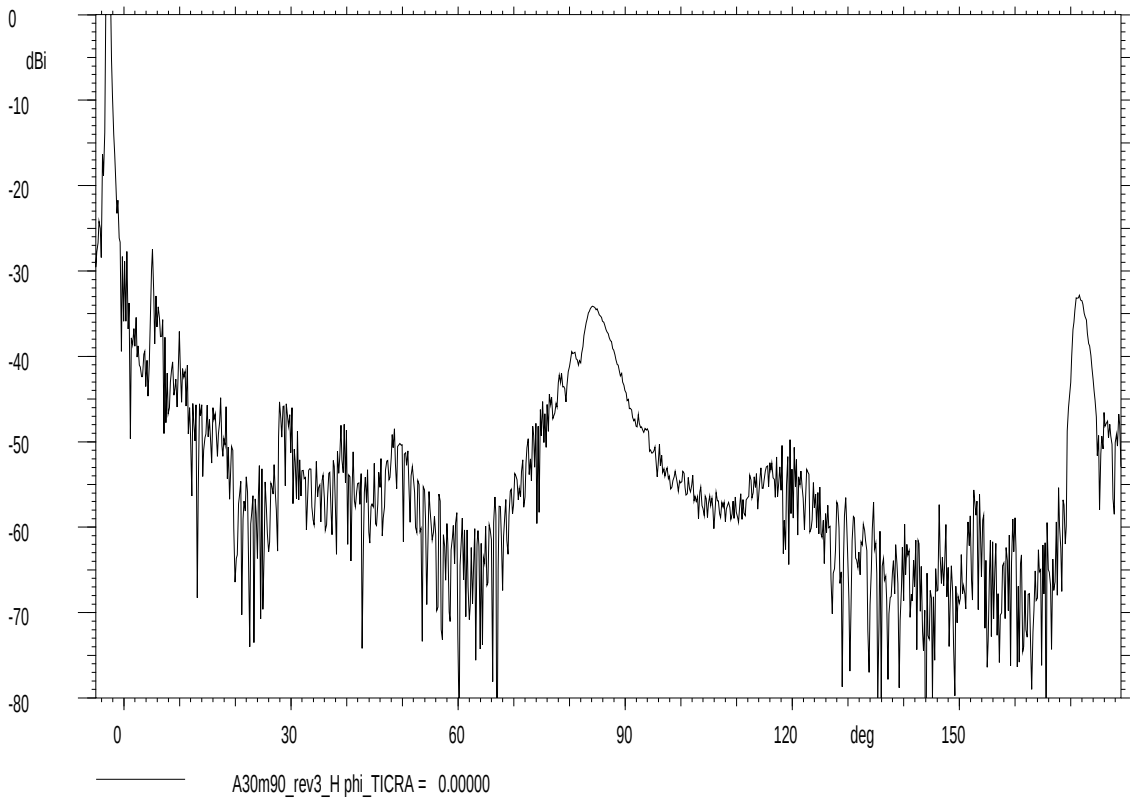

Figure 6-7 : MI Technology set up (vectorial network analyser)φ=0°, wo baffle

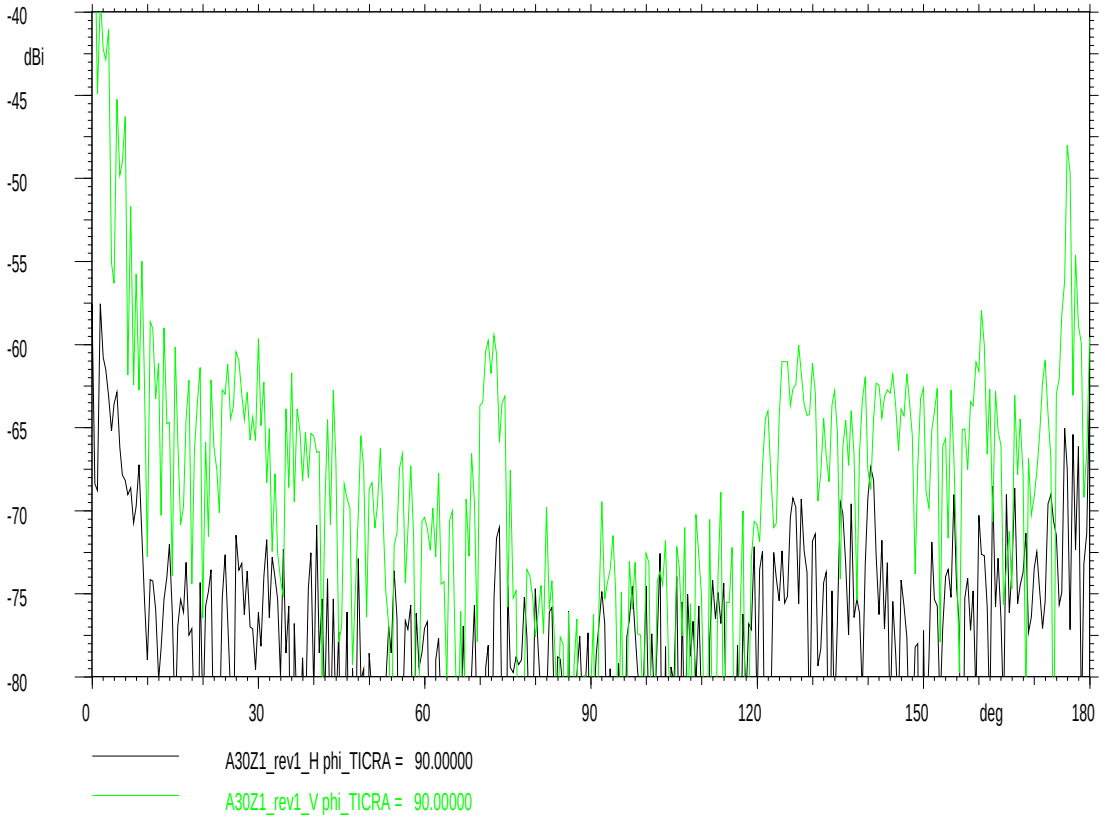

Figure 6-8 : MI Technology set up (vectorial network analyser) φ=90°, wo baffle.

6.2.2 Far out side lobe measured with spectrum analyser set up (telescope without baffle) cut for φ=0°.

The figure 6-9 displays the measured cut fot φ=0° using the spectrum analyser set up. All other plots are displayed in the reference document [RD 4].

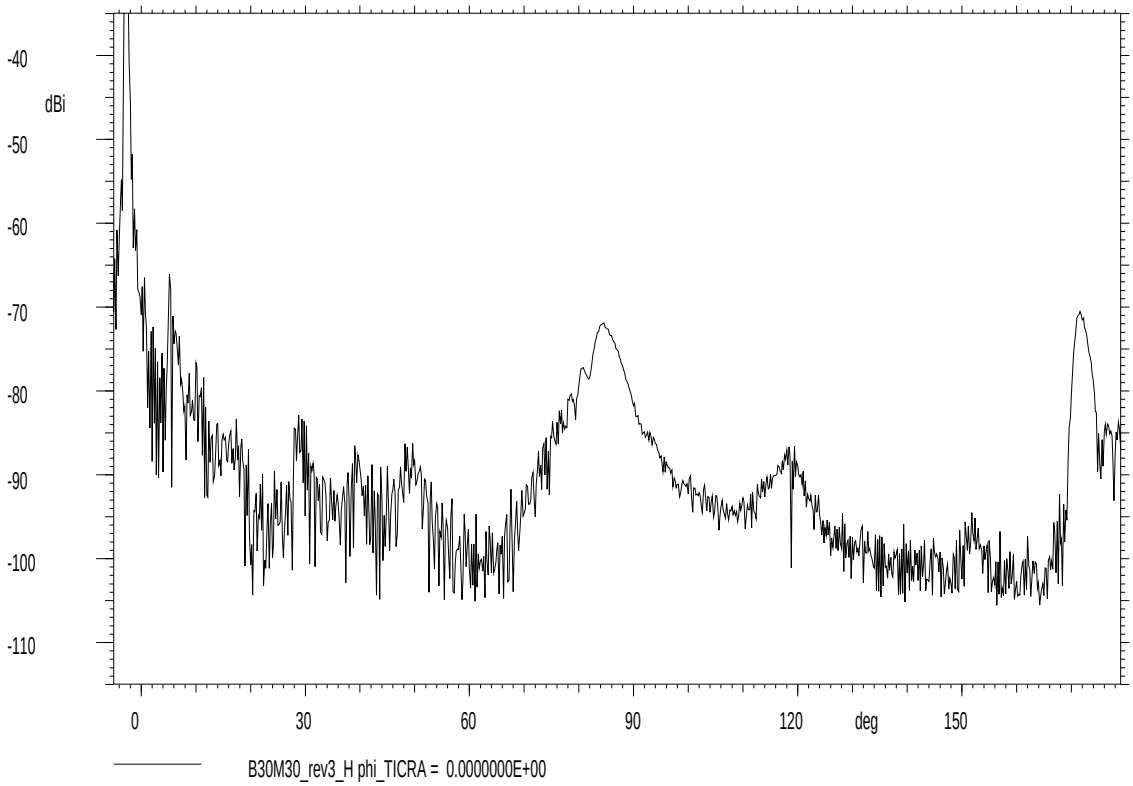

Figure 6-9 : measurement with the Spectrum analyser set up φ=0°, wo baffle

6.2.3 Comparison of both measurement (MI Technology set up (vectorial network analyser)& Spectrum analyser set up) methods

All data from this section are extracted from reference document [RD4]. The document [RD4] and the present one are fully complementary.

The figure 6-10 displays the measured cuts fot $\varphi = 0°$ using the two available set ups. The aim of this comparison is to cross-validate the two different measurement set-ups. At 100 GHz and higher frequencies the only available set up is the spectrum analyser one. Those two curves have been superimposed and show a nice correlation between the two diagrams . The MI Technology set up (vectorial network analyser) is more noisy at 70 dB below the maximum (spill over lobe max at –48dB/ max_co_pol). This is visible close to $\theta = 20°$, $\theta = 60°$ and over $\theta = 120°$. The spectrum analyser with the set up detailed in [RD4] has not been optimized to provide the best dynamic as this was not useful for correlation purposes. This operation has been performed at 100 GHz only.

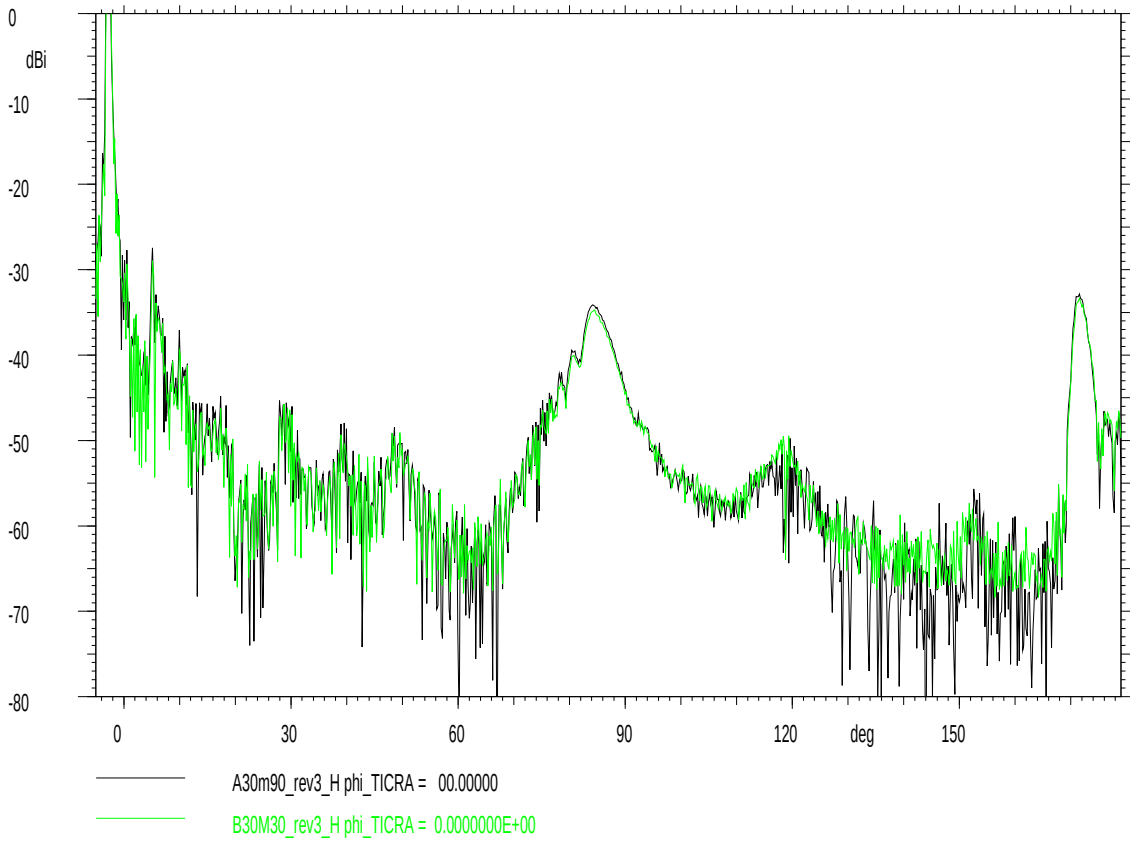

Figure 6-10 : Vectorial Network Analyser & Spectrum analyser measurements comparison in plane $\varphi = 0°$.

The test procedure (detailed in RD4) is mainly composed of one and only one alignement wrt the angle of arrival of the CATR. The first acquistion (main lobe acquisition) is performed in an aligned and known configuration. For the cut acquisition, it is necessary to rotate the RFDM around the revolution axis of the Cassini ring interface. This is performed by releasing the brake along the circular track (see fig 6-11), the RFDM has then some gap or degree of freedom , in other word the alignement wrt the CATR angle of arrival is slightly degraded. This is not critical for the result analyses because the telescope itself remains aligned, the plots results have just to be translated to be overlapped. Then after rotation, the RFDM is turned and locked. The device under test has no more gap, but remains mis-aligned in the CATR. At this stage to save time in the CATR no re-alignements have been performed. A re-alignement is technically feasible (same as the initial one) but requires some time which is not often really compatible with an industrial planning of a Compact antenna test range.

Figure 6-11 : RFDM under test configuration in CATR.

The figure 6-12 (respectively 6-13) displays the near-in side lobe cut using the MI Technology set up (vectorial network analyser) (respectively the spectrum analyser set up). This cut is passing close to the vertical line defined by u=0 in figure 6-1 (respectively 6-3). The cuts are not passing through the line (u=0) because the cassini ring has been released. Hence the direct and accurate comparison of the different main lobe cuts should not be performed. Nevertheless it is possible ot observe that the curves have globally the same shape. This means that the induced depointing by the cassini ring release is small.

The comparison of the two X pol curves in figure 6-14 shows that the spectrum analyser measurement is reaching a noise level at 70 dB below the maximum. In fact this limited dynamic comes from the spetrum

analyser parameters set up. These parameters are provided in [RD4]. The aim of this measurement was not to optimize the dynamic but to show the cross validation with the standard technologie (MI one).

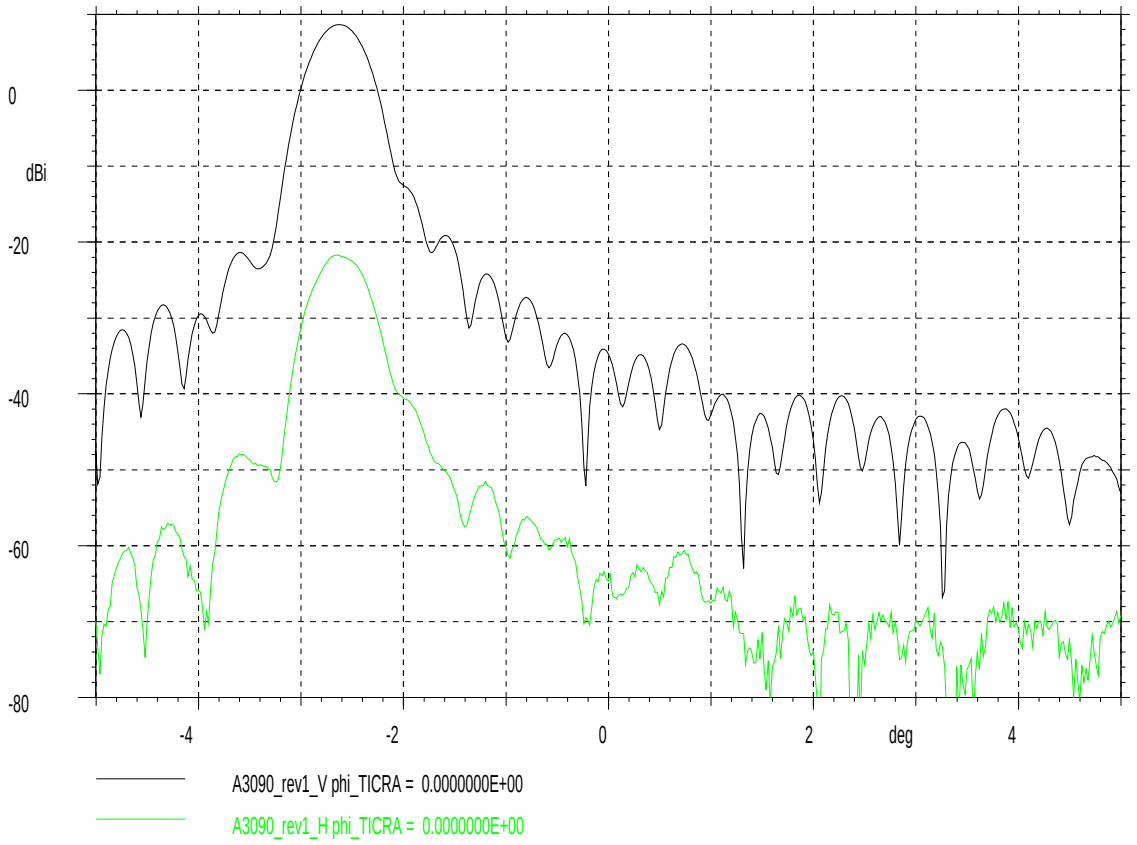

Figure 6-12 : MI Technology set up (vectorial network analyser) measurement in Co& Cross polarization in plane φ=0°.

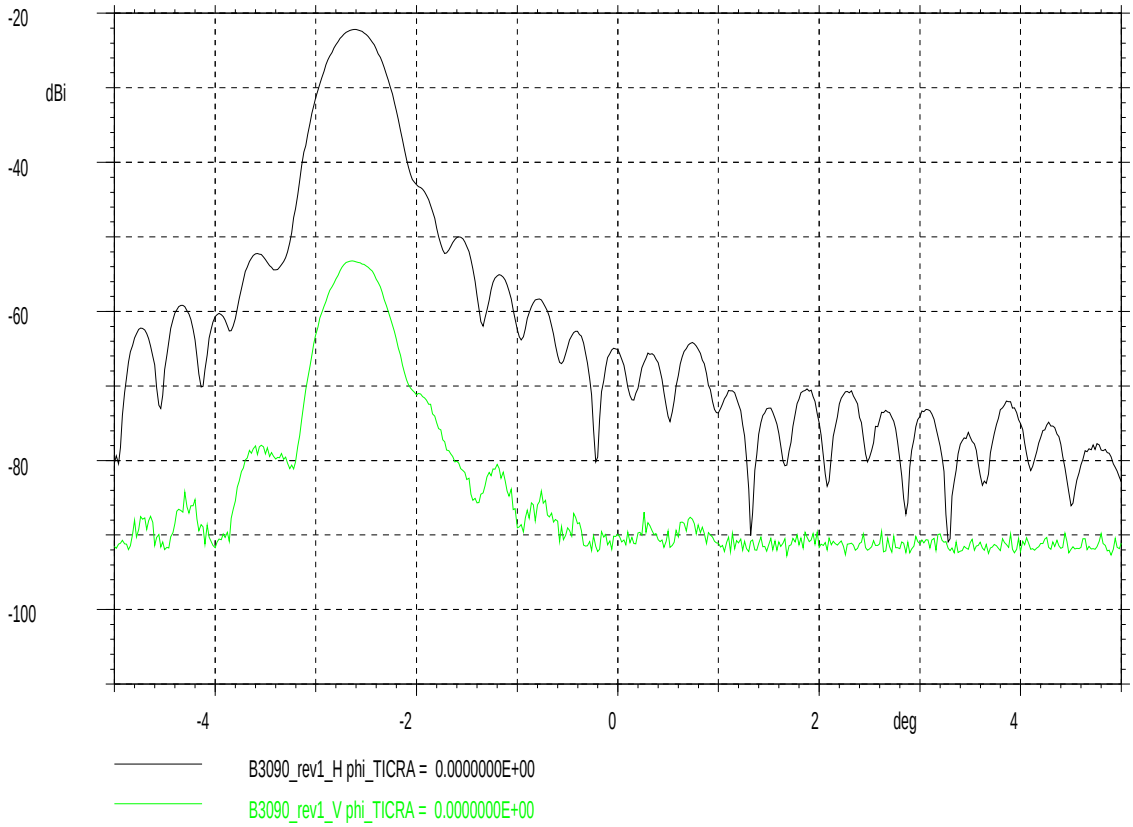

Figure 6-13 : spectrum analyser measurement in plane φ=0°.

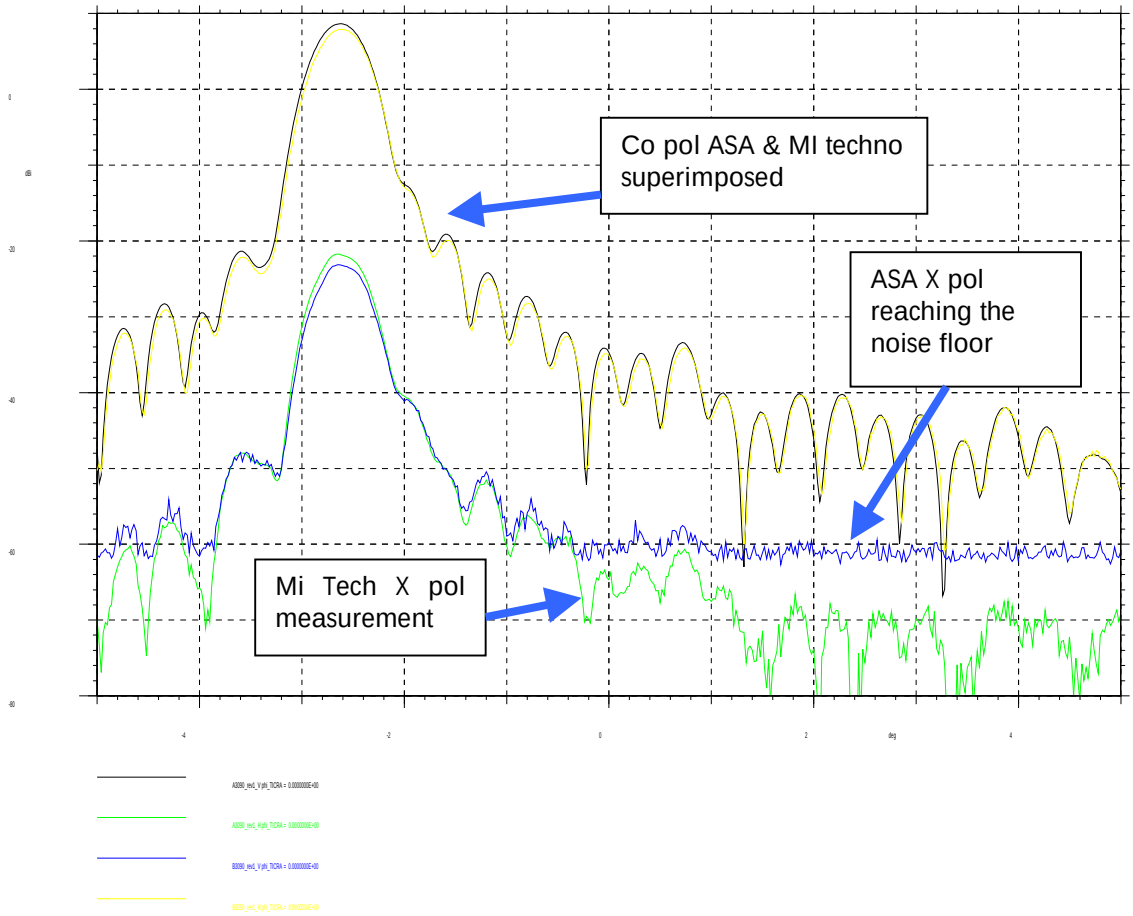

Figure 6-14 : superimposition of the two measurement techniques.

7. LOSS BUDGET EVALUATION AT 30 GHZ

7.1 Integration of the measured main lobe

The main lobe displayed in section 6.1 have been integrated in order to obtain the integrated directivity. The 3 results are within less than 0.14 dB difference.

		Window size					
	Directivity max(dBi)	Azimuth min (°)	Azimuth max (°)	Azimuth range (°)	Elevation min (°)	Elevation max (°)	Elevation range (°)
MIT, without baffle	52.21	-1.5	1.5	3	1.15	4.15	3
Spectrum analyser, without baffle	52.22	-1	1	2	1.65	3.65	2
MIT with baffle	52.08	-1	1	2	1.65	3.65	2

table 7-1 : integrated directivity and associated window.

The integrated directivity takes into account the ohmic losses but not the spill over. The computed (grasp8) directivity includes the spill over but not the ohmic loss. The table 7-1 displays the loss budget in distinguishing the prediction and the measurement. Then this loss budget is applied to the directivity obtained through a grasp8 computation or by integration of the measurements (see table 7-3).

On final the gain difference is less than 0.13 dB.

	Prediction	Measurement
Feed VSWR	1.061	1.125
Insertion loss (dB)	-0.004	-0.015
Ohmic loss (dB)	-0.05	NA
Spill over (dB)		-0.024
Loss (dB)	-0.054	-0.039

table 7-2: loss budget.

	Prediction	Measurement A	Measurement B	Measurement C
Directivity (dBi)	52.11	52.21	52.22	52.08
Loss	-0.05	-0.04	-0.04	-0.04
Gain (dBi)	52.06	52.18	52.18	52.04
Difference with prediction (dB)	0.00	0.12	0.13	-0.02

table 7-3 : comparison of the gain obtained through measurement or prediction .

8. 30 GHZ FLIP TEST ANALYSIS

The flip test consists in measuring one cut of +/-90 ° range excursion from left to right in the horizontal plane. This cut corresponds to the cuts for $\varphi = -/+90°$ and θ varying from -90° to 90°. The telescope being in the nominal position (plane of symmetry vertical , primary reflector on top) and then in the flipped direction : plane of symmetry vertical and primary reflector upside down (see fig 8-1)

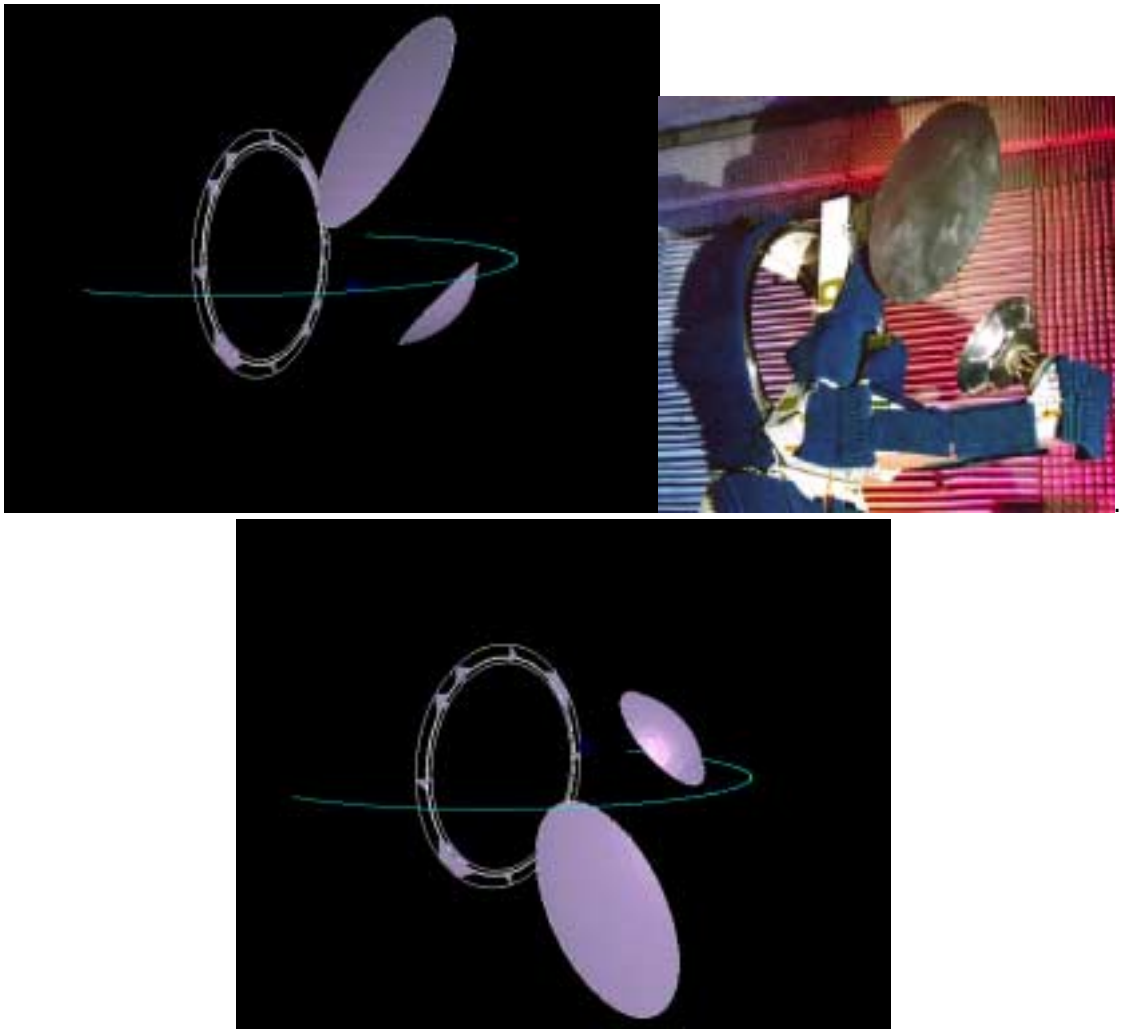

Figure 8-1 : flip test configuration

When the telescope has the primary toward the ceiling, its center is located at 5.25m from the ground. When the telescope is flipped, its center is located at 6- 1.5 = 45 m.

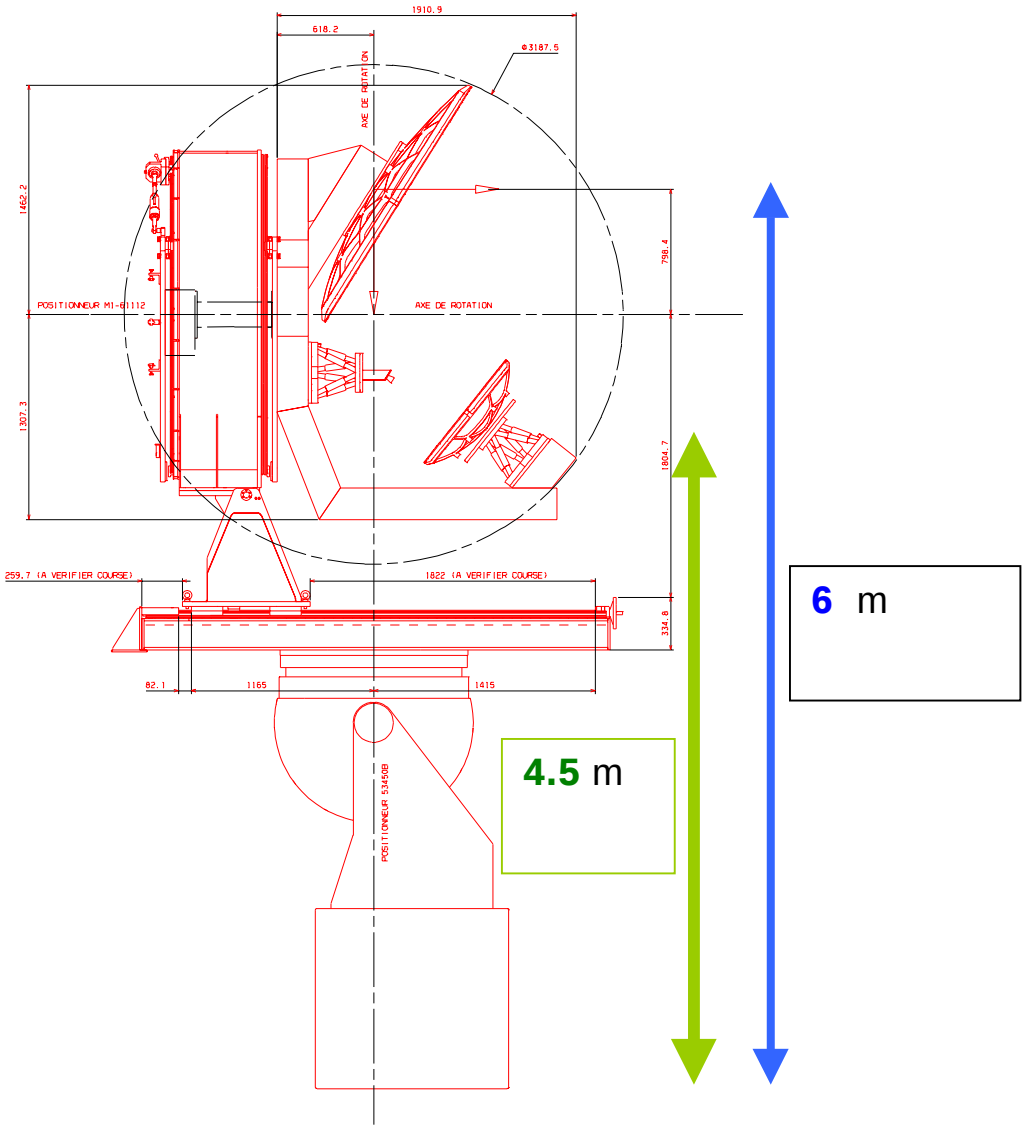

Figure 8-2 : telescope on the positioner with the two chief rays height wrt the ground floor, corresponding to the initial position, and the upside down one.

During the flip test, the telescope configuration is such that the plane of symmetry remains vertical. When the telescope is rotated in azimuth only by 35°, the plane of symmetry of the telescope is passing through the CATR illuminator (see fig 8-3). In other word, the telescope is globally pointing toward the feed room and thus create a fake signal called the direct view. The telescope is pointed twice toward the feed room, the first time in the intial configuration and the second time in the upside down configuration. In order to assess the level difference between the two configurations for the fake lobe, it is neccessary to know the diagram in the plane of symmetry. This measured pattern is displayed in figure 8.4.

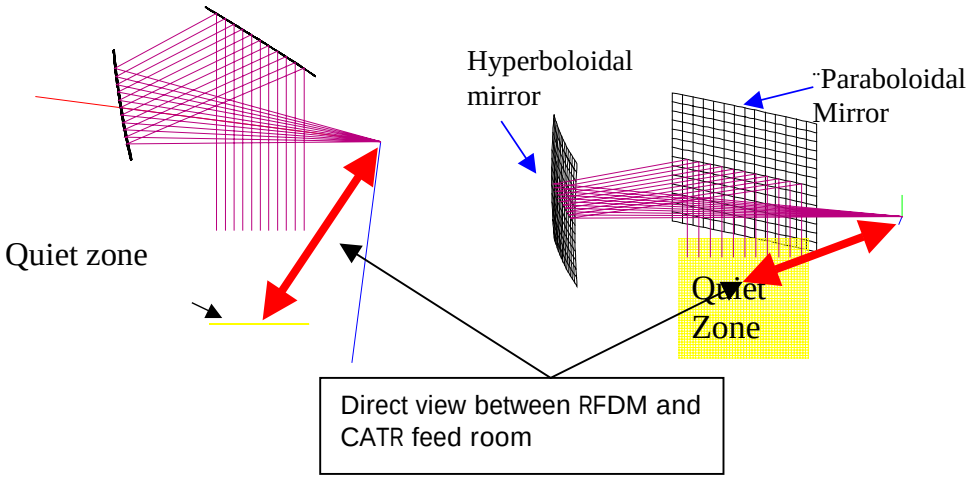

Figure 8-3 : direct view in the CATR

The two main lobe cuts are not perfectely overlapping due to the cassini ring interface release for the flip operation. The cut is performed in the primary reflector coordinate system M1 (see mathematical model RD 5). The maximum of the main beam is pointing at $\theta = -2.65°$ in the plane of symmetry. Hence the measured level at $\theta = 0$ is nothing else than the trail of the main lobe at 46 dB/max.

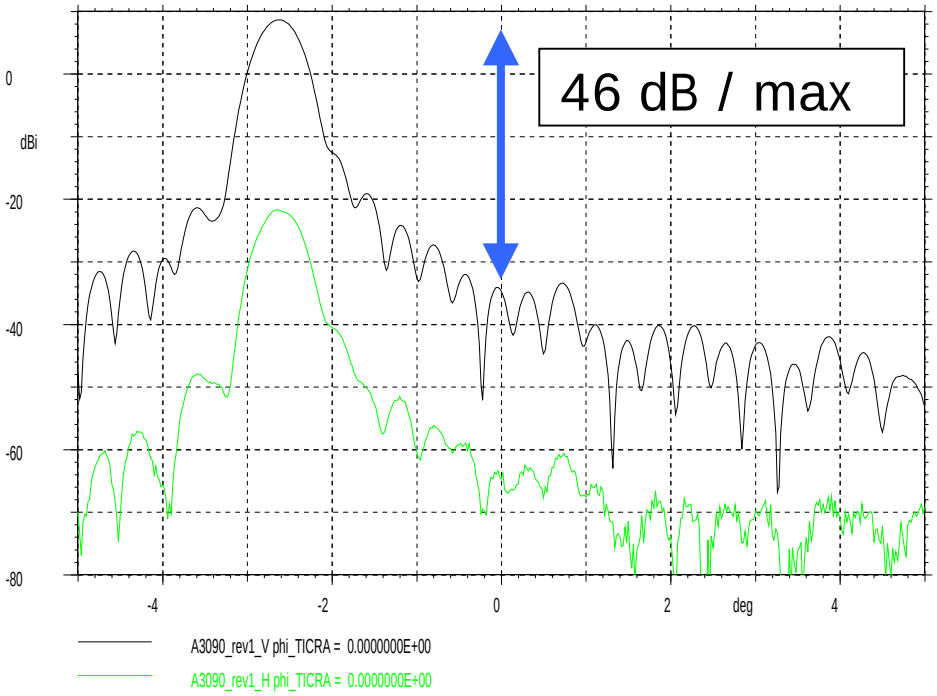

Figure 8-4 : measured pattern in the plane of symmetry.

Nevertheless all other directions of the diagram have the general same behaviour. A special attention shall be paid for the lobe at 35°. This corresponds to the direct illumination of the feed room by the telescope main lobe. In that case the spurious signal form the telescope is greater than the level of be measured signal. As far as the telescope axis is moved down by 1.5 m and the feed room located at 13 m, then the corresponding angle variation is of order of 6.5°. As the gain variation is rapid versus θ a deviation of 20 dB is measured.

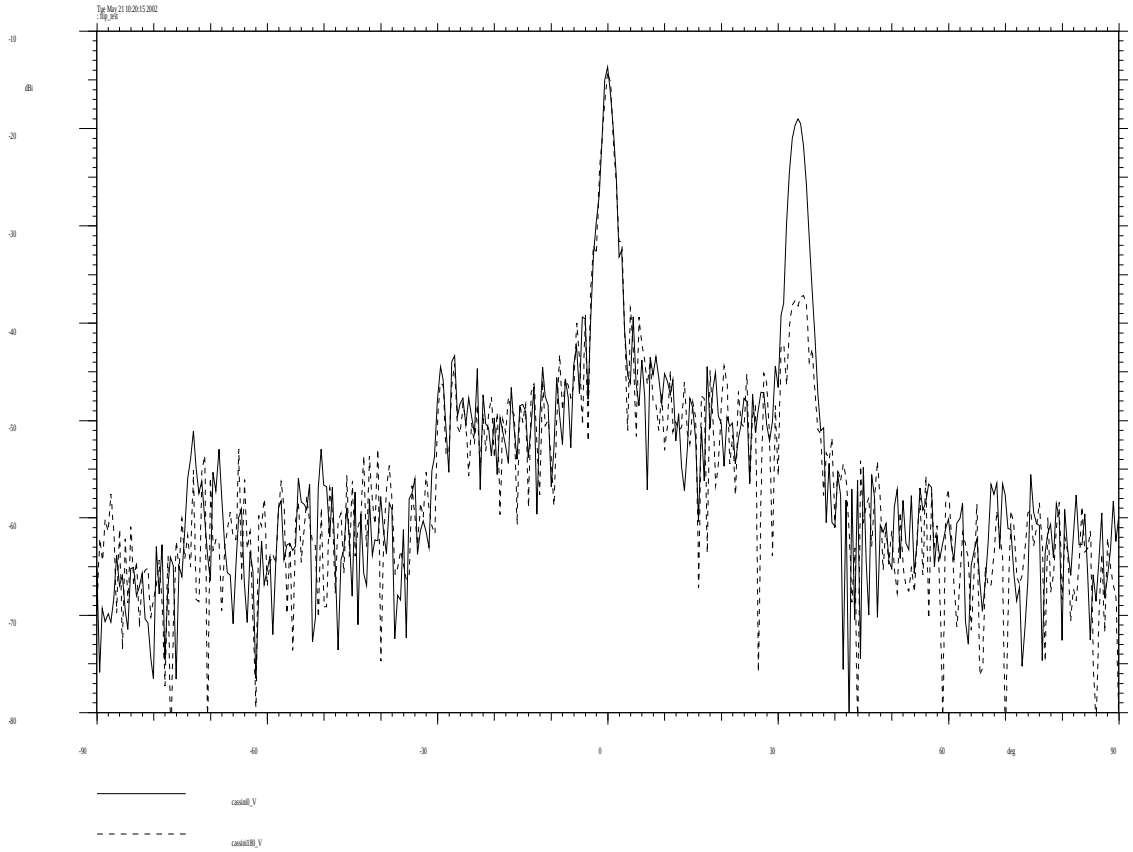

Figure 8-5 : flip test radiation pattern: superimposition of the two acquistions.

9. 30 GHZ MEASUREMENT AND PREDICTION COMPARISON

9.1 Main lobe co polarisation comparison.

The main lobe computed using grasp8 (see section 5.2 for the details) is compared to the measured one (see section 6.1.1).

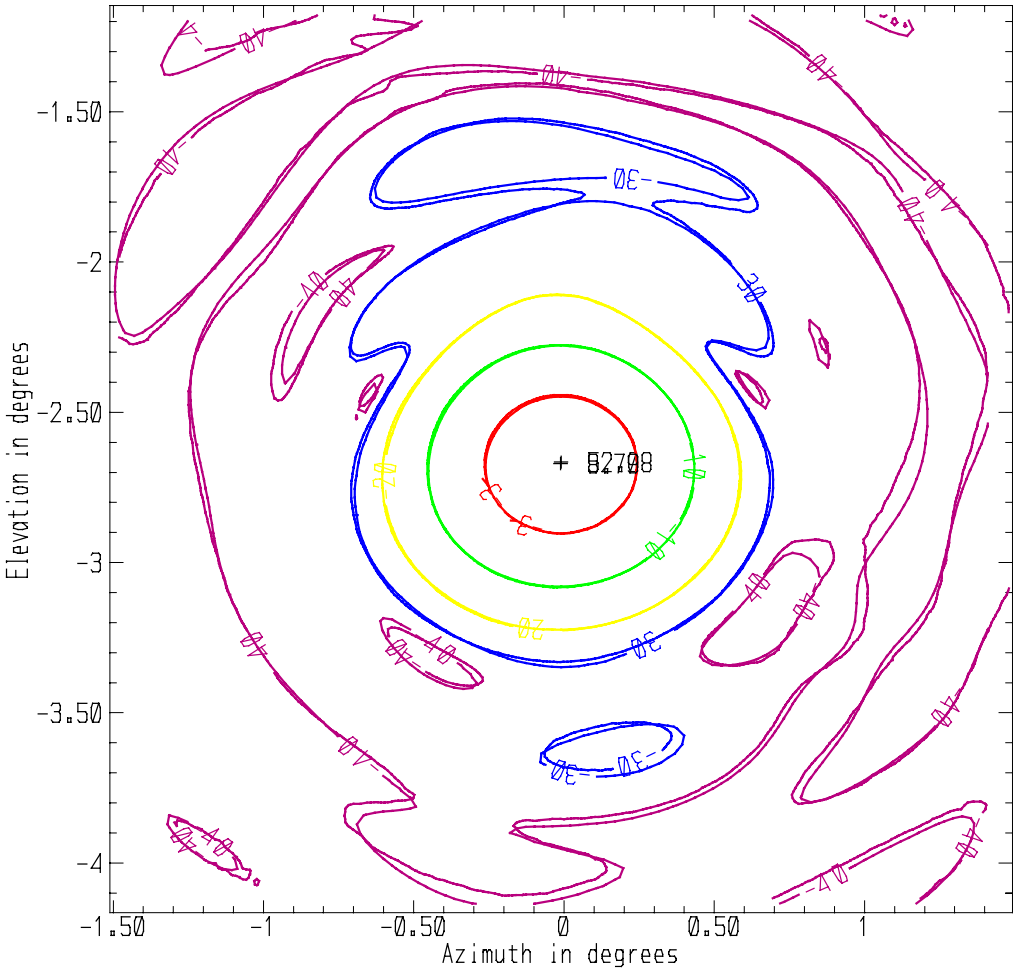

Figure 9-1 : prediction & measurement comparison at 30 GHz, -3 –10 –20 –30 –40 dB/max.

As a conclusion, a nice correlation is obtained. Moreover an even better correlation should be obtained by using the videogrammetry data of the secondary reflector (see section 3.3) .

9.2 Main lobe cross polarization comparison.

The main lobe measured cross polarization (introduced in section 6) is compared to the prediction (introduced in section 5). The comparison is displayed in figure 9.-2 The general shape of the pattern is globally the correct shape, nevertheless by looking careffuly it is possible to observe that :

-the predicted x pol is composed of two quasi symmetrical lobes with the same amplitude.

-the measured x pol is composed of two lobes with a difference of 2 dB.

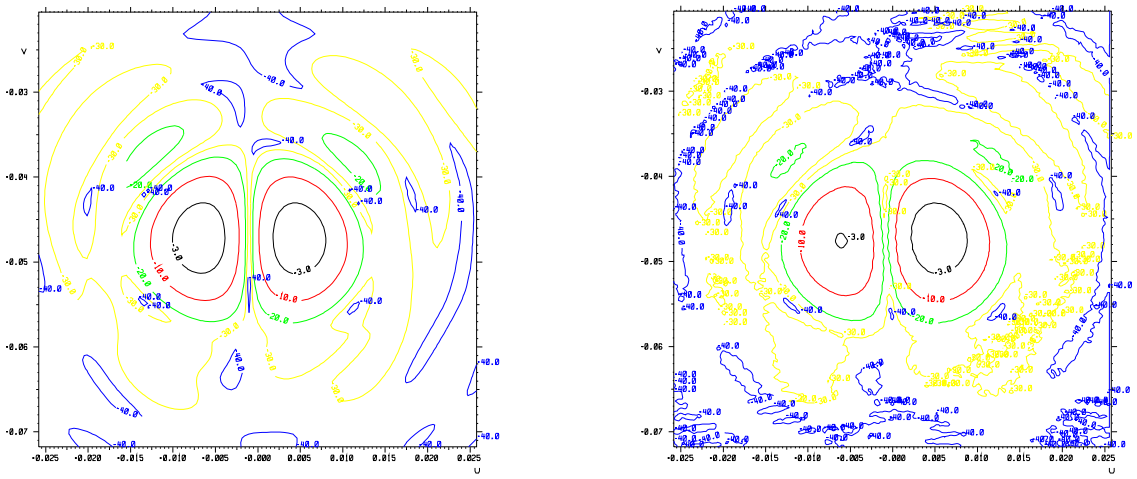

Figure 9-2 : Cross polarization comparison : prediction (left)& measurement (right).

The somewhat poor correlation on the x pol is due to the primary feed radiation pattern. There's a difference between the primary feed radiation pattern used in the numerical model and the actual one measured in France Telecom R&D facility la Turbie. This has been shown in section 4 . The actual feed xpol is globally the image of the copolarisation attenuated by 30 dB. Hence the primary xpol level is too high when compared to the predicted one.

The measured telescope xpol is the sum of the telescope intrinsic/geometrical depolarization and of the image of the lobe of xpol of the feed.

The geometrical depolarization is generated by the geometry itself, the telescope is compliant with the Dragone Mitzugushi condition, but this is true for a feed located at the prime focus. In the measured case, the feed has been displaced away from the primary focus. So, the Dragone Mitzugushi is altered and the geometry induces xpol.

The primary feed has a lobe of xpol corresponding roughly in shape to the image of the co-pol. This xpol lobe is producing a lobe in the telescope far field. This last lobe is added to the geometrical xpol lobe.

That's the reason why there's not a good correlation between the measurement and the prediction for the xpol in the main lobe.

The measured data from France Telecom R&D have been delivered, the final analysis to conclude is to convert the measured data into a grasp8 compatible format and perform the modelisation. This analysis has not yet been performed.

9.3 far out side lobe comparison

The far out side lobe computed using grasp8 (see section 5.3 for the detail) is compared to the measured one (see section 6.2.1). This sections analyses the differences.

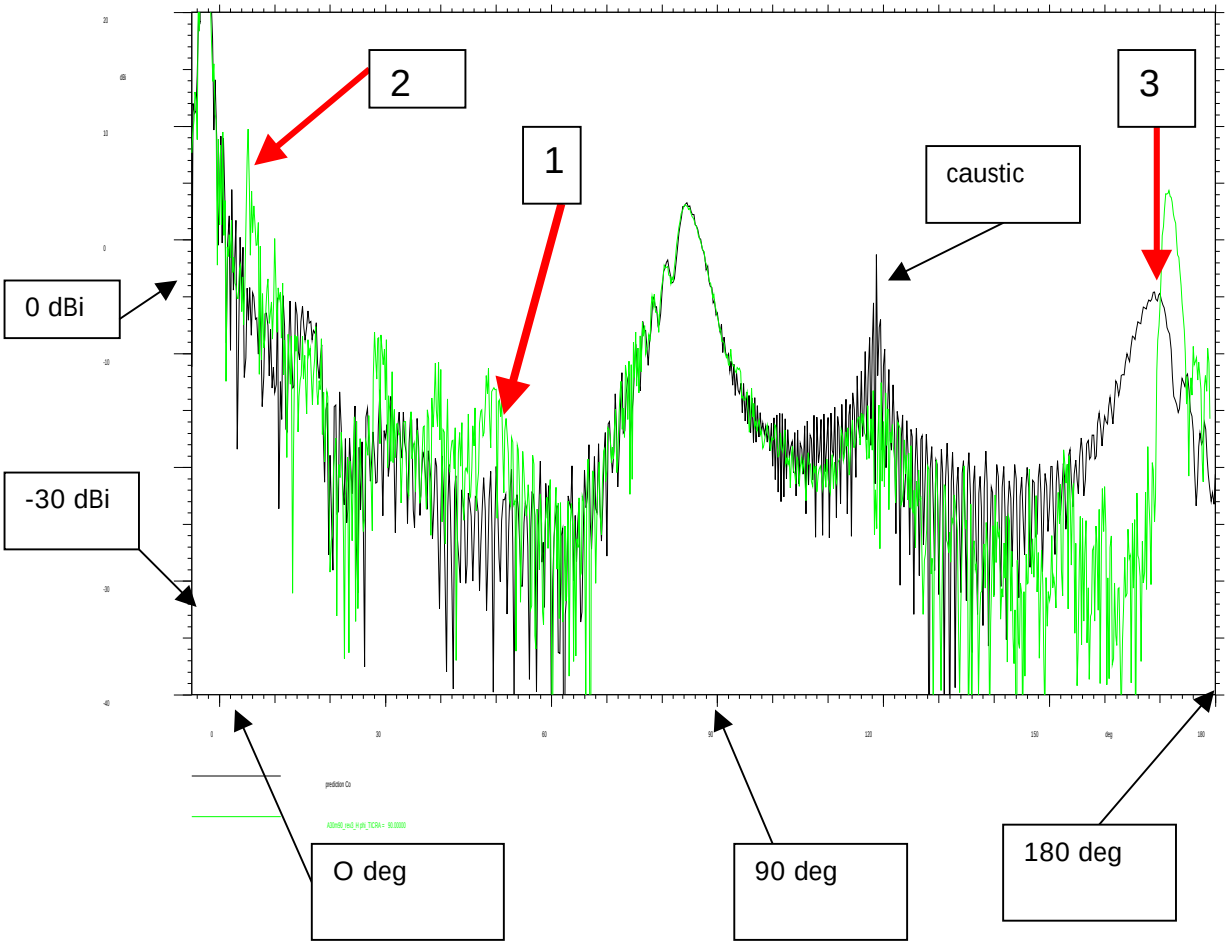

Figure 9-3 : superimposition of the predicition and measurement for the far out side lobe.

The differences in the correlation can be explained by looking the RFDM configuration in the CATR. The CATR is implemented in grasp8. The geometry is displayed in figure 9-4. This geometry displays only the effective surface of the CATR reflector, the serrations and the bill board are not displayed on this figure. The RFDM telescope has also been implemented in the CATR at its location under test. Then rays are traced from the feed in the focal plane of the RFDM.

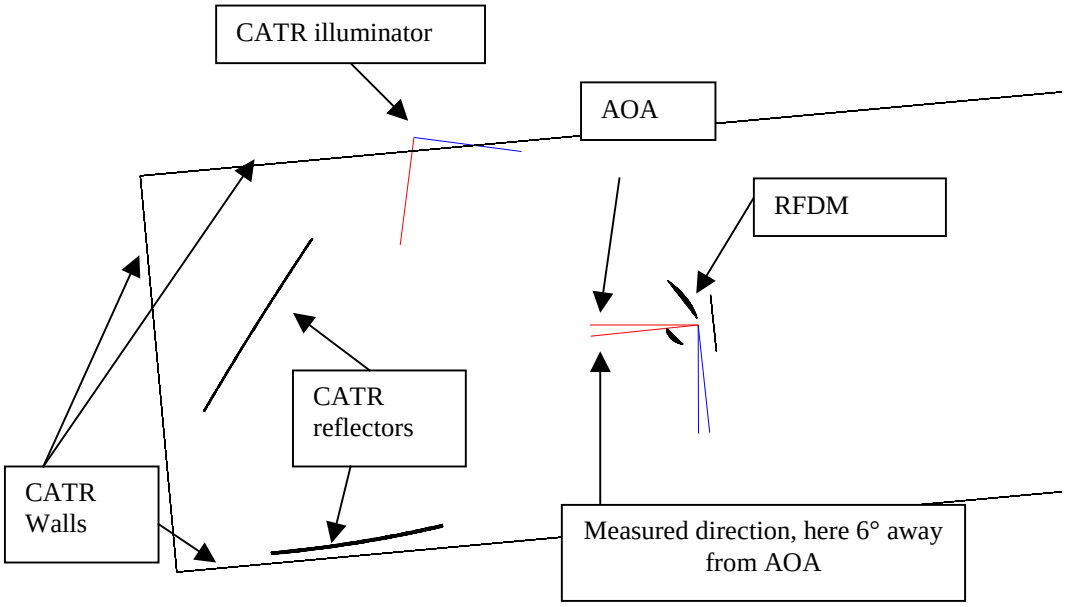

Figure 9-4 : CATR model implemented in grasp8 including the RFDM.

The Lobe area with the flag 1 (θ ranging from 30° up to 50°) displayed in figure 9-3 corresponds to the case where the RFDM is in a such posution that the spill over past the primary reflector is direclty illuminating the feed room. This is highlighted by the ray tracing displayed in figures 9-5 to 9-7.

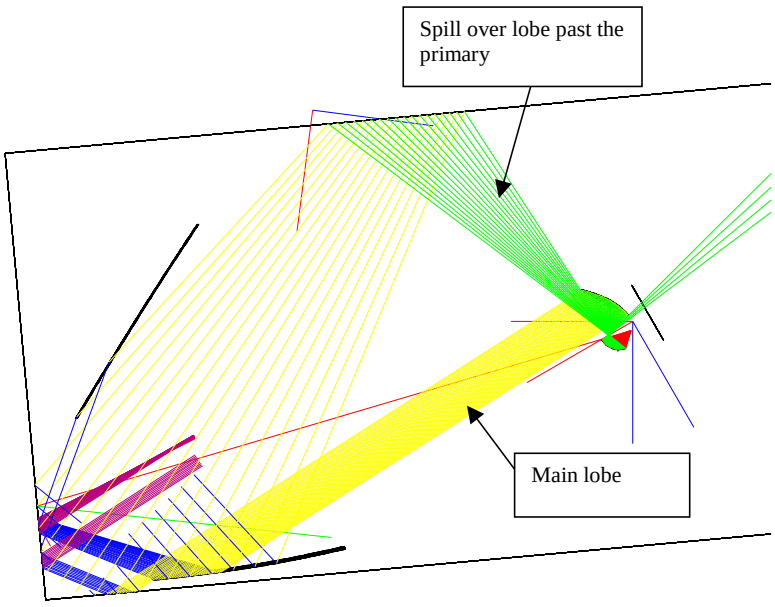

Figure 9-5 : ray tracing of the RFDM under test configuration for the cut φ=0°, pointing in θ=30°

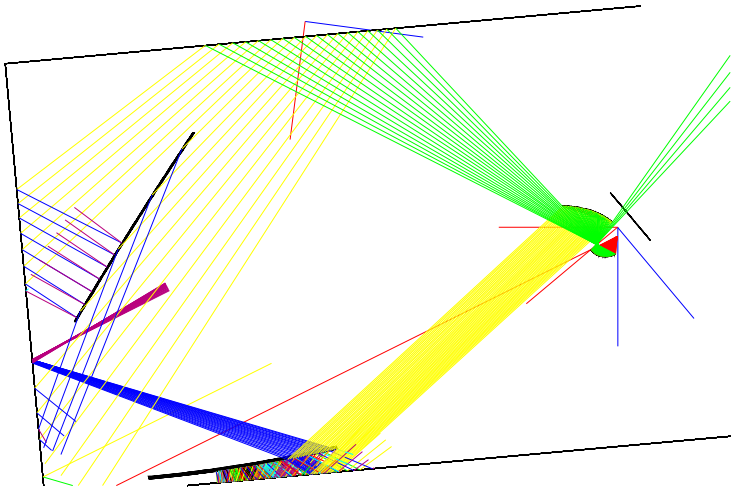

Figure 9-6 : ray tracing of the RFDM under test configuration for the cut φ=0°, pointing in θ=40°

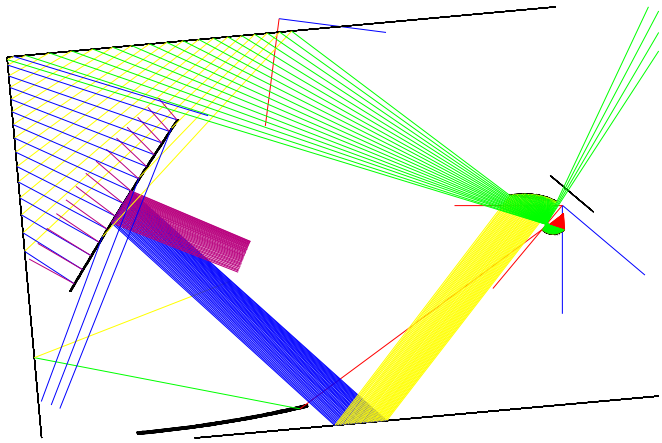

Figure 9-7 : ray tracing of the RFDM under test configuration for the cut φ=0°, pointing in θ=50°

The difference associated to flag 2 corresponds to a triple reflection. First on the CATR reflectors and then on the billboard. The ray combination is as follows (let's assume the RFDM is a transmit antenna) :

-reflection number 1 on the CATR primary reflector (incident yellow beam, reflected in blue)
-reflection number 2 on the CATR secodary relfector (incident blue beam reflected in purple)
-reflection number 3 on the CATR bill board wall (TBD dB attenuation) (incident purple beam, reflected in clear blue)

The final reflection is send close to the CATR illuminator. In fact the bill board is metallic and then covered by flat anechoids. This is displayed in figure 9-9. The shape of the billboard is considered in the model as being the primary CATR reflector extension, in fact the bill board has an other shape so the rays are not reflected exactly as in the ray tracing. In addition the flat anechoid for low incidence rays (80° from the normal) might have a non negligible reflection coefficient. Hence part of the incident energy might be reflected. The third source of ray deviation is the edge composed by the flat anechoid edge.

As a preliminary conclusion the billboard is suspected to deflect some energy toward the feed room due to its shape and flat anechoid coverage.

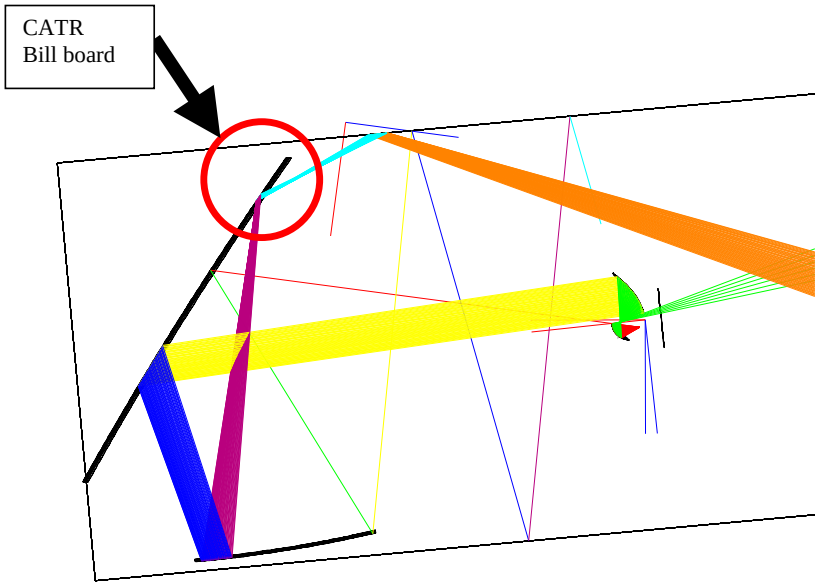

Figure 9-8: ray tracing of the RFDM under test configuration for the cut φ=0°, pointing in θ=6°

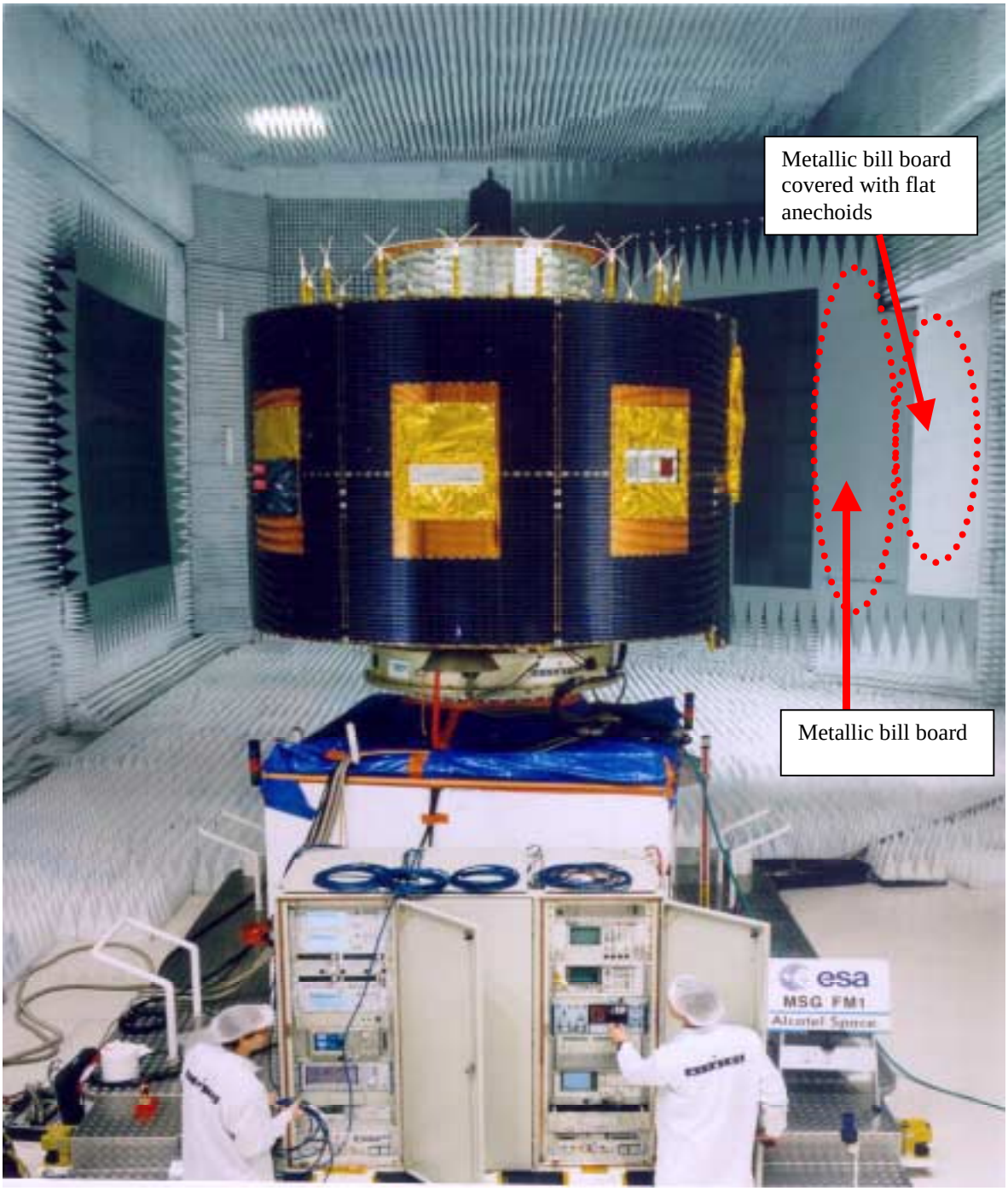

Figure 9-9 : picture of the CATR and the billboard.

The lobe near $\theta = 120°$ is a numerical caustic. Around this value, predictions are false.

The spill over lobe past the primary reflector is an annular lobe all around the primary. The lobe direction is obtained by ray tracing on the RFDM geometry. The ray tracing is presented in figure 9-10. The cut $\varphi = 0°$ corresponding to the plane of symmetry is cutting the spill over in two directions : around $\theta = 85°$ and around $\theta = 175°$. Those two lobes are visible on the figure 9-3. For the lobe at 175° a poor correlation is obtained. This is due to the supporting structure (see fig 9-10) which is not taken into account in the numerical model. This stucture acts as a ray blocking and thus modifies the expected lobe.

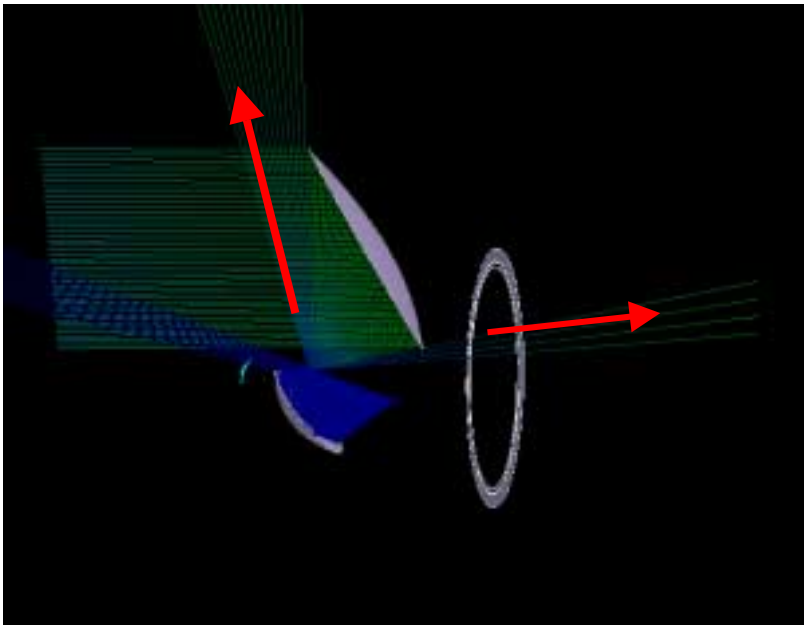

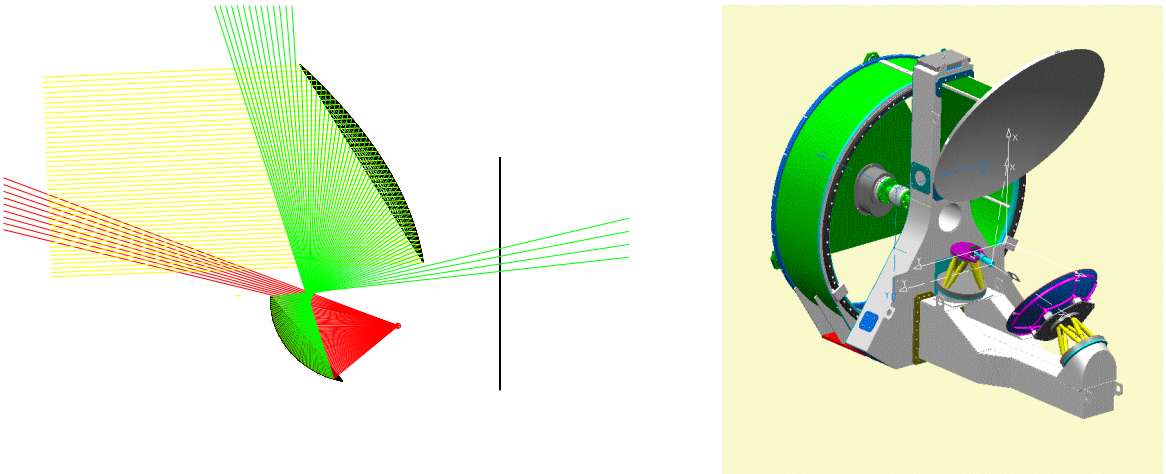

Figure 9-10 : test configuration implemented in grasp8. And test configuration in CATR.

The spill over lobe in direction $\theta = 85°$ (see fig 9-11) is nicely correlated with the prediction.

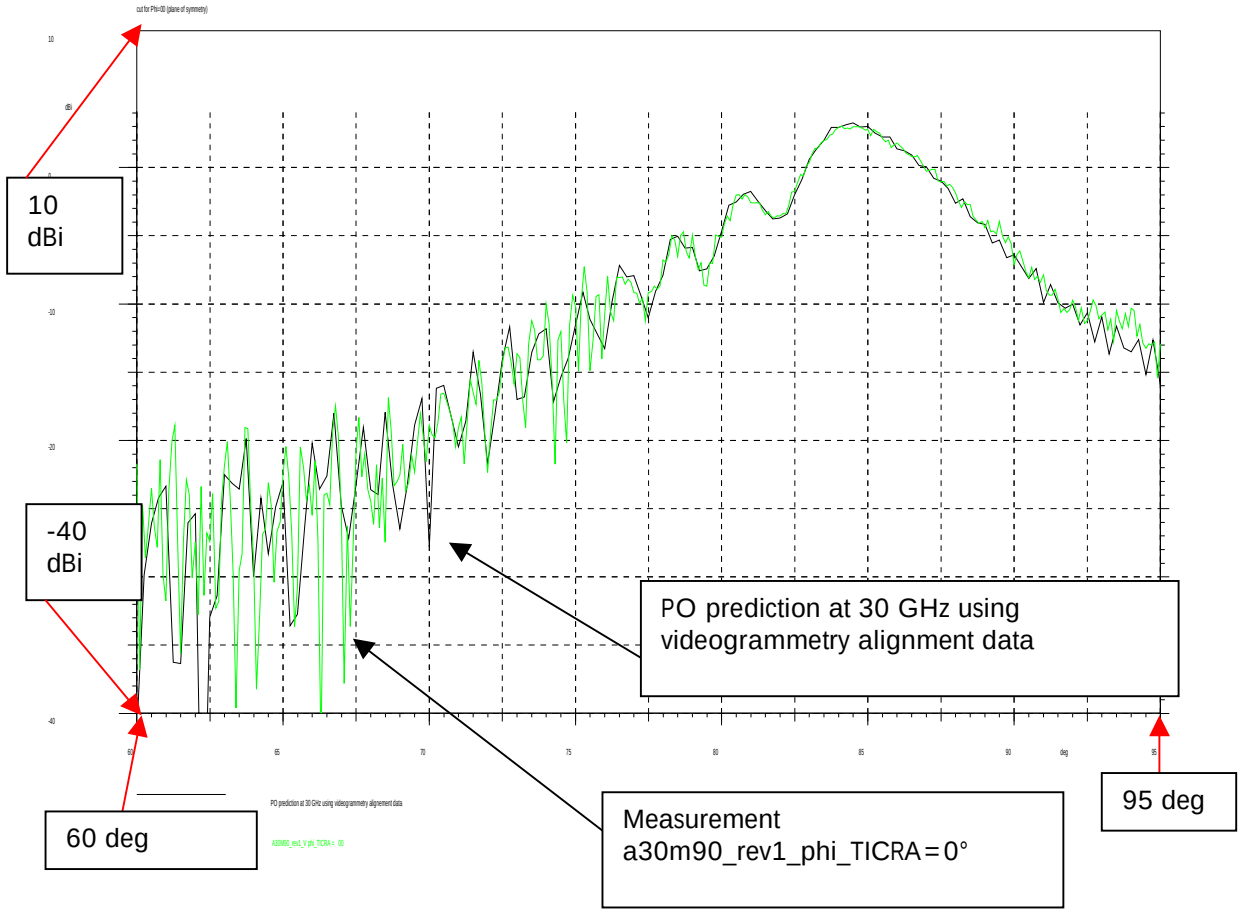

Figure 9-11 : superimposition of prediction and measurement : abscissae range from 60° up to 95 °, ordinate range from –40 dBi up to 10 dBi.

10. TELESCOPE FAR FIELD RADIATION PATTERN PREDICTION AT 100 GHZ.

10.1 Main lobe prediction.

This section presents the prediction. Detailed analyses (correlation with measurement) are provided in the next section.

The main lobe is computed using the grasp8 software and the telescope mathematical model [RD 6]. This model corresponds to the nominal geometry realigned with the distance data provided by the videogrammetry. The primary reflector surface is composed of the cloud of points measured with the videogrammetry, the secondary surface is composed of the set of points measured with the 3D mechanical machine. A cross check will nevertheless be performed with the surface data provided by the vidogrammetry measurement of the secondary reflector. As it has been seen the correlation is excellent at 30GHz. But very small discrepancies at 30 GHz are highlighted with the frequency increase.

The results of this section are going to be updtated thanks to the future videogrammetry data (mid july 2002).

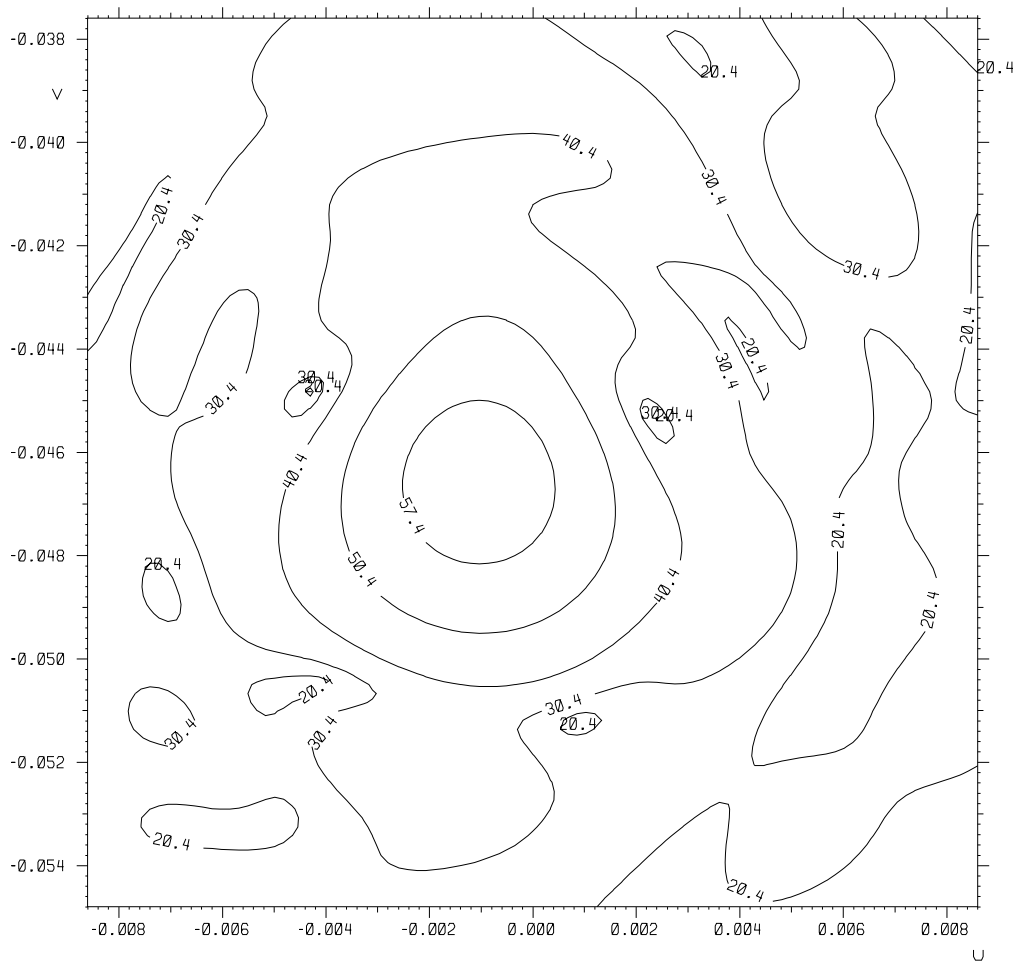

Figure 10-1 : predicted pattern at 100 GHz.

10.2 Far out side lobe prediction

The far out side lobes are computed using the grasp8 software and the telescope mathematical model [RD 6]. The diagram is computed in one cut : the horizontal cut passing through the main lobe. In the M1 coordinate system a coordinate system pointing in the main beam direction is defined. Then in this new coordinate system, the cut is performed in the plane defined by the two half cuts φ=-90 and φ=+90°.

The figure 10-2 displays the prediction in the plane φ=+/-90°. This cut is passing through the main lobe (pointing in θ=-2.65°, φ=0° in M1 coordinate system). This cut should be symmetrical in the nomical case (ideal surface), the non symmetry is induced by the surface shape errror and the reflector relative misalignement. Rem : the predictions are performed using the alignement data measured on the actual RFDM prior to the RF test.

These predictions should be improved thanks to the use of the videogrammetry data of the secondary reflector. See section 3 for details on the vidoegrammetry.

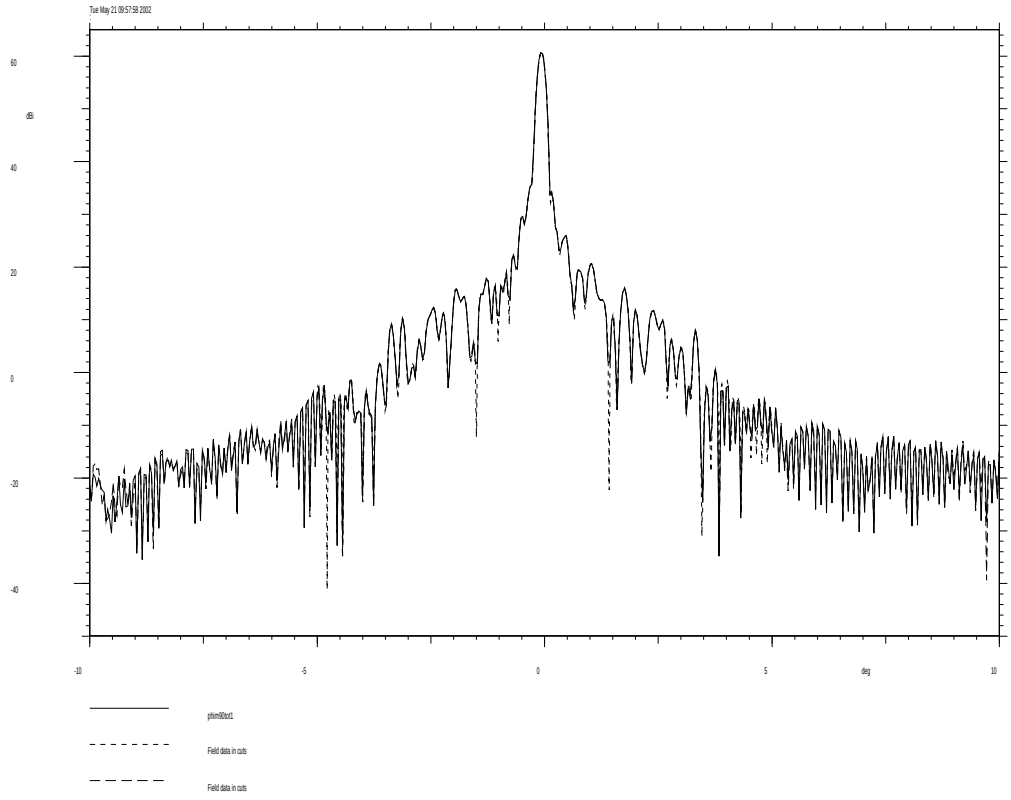

Figure 10-2 : 100 GHz prediction for the side lobes (+/- 10°) in the horizontal cut passing through the main lobe.

11. 100 GHZ RFDM MEASUREMENT

This section introduces some measurements performed at 100 GHz. These measurements will be compared in future section (13) with predictions. All measurements plots are available in the reference document [RD 4]. The test has started by a millimetric module setting. For this measurement the dynamic has been optimized, a 97 dB dynamic has been highlighted (see detailed parameters in [RD4]) for the "horizontal cut". This dynamic is sufficient for the 100 GHz pattern because the telescope is not directive enough at this low frequency. There are no side lobes lower than 100 dB in the investigated part of the sphere around the telescope. Then a main lobe acquisition has been performed. On final the same cut has been performed to check the measurement reproducibility over time. The final acquisition has been the spill over lobe past the primary cut. For this acquisition, it has been necessary to release the Cassini ring and thus to slightly deviate from the initial alignment wrt the angle of arrival in the CATR.

11.1 Main lobe measurement

The main lobe has been measured in a window (3 times smaller than the 30 GHz one) in order to reach levels down to 40 dB below the maximum. The main lobe is displayed in figure 11-1.

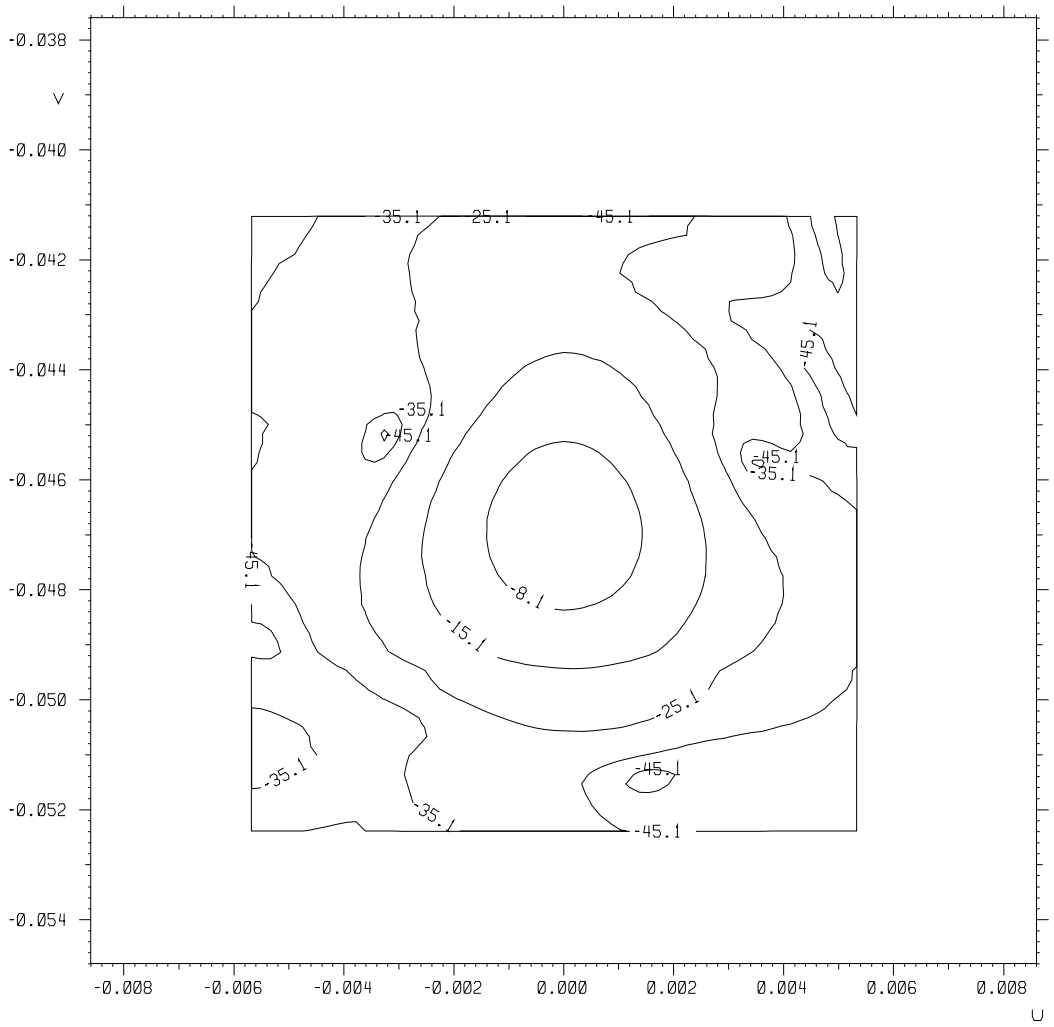

Figure 11-1 : Measured pattern at 100 GHz.

11.2 Far out side lobe measurement

This section displays the far out side lobe in the horizontal cut (see figure 11-2). And the spill over lobe past the primary reflector (see fig 11-3).

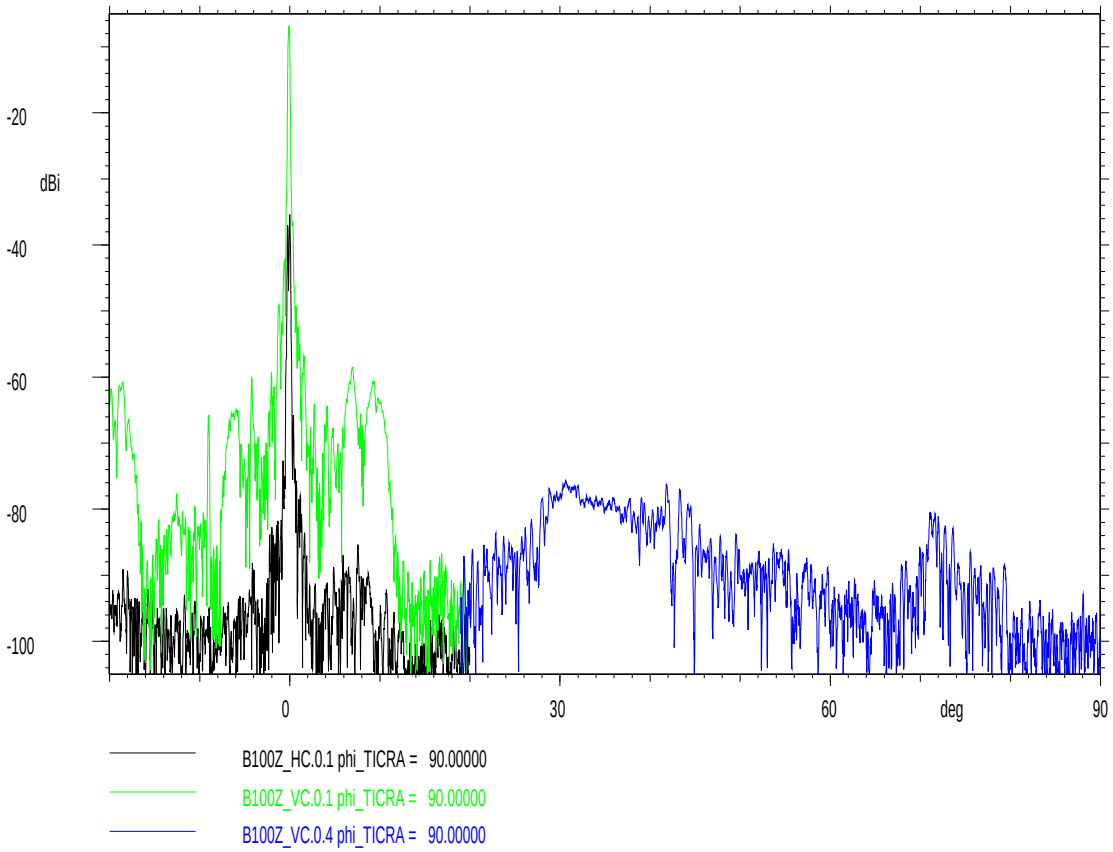

Figure 11-2 : far out side lobe measurement in the horizontal plane passing through the main lobe.

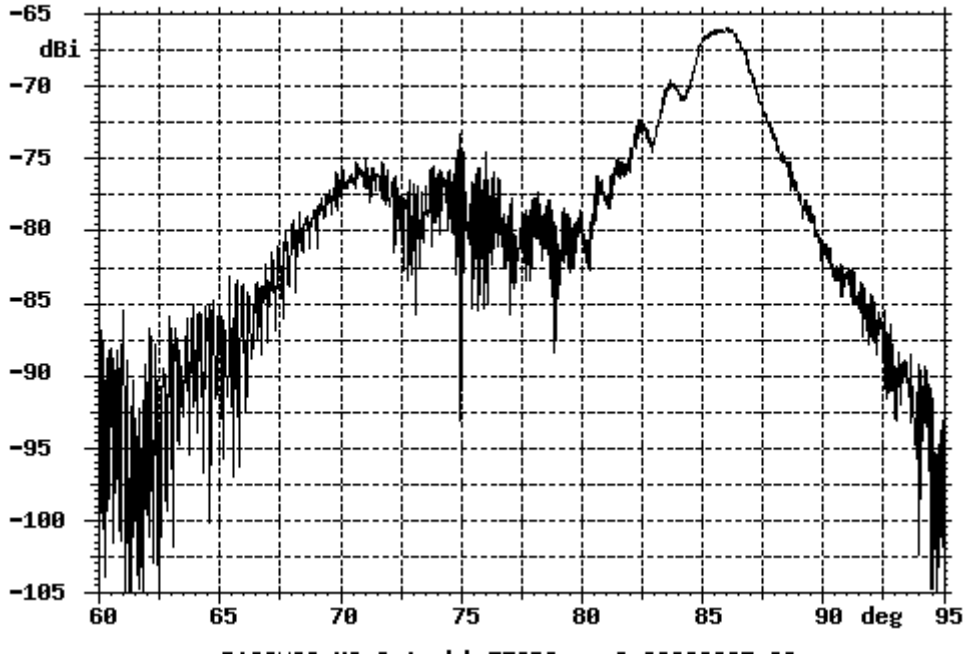

Figure 11-3 : spill over lobe past the primary reflector.

12. LOSS BUDGET EVALUATION AT 100 GHZ

The main lobe displayed in section 11.1 have been integrated in order to obtain the integrated directivity.

Feed VSWR	1.061	1.2
Insertion loss (dB)	-0.004	-0.036
Ohmic loss (dB)	-0.2	NA
Spill over (dB)	NA	-0.024
Loss (dB)	-0.204	-0.060

	Prediction	Measurement
Directivity (dBi)	60.4	60.90
Loss	-0.20	-0.04
Gain (dBi)	60.20	60.86
Difference with prediction (dB)	ref	0.67

table 12-1

The integrated directivity takes into account the ohmic losses but not the spill over. The computed (grasp8) directivity includes the spill over but not the ohmic loss. The table 12-1 displays the loss budget in distinguishing the prediction and the measurement. Then this loss budget is applied to the directivity obtained through a grasp8 computation or by integration of the measurements.

13. 100 GHZ MEASUREMENT AND PREDICTION COMPARISON

13.1 Main lobe co-polarization comparison

This section introduces the comparison with the measurements. As it has been written in section 10.1 there's some remaining uncertainties to be removed wrt the knowledge of the surface shape and relative alignment. The comparison displayed in figure 13.1-1 is less satifying than the the comparison performed at 30 GHz (see section 9.1). Nevertheless the general shape of the diagram is found down to 40 dB below max. The slight differences can be removed by using the videogrammetry data of the secondary reflector.

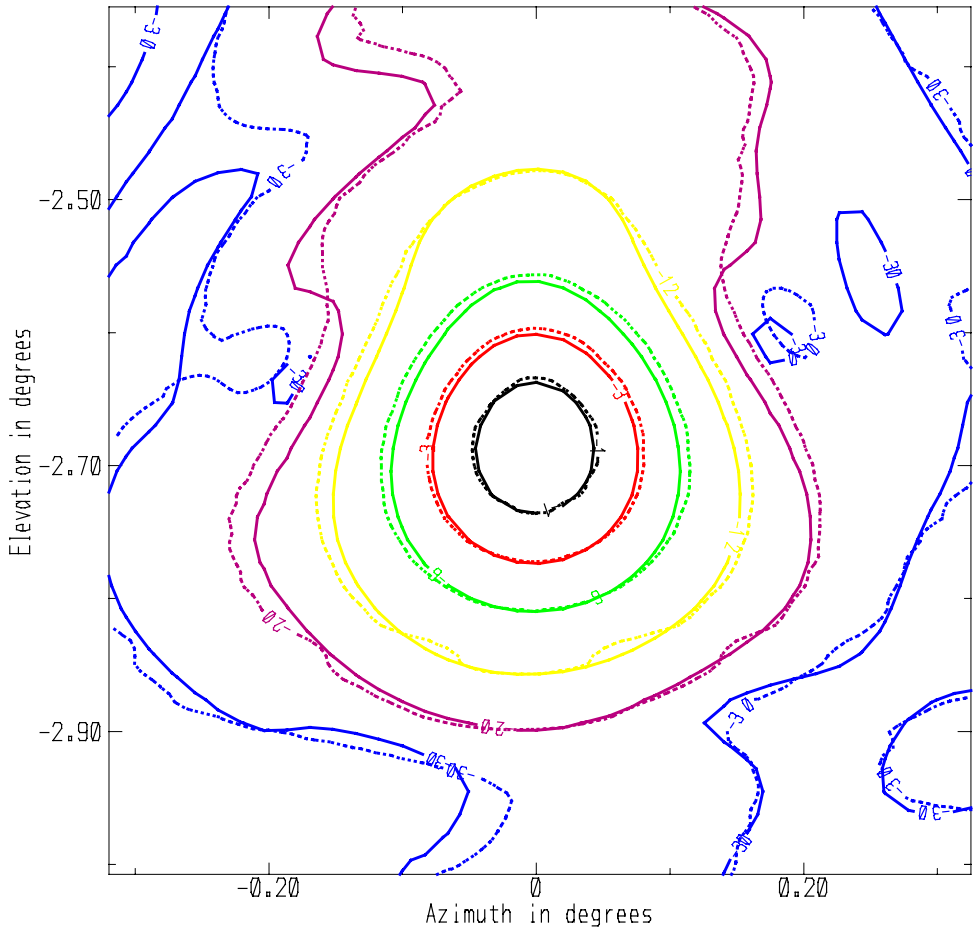

Figure 13-1 :main lobe prediction superimposed with measurements (displayed for levels : -3 dB -10 dB, -20 dB, -30 dB below max).

13.2 100 GHz far out side lobe measurement comparison with prediction

The measured far out side are superimposed to the prediction. The blue arrows are pointing the most significant discrepancies. Those differences are explained by a ray tracing in the CATR with the RFDM in nominal position (ie : plane of symmetry perpendicular to the ground).

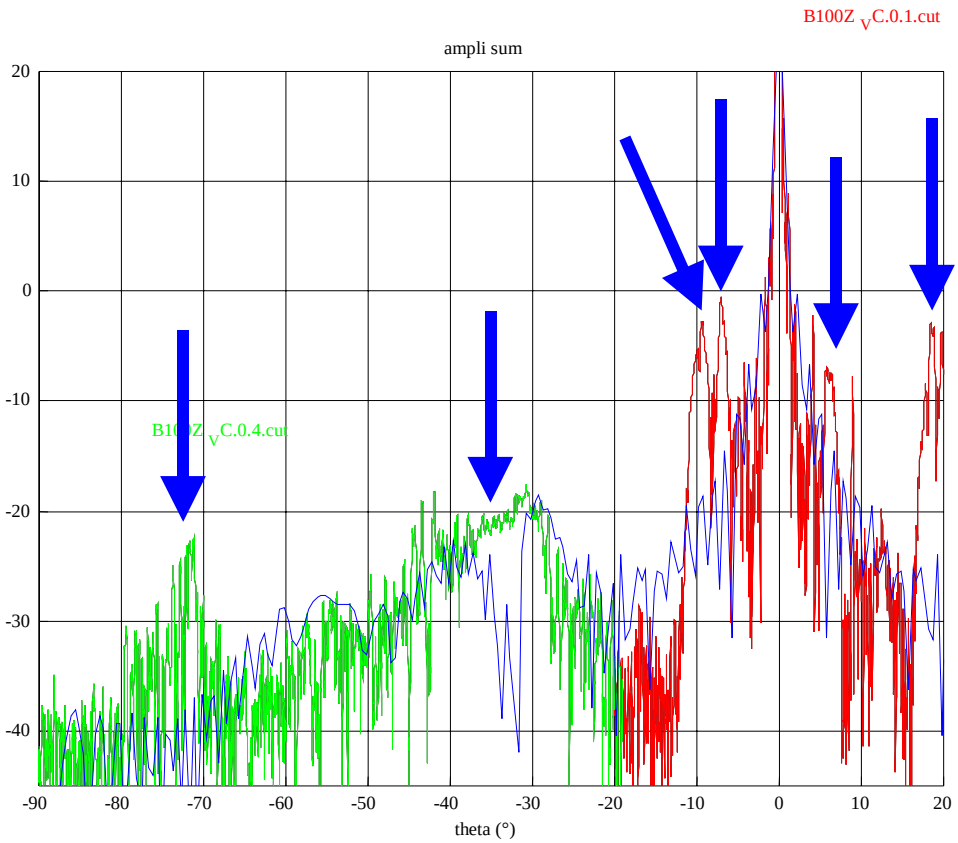

Figure 13-2 : prediction & measurement superimpostion.

Each significant discrepancy is explained one by one starting form the one at –70° then –35° ,-10°,-7°,+7, +20°.

The abnormal level at θ=-70° comes from a reflection on the Anechoid wall, from the measured value (see section 15) the anechoids have an attenuation of 50 dB (see link budget in [RD4]).

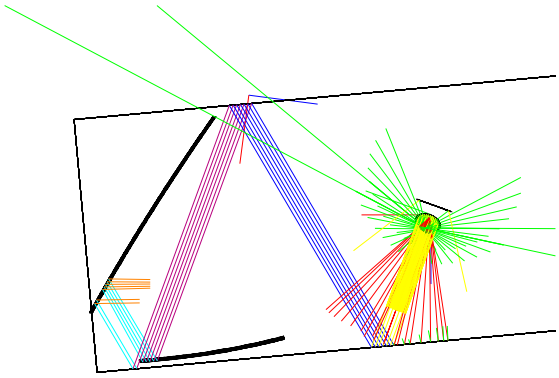

Figure 13-3 : ray tracing for measured direction of θ=-70°

The CATR secondary reflector has been enlarged by 1m on each edge in order to simulate the serration from a ray tracing point of view. Then at θ=-35°, the main lobe is pointing directly to the serration area. The serraction might diffract toward the feed room. This assumption has to be consolidated by detailed analysi (grasp8 modeling of the CATR using multigtd method).

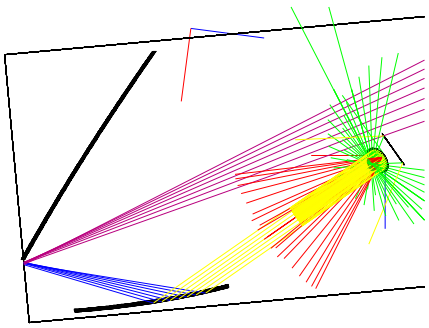

Figure 13-4: ray tracing for measured direction of θ=-35°

For θ =-10° or θ=-7°, two main hypothesis can be discussed. The first hypothesis being the triple reflected rays. The second hypothesis being an array lobe induced by the primary CATR reflector periodic milling.
This kind of lobe should be more and more amplified with the frequency increase (the surface error are becoming larger compared to the wavelength).
This lobe is apparently due to the CATR concept itself. The following publication (AMTA 2001) shows the same phenomenon at 503 GHz :

-“calibration and verification measurement in compensated compact ranges up to 500 GHz”-J. Hartmann et al – AMTA 2001.

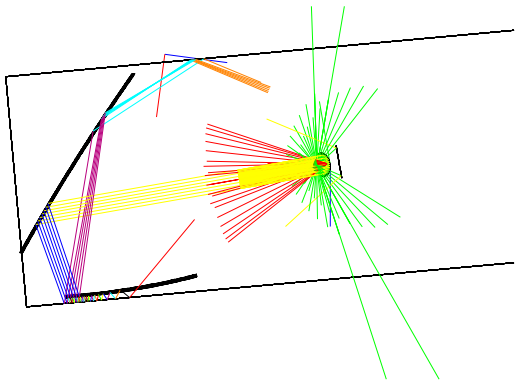

Figure 13-5: ray tracing for measured direction of θ=-10°

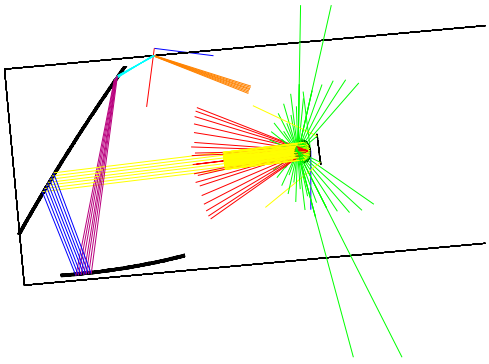

Figure 13-6: ray tracing for measured direction of θ=-7°

For the θ = +7° lobe the energy reaching the CATR illuminator might come form the reflection/diffraction of the serration on the secondary CATR reflector. The other possibility is the direct illumination of the feed room by the primary feed in the RFDM focal plane.

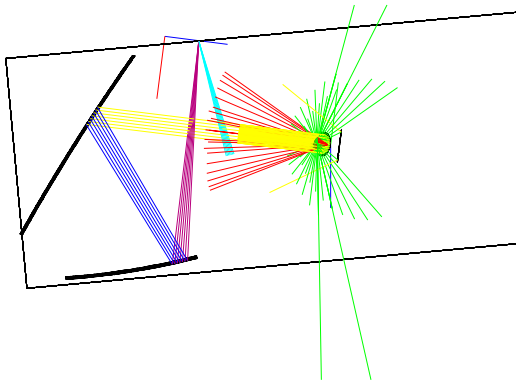

Figure 13-7 : ray tracing for measured direction of θ = +7°

For θ = +20° the lobe might come from the diffraction of the flat anechoid edge on the billboard.

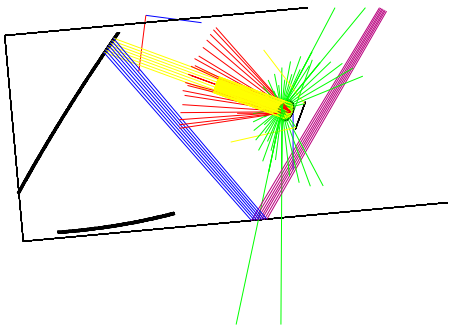

Figure 13-8: ray tracing for measured direction of θ = +20°

The final correlation is the spill over lobe past the primary reflector. A nice correlation is obtained. Anyhow the spill over lobe past the primary reflector is mainly due to the reflection on the secondary reflector and diffraction on top of the primary reflector. The correlation can be improved by using the videogrammetry data of the secondary reflector. The abnormal lobe at 70 dB can be explained by a reflection on the wall covered of anechoid in the CATR.

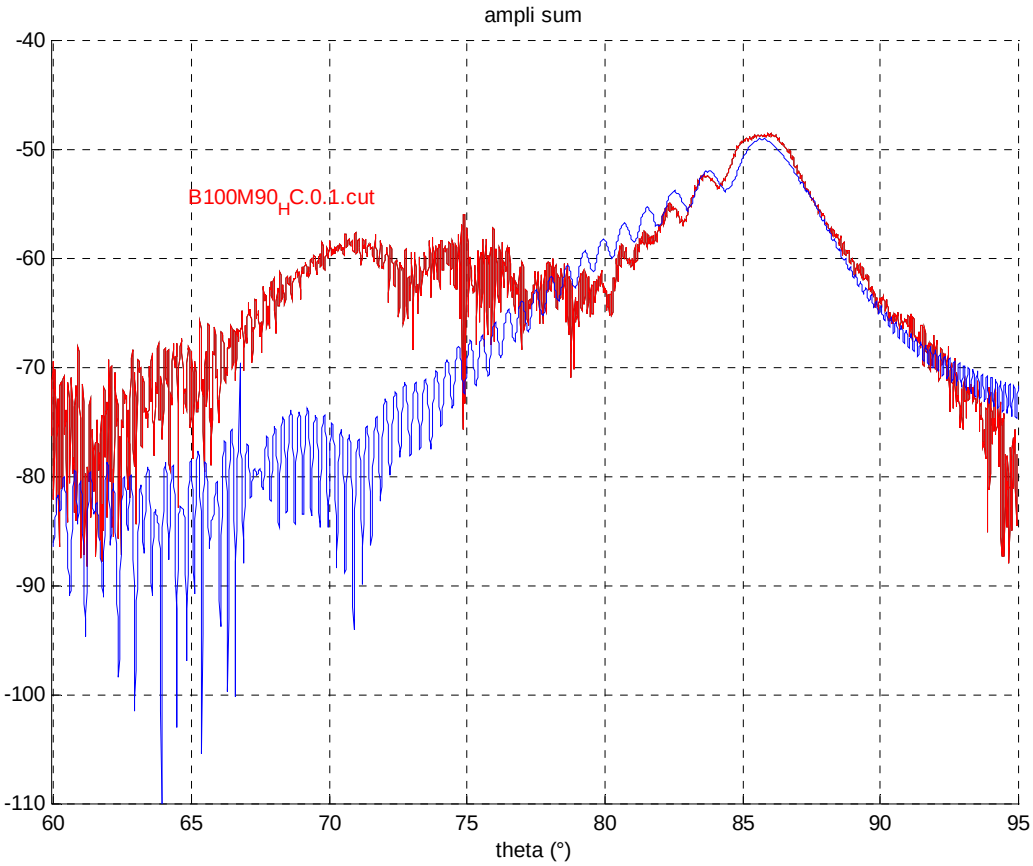

Figure 13-9 : superimposition of the spill over lobe measure and predicted.

14. LESSONS LEARNT FOR THE RFQM/FM TESTING.

The RFDM campaign has shown the necessity to have an accurate knowledge of :

- -theoretical primary feed diagram.
- -primary feed measured diagram.
- -accurate knowledge of the reflector surface.
- -accurate knowledge of the reflector relative alignement.
- -knowledge of the potential mispointing induced by the structure of the telescope under test.
- -the overall diagram of the telescope (spill over lobe direction and level).

Now for the test facility it is necessary to know :

- -the geometry (optical combination of the CATR reflector)
- -the CATR accomodaton (walls,ceiling)
- -the RF properties of the CATR anechoids.

In addition it is neccessary to know the location of the telescope in the CATR.

It is also necessary to know the CATR RF set up and RF chain performances.

All the lessons learnt in the RFDM test campaign are highly valuable for the future specification of the RFQM model and flight model.

15. ALCATEL CANNES COMPACT ANTENNA TEST RANGE QUALIFICATION STATUS.

15.1 description

The Alcatel Space Industries Compact Antenna Test Range (CATR) is a dual reflector antenna facility designed for adjustment and measurement of satellite antennas & and RF payloads in a clean room (class 100 000) environment.

The dimensions and specifications of the CATR are the following :

- Compact antenna test range model : dual shaped compensated Cassegrain reflector system.
- Surface accuracy of the large iron reflectors is better than 17 μm r.m.s.
- Range of validated frequencies:
- from 1.5 to 40 GHz
- Linear and circular polarisations
- Anechoïc chamber dimensions : 14.32 x 36.17 x 11.15 meters (W x L x H).
- Central quiet zone: 5.5 x 5 x 6 meters (L x H x P).
- West door dimensions : 4.55x 5.2 meters (W x H).
- Plane wave quality (average values *) :
- Amplitude ripple = ± 0.3 dB
- Amplitude taper = 2 dB maximum
- Phase ripple = ± 4°
- measurement Accuracy (gain, EIRP, GT) : ± 0.25 dB
- ** This characteristic is dependent on the chosen illuminator.*

- The shielding of the CATR has the following minimum attenuation characteristics :
- Magnetic fields 200 KHz : 61 dB
- Electric fields 10 MHz : 100 dB
- Planes Waves 1 GHz: 76 dB
- External Isolation (Faraday cage) : 100 dB (characteristic)
- Internal Isolation (absorbers) > 50 dB one way (in Ku band)
- Absorbers M2 type

15.2 Anechoids test

The CATR CFR 75/60 implemented in Cannnes has the walls covered with standard anechoids (APM30 or APM 45 manufactured by Hyfral). In case of high frequency measurements, the reflecting coefficient of those anechoids has to be determined. In this frame a measurement has been performed using an Abmillimetre network analyser (MVNA 8-350) from frequencies ranging within 50-70 GHz and 90-110 GHz.

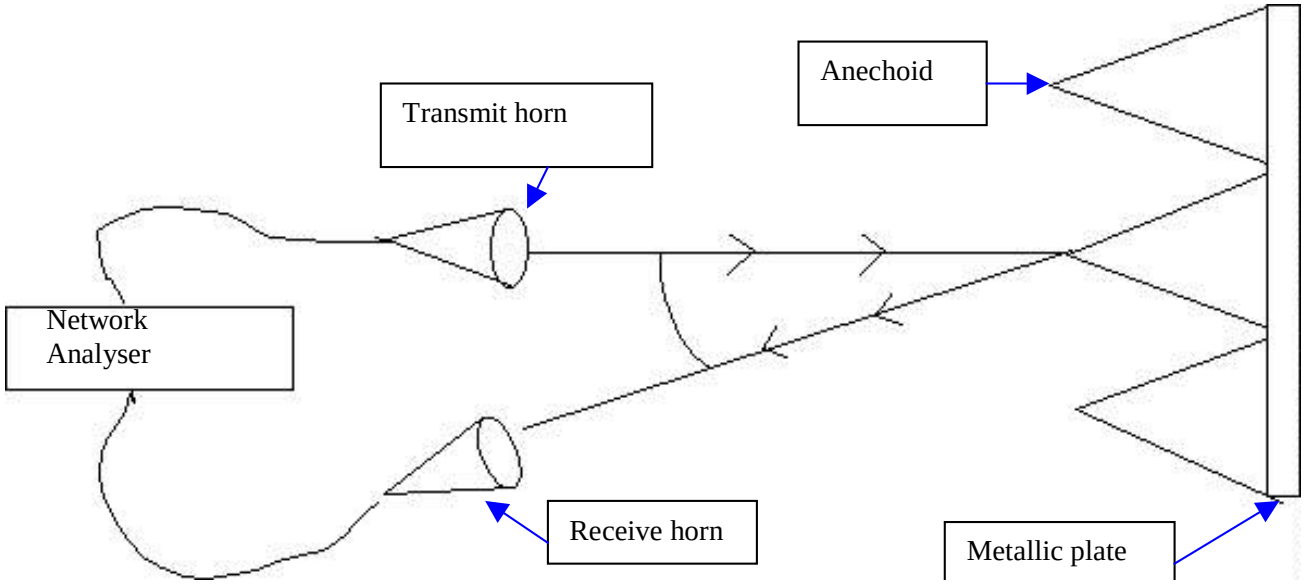

Figure 15-1 : Measurement test Bench

Calibration measurement: The reference value (0 dB) is obtained with the metallic plate alone then absorbers reflection measurement are obtained by comparison with this reference. The results are displayed in figures 15-2&15-3

APM30		5°	15°	45°
Manufacturer (Hyfral) data		-50 dB	NC	NC
50-70GHz	Max	-40 dBc[1]	-40 dBc	-50 dBc
	Min	-55 dBc	-48 dBc	-55 dBc
90-110 GHz	Max	-35 dBc	-32 dBc	-50 dBc
	Min	-38 dBc	-38 dBc	-55 dBc

Figure 15-2 : measurement results for the anechoids APM30

APM45		5°	15°	45°
Manufacturer data		-50 dB	NC	NC
50-70GHz	max	-40 dBc	-45 dBc	-55 dBc
	min	-50 dBc	-55 dBc	-60 dBc
90-110 GHz	max	-40 dBc	-40 dBc	-55 dBc
	min	-43 dBc	-50 dBc	-60 dBc

[1] dBc : dB compared

Figure 15-3 : measurement results for the anechoids APM45

The graphical measurement results are provided in Figure 15-4. The legend of each curve is defined for example as 5A30HH1 with:

5 : incidence angle
A30 : APM30 Foam
HH : same polarization for transmit and receive
1 : first measurement with horns pointing on absorber peak
2 : second measurement with horns pointing to absorber bottom

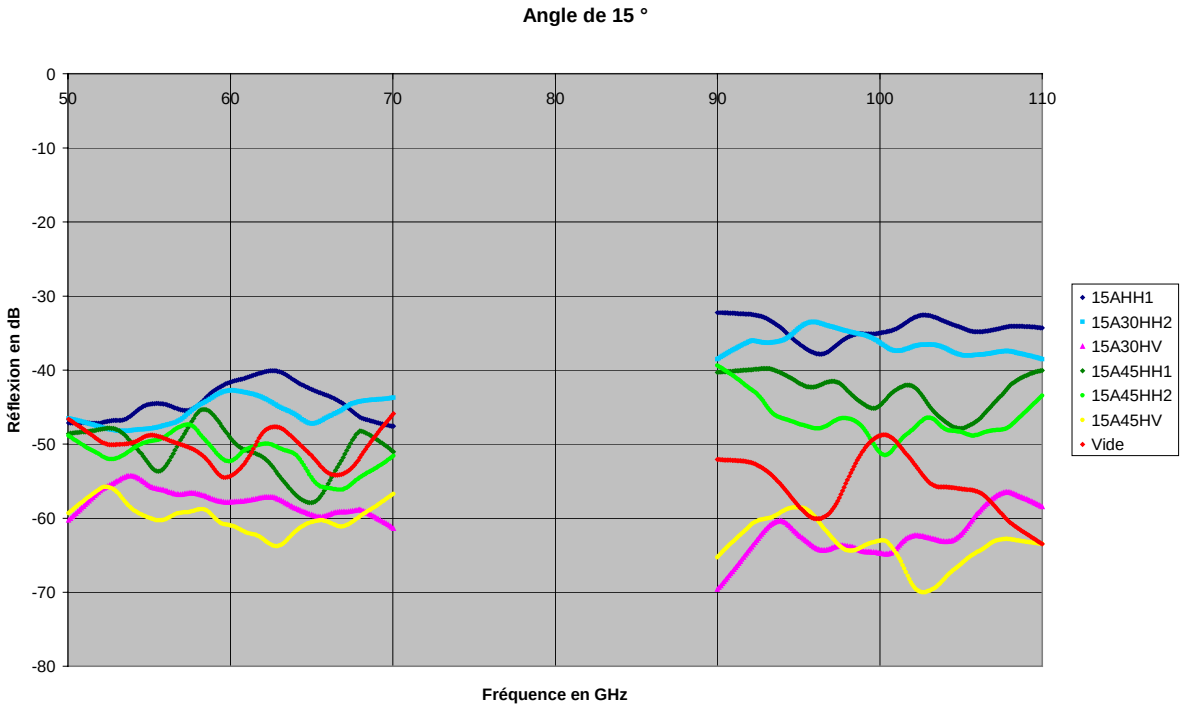

Figure 15-4 : Measurements curves for 15° incidence angle

This measurement shows the excellent behavior of anechoids over a wide frequency range.

15.3 Quiet zone analysis.

Quiet zone gridding have been performed in the frame of the CATR validation campaign.

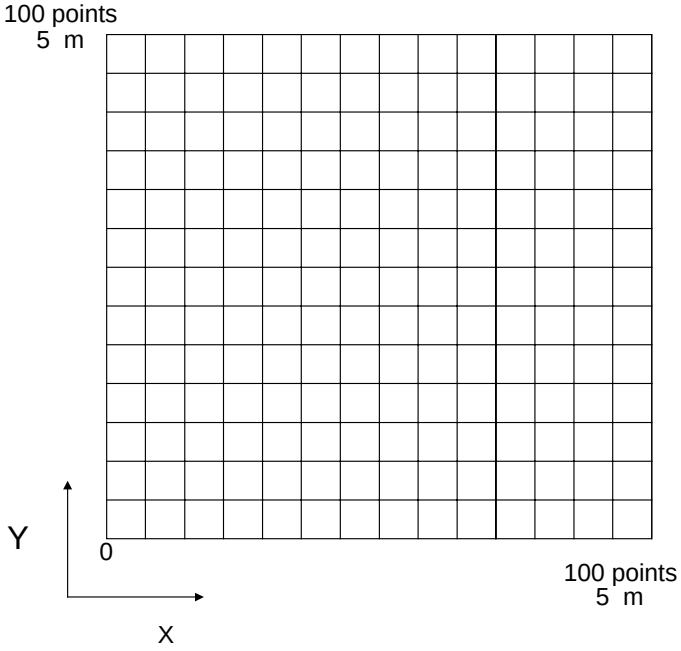

Figure 15-5 : CATR Quiet zone measurement : acquisition grid

Figure 15-6 : Curves plots

In order to compare the phase variation and obtain a overall view of the variation, the curves have been plotted as described in Fig. 15-6 instead of contour plots.

In a plane, the phase for two frequencies f and f' is respectively $\varphi = 2\pi l/\lambda_g$ $\varphi' = 2\pi l/\lambda_{g'}$. where l is the physical distance between the phase centre and the plane. The measure correspond in fact to $2\pi dl/\lambda_g$ [$2k\pi$] and $2\pi dl'/\lambda_{g'}$ [$2k'\pi$]. Then, it is possible to write $l = 2\pi k/\lambda_g + dl = 2\pi k'/\lambda_{g'} + dl'$.

The following relation is then verified on the measures.

$$k' \lambda'_g - k \lambda_g = \frac{(dl' - dl)}{2\pi} = cste \qquad (1)$$

With k and k' being integers. This shows there's no dependency of the frequency in the results.

FIGURES15-7 and 15-8 show the validation of (1) for four frequencies in the Ku band for polarization H and V. The rms value still constant over all positions. The ppm value is $\pm$ 0.1mm.

The same verification have been done in Ka band (see FIGURES 15-9 & 15-10) and the results show a good accuracy (constant rms value and ppm value less than 0.02 mm). Consequently, at higher frequencies , diffraction which depend on frequency has a reduced impact on phase. The ppm value is more significant in Ku band than in Ka band. This is due to an offset of 1 cm during scanning in x plan and sweeping in frequency in Ku band measurements.

These last investigations allow to verify if the diffraction effect (due to the edge of the reflectors) has a significant impact in the QZ.

The quiet zone gridding is performed over 5m by 5m the actual quiet zone is 4m by 4m, hence the regular peaks on the curves 15-7 correspond to the edge of the measured area. This area is the more affected by diffraction. Those peaks are decreasing with the frequency increase (see fig 15-7at 11-13-14 GHz and fig 15-9 at 29.5-30-30.5 GHz). This shows the nice quiet zone behaviour wrt frequency increase .

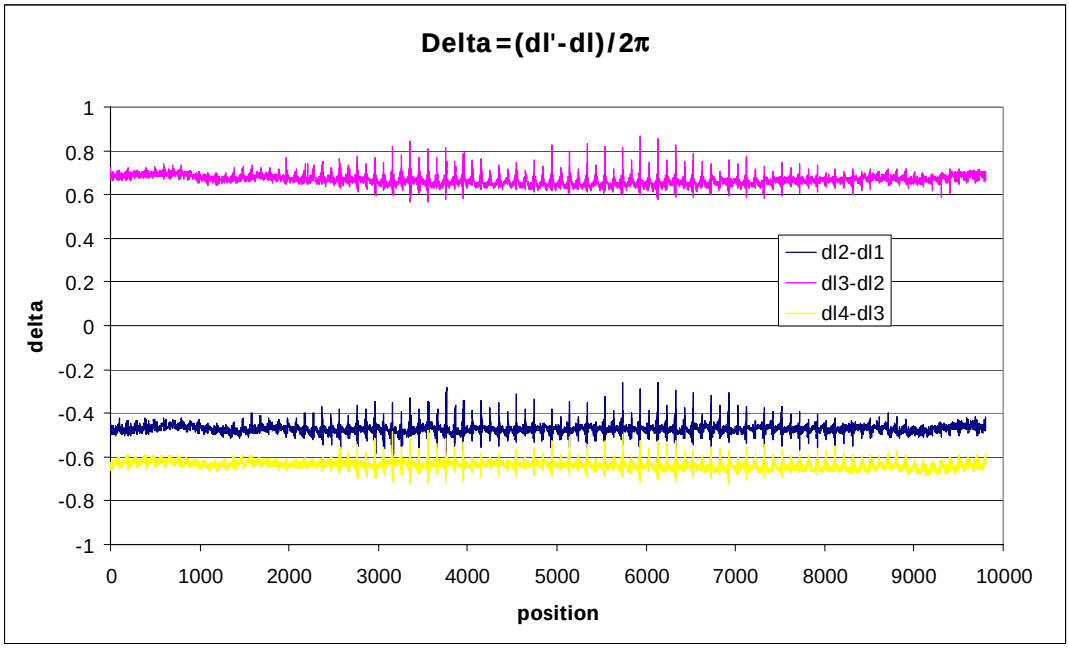

Figure 15-7 : verification of (1) for Polar H, frequencies (dl_1 (11GHz),dl_2 (12 GHz), dl_3(13 GHz),dl_4(14 GHz)

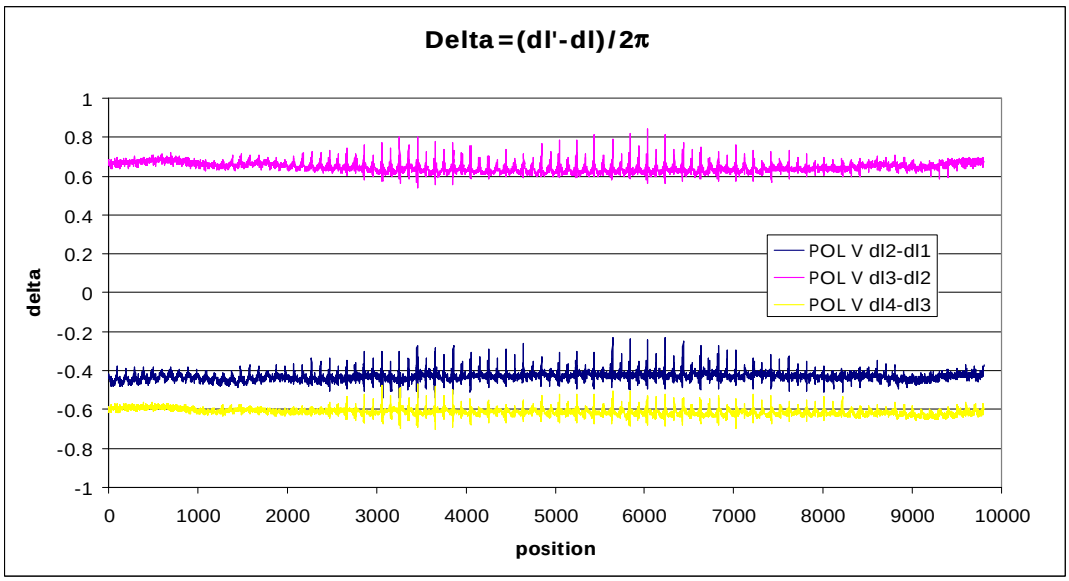

Figure 15-8 : verification of (1) for Polar V, frequencies (dl_1 (11GHz),dl_2 (12 GHz), dl_3(13 GHz),dl_4(14 GHz)

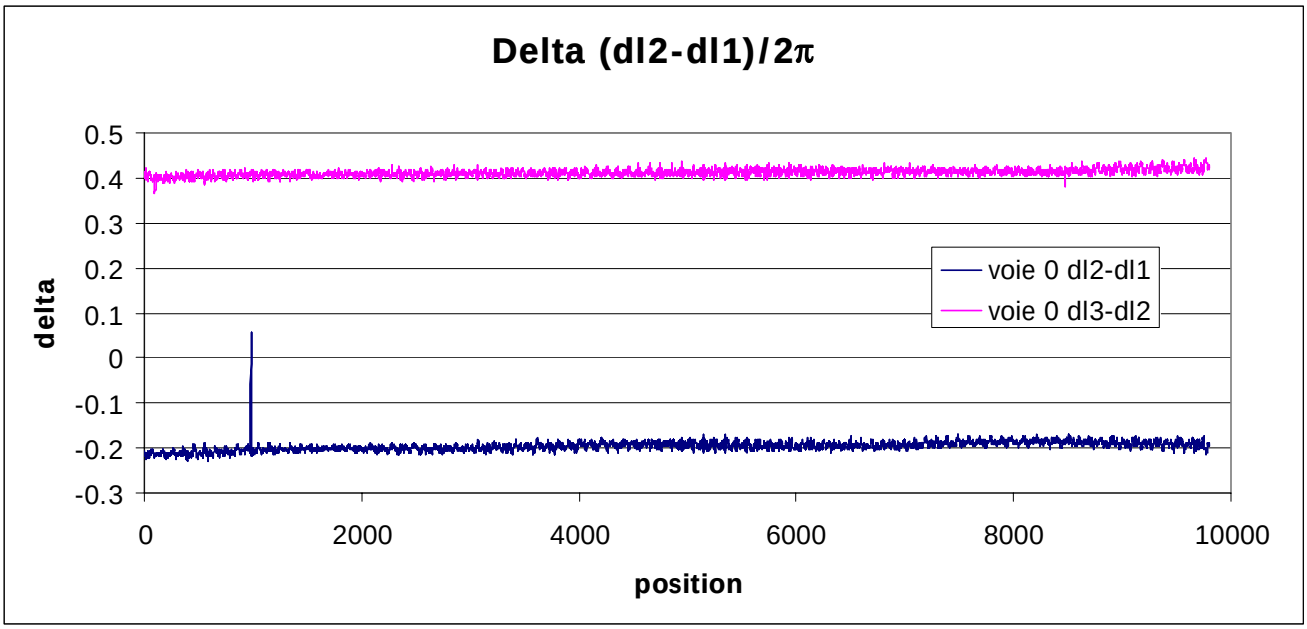

Figure 15-9 : verification of (1) for Polar V, frequencies (dl_1 (29.5 GHz),dl_2 (30.0 GHz), dl_3(30.5 GHz)

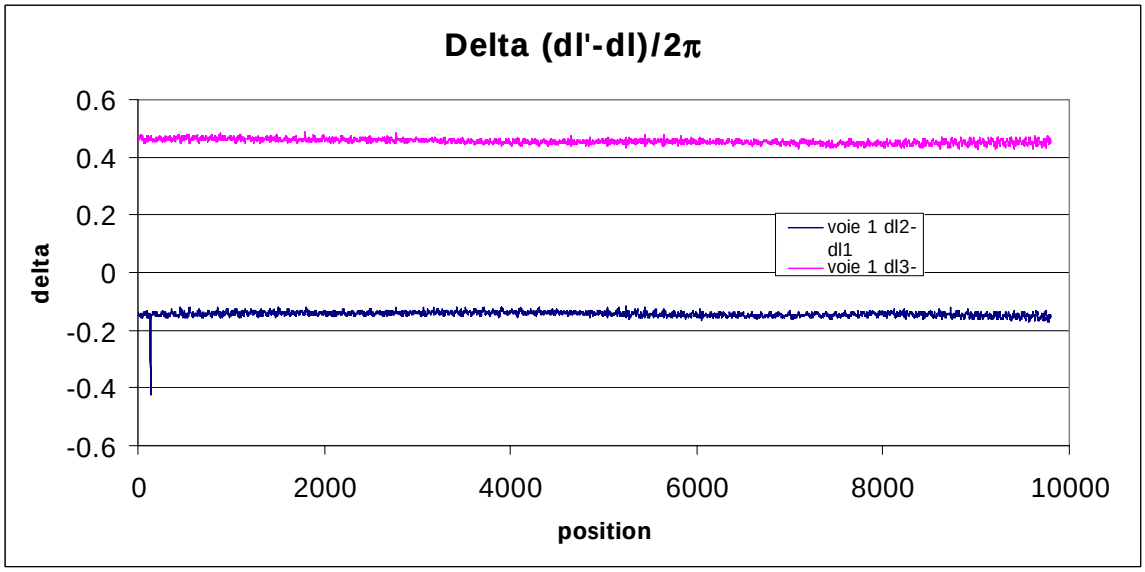

Figure 15-10 : verification of (1) for Polar H, frequencies (dl_1 (29.5 GHz),dl_2 (30.0 GHz), dl_3(30.5 GHz)

The distortion on reflectors and on scanner stability have to be quantified in term of phase.

The CATR reflector have been manufactured with a surface error of 0.017 mm. The scanner has a positionning surface errror of 0.120 mm. Hence the phase measurement is mainly altered by the scanner deviation. A comparison of the measured phase and the surface deviation is displayed in figure 15-11. The scanner deviation are clearly visible in the phase measurement.

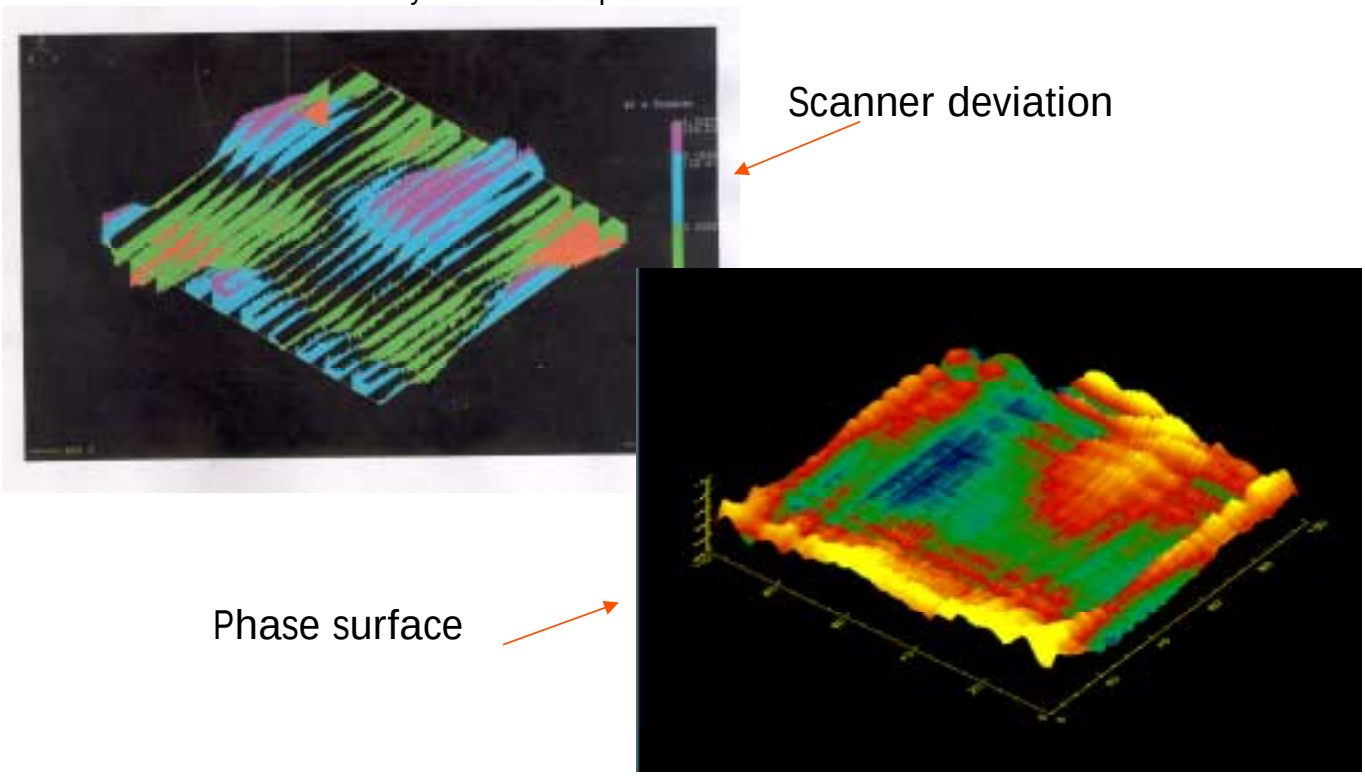

Figure 15-11 : phase measurement compared with scanner deviation.

15.4 Antenna tested at 30 GHz, 32 GHz.

15.4.1 Hot bird 6 Ka band antenna test.

The figure 15-6 displays a telecom satellite Ka band (30 GHz) antenna tower mounted on the positionner for the ALCATEL Cannes compact antenna test range.

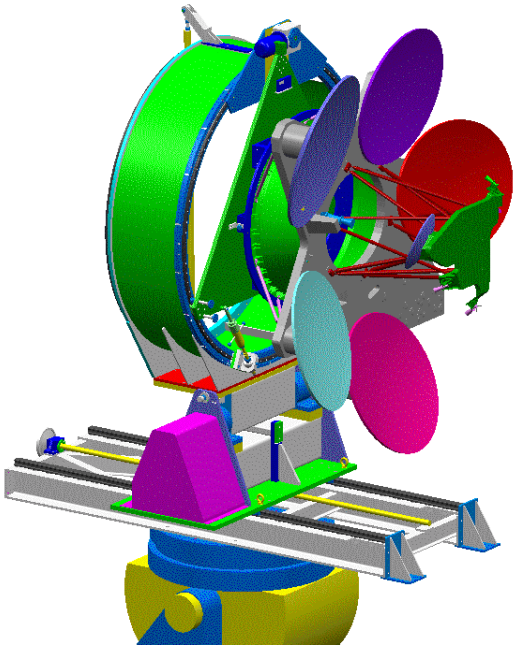

***Schéma7**: Configuration d'essais*

Figure 15-12 : antenna under RF test at 30 GHz.

15.4.2 Cassini antenna

The 4m Cassini antenna has been tested in the ALCATEL Cannes CATR (see fig 15-13).

Figure 15-13 : 4m Cassini Antenna under test in the ALCATEL CATR

For the Ka Band the main parameter are displayed in following table. It is interesting to highlight the fact that the angular resolution of the beam at half power is of the same order of magnitude at the Planck angular resolution at 100 GHz. This is due to the antenna diameter ratio being quite close to the frequency ratio.

Frequency (GHz)	Measured Peak gain (dBic) LHCP	Measured HPBW(°) (*)
31.750	56.88+/-0.3	0.15
32.128	56.43+/-0.3	0.165
34.416	55.60+/-0.3	0.16

(*) with a resolution of 0.005°

The Cassini antena has also been test in S-band the figure 15-14 displays the in-flight antenna measurement performed by JPL with the on ground measurement performed in the CATR.

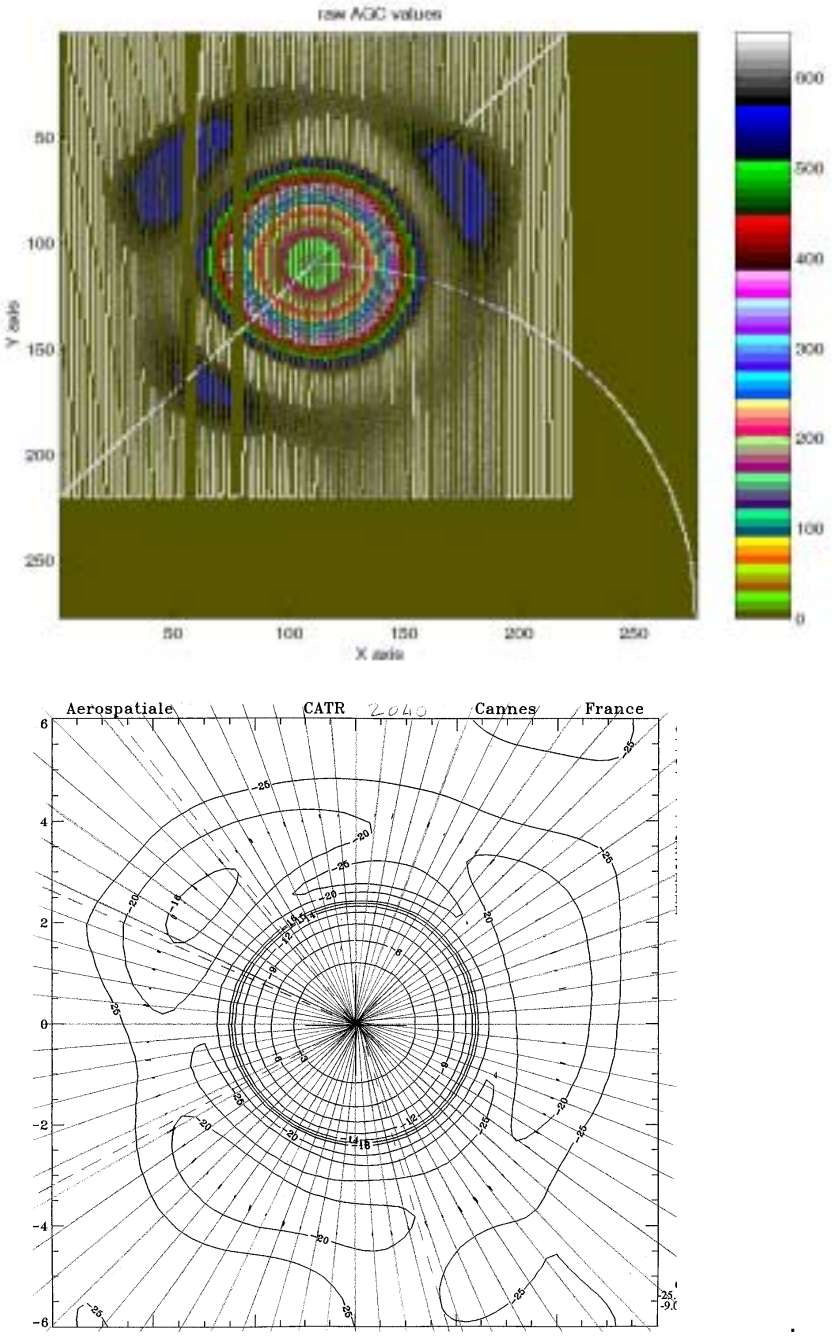

Figure 15-14 : In fligt Cassini antenna measurement compared with on ground CATR measurements.

15.5 Compact Antenna Test Range qualification status conclusion.

As a conclusion the Alcatel Cannes Compact antenna test range has been qualified and used at 30 GHz. Different antenna have already been tested, telecommunication antenna (Hot Bird 6 Ka Band antenna) as well as scientific and high gain antenna (Cassini).

The anechoids or absorbers have been tested in reflectivity, 100 GHz is well inside the frequency range of operation.

The quiet zone gridding for different frequencies shows that the diffraction effect is going down when the frequency is increased. By extension the 100 GHz diffraction is expected to be less than the 30 GHz one.

As a conclusion, the early test at 30 GHz on the RFDM is sufficient to validate the numerical model and associated tool, this corresponds to the RFDM test objective. The 100 GHz extension test is only a step toward higher frequencies for future test on the RFQM.

16. MISCELLANEOUS

All the measured data used as input in this document have been provided by the long term effort of the Alcatel team composed of different expert and specialists.

For this reason a special thanks should be adressed to :

- **G. Forma** who has performed the project management for the mock up and tests.
- **H Garcia** who has given all his physical and intellectual power to ensure the success of the project
- **C. Bouvin** who has been deeply involved in the numerical optimization of the feed matching, and data post processing.
- **C. Nardini** who has widely shared his know how and contributed to the success of the collaboration with Farran company.
- **D Allenic** and **JF Lecomte** who have provided many good advice and engineering feeling thanks to their wide experience.
- **B. Martel** who has been mostly available for the night and early morning slots of RF test.
- **JM Carrere** who has performed the very unpleasant files crash recovery.
- **H. Jaillet** who has carried out the alignments.
- **P Baussart** who has provided the powerfull videogrammetry views using an innovative method.
- **JF Clement** who has designed the mechanical structure.
- **B. Buralli** who has been motivated since the first second to ensure the succes of the RF test and who has performed the first 100 GHz cut acquisition in the history of the CATR.

17. CONCLUSION

This campaign has allowed to cross validate the numerical model (mainly the grasp8 software). This software has originally been develloped for the antenna main beam and near in side lobe prediction. Thanks to the Planck program, the pattern computation has been extended to all directions around the telescope in addition to the use of a new frequency range. The antenna testing has raised many technological issues in the usual RF field of activities (knowledge of surface, alignement, implementation of new RF set up, high directivity antenna testing, impact of the test facility). The measurement results have to be carefully studied, any abnormal lobes have been explained for the investigated cuts. This study is not completely frozen, this document has highlighted different explanations for abnormal lobes (ie not correlated with prediction).

This RFDM test campaign has allowed Alcatel to extend its RF measurement experience in acquiring high frequency measurement techniques. From a programmatic point of view, this test campaign allows the Planck prime contractor to gain sharper know how in high frequency RF tests. This know how will be valuable either to perform the future Planck RF tests on the qualification model or to sub contract and manage these tests in an external test facility. In this frame the RFQM test requirement is going to be released after discussion with the instrument teams and will take fully benefit of the ALCATEL recent know how.

END OF DOCUMENT